MICROBIAL DYNAMICS DURING GUT INFLAMMATION AND INFECTION

A Dissertation

Presented to the Faculty of the Weill Cornell Graduate School

of Medical Sciences

in Partial Fulfillment of the Requirements for the Degree

of Doctor of Philosophy

by

Krista Alexandra Dubin

December 2018

MICROBIAL DYNAMICS DURING GUT INFLAMMATION AND INFECTION

Krista A. Dubin, PhD

Cornell University 2018

The gastrointestinal (GI) tract is colonized with complex microbial communities, known as the microbiota, that contribute to the health of the host. The intestinal microbiota plays an important role in determining susceptibility to enteric infection and therapeutic response to cancer treatment. The composition of the microbiota is known to influence the efficacy of a range of cancer therapies. We found that differences in the microbiota's composition affects patients' risk of developing inflammatory complications of immunotherapy. Increased representation of the Bacteroidetes phylum as well as B vitamin biosynthesis pathways are correlated with resistance to checkpoint-blockade-induced colitis. The microbiota's composition is also known to impact the colonization density of antibiotic-resistant pathogens, an important cause of bacteremia in cancer patients receiving allogeneic hematopoietic stem cell transplants. We found that obligate anaerobes provide colonization resistance to *Klebsiella pneumoniae*, which is inhibited by short-chain fatty acids. Once colonized, enteric pathogens can evolve in the GI tract. This evolution can be tracked by the accumulation of single nucleotide polymorphisms (SNP) over time. In a mouse model of *Enterococcus faecium* colonization, SNPs were acquired at a rapid and regular rate, enabling us to study its diversification in real-time. Our work indicates that *E. faecium* can rapidly adapt in the gut by acquiring mutations in the pencillin-binding protein 5 while exposed to long-term ampicillin treatment.

BIOGRAPHICAL SKETCH

Krista Dubin completed a Bachelors of Arts in Biology at Bowdoin College in 2007 and matriculated into the Weill Cornell/Rockefeller/Sloan Kettering Tri-Institutional MD-PhD program in 2010. She joined Dr. Eric Pamer's laboratory in 2012.

PUBLICATIONS

Taur Y, Xavier JB, Lipuma L, Ubeda C, Goldberg J, Gobourne A, Lee YJ, **Dubin K**, Socci ND, Viale A, Perales MA, Jenq RR, van den Brink M, Pamer EG. 2012. Intestinal domination and the risk of bacteremia in patients undergoing allogeneic hematopoietic stem cell transplantation. Clin Infect Dis. (7):905-14. PMID: 22718773

Dubin K, Callahan MK, Ren B, Khanin R, Viale A, Ling L, No D, Gobourne A, Littmann E, Huttenhower C, Pamer EG, Wolchok JD. 2016. Intestinal microbiome analyses identify melanoma patients at risk for checkpoint-blockade-induced colitis. Nat Commun (7):10391. PMID: 26837003

Dubin K, Pamer E. 2017. Enterococci and their interactions with the intestinal microbiome. Microbiol Spec 5(6): doi:10.1128/microbiolspec.BAD-0014-2016

For my mother Randi

ACKNOWLEDGEMENTS

First and foremost, I would like to thank my advisor, Eric Pamer. Working on these projects with Dr. Pamer fundamentally shaped what I want to do as a physician scientist — how I think through problems, what challenges I want to tackle and ways I think can contribute. These are questions and challenges that I would not have thought to take on, and Dr. Pamer's mentorship provided the guidance to complete these projects. Dr. Pamer has a great ability to identify clinical questions and translate them into research projects and is an excellent communicator (both scientifically and personally), which are qualities that I believe make him such a successful physician-scientist. I appreciate his patience with seeing me through these projects start to finish. It has been a privilege to work in a lab that operates at such a high level of scientific rigor and that is comprised of people who are both talented and kind, and I'm leaving Dr. Pamer's lab with some very close relationships. I would thank both former and current members of the Pamer lab for their support over these years. I would also like to thank my thesis committee members, Dr. Alexander Rudensky, Dr. Luciano Marraffini and Dr. Marcel van den Brink, for their guidance and advice on these three diverse projects. I would like to thank Dr. Joao Xavier as a collaborator for his generosity with both his time and teaching. I am also thankful to have the support of the Tri-Institutional MD-PhD program, especially Dr. Olaf Andersen and Ruth Gotian, who have shaped and led a program that I am very proud to be a part of.

TABLE OF CONTENTS

LIST OF FIGURES

LIST OF TABLES

CHAPTER 1

INTRODUCTION

1.1 OVERVIEW

The GI tract harbors a rich community of bacteria, reaching densities as high as 10^{11}-10^{12} CFU/g (1). Intestinal microbes have coevolved with their hosts over millennia and aid in numerous functions from energy harvesting to immune system development (2). The intestinal microbiota of healthy individuals is composed of a diverse consortium of bacteria (3-5). Individuals harbor a range of bacterial compositions, consisting of hundreds of microbial strains in the colon that mainly fall into two major phyla: gram-negative Bacteroidetes and gram-positive Firmicutes (3,6,7). In addition to variations among individuals, differences in community structure are also found across body sites that exhibit different levels of stability over time, such as between the stable lower (fecal) and variable upper (oral) regions of the alimentary canal (8). The composition of the intestinal microbiota impacts the health of the host broadly as it has been associated with the development of diseases ranging from obesity, arthritis, Parkinson's, depression, to cancer (9-13).

Following antibiotic-induced perturbations of the microbiota's composition, colonization resistance is impaired, which allows pathogens such as *Enterococcus faecium* and *Klebsiella pneumoniae* to colonize the GI tract and rapidly reach high densities. In this introduction, we discuss how pathogens expand and evolve within hosts during infections (section 1.2). We then discuss mechanisms that commensal microbes utilize to prevent enteric infection with a particular focus on these two pathogens (section 1.3) and how rationally designed bacteriotherapy may rescue resistance in colonized patients (section

1.4). We conclude with a discussion of the role that the composition of the microbiota plays in maintaining mucosal homeostasis and modulating the effect of drug therapy (section 1.5).

1.2. EXPANSION AND DIVERSIFICATION OF COLONIZING PATHOGENS WITHIN PATIENTS

Administration of broad-spectrum antibiotics allows bacterial pathogens to expand dramatically in the gut by perturbing this sensitive microbial ecosystem (14-17). The clinical consequences of vancomycin-resistance Enterococci (VRE) serves as an excellent case study. VRE can expand to 99% of the intestinal lumen's microbiota in both antibiotic-treated mice and hospitalized patients (15). Dense colonization is associated with translocation into the bloodstream and subsequent bacteremia (15,16). In patients undergoing allogeneic hematopoietic stem cell transplantation (allo-HSCT), VRE colonization was found in over one-third of recipients and these dominated patients had a 9-fold greater risk for VRE bacteremia (16). This risk persists over time; ampicillin administration leaves mice susceptible to VRE colonization for up to 4 weeks post-treatment, and VRE stably persists in the cecum for at least 60 days (15). Bacterial pathogens and commensals can accumulate mutations as they adapt to the host environment during acute infection and chronic colonization. How microbes evolve within patients is of clinical importance. Colonizing pathogens improve their fitness within a host by increasing virulence, drug resistance and immune evasion (18). The genetic changes acquired within patients can also be used to track infections, providing higher-resolution insight into the dynamics of patient-to-patient spread than traditional typing methods (19-22).

SNP-based genomic comparisons have been employed to carefully characterize bacterial evolution. During chronic colonization in patients, bacteria acquire genetic changes

within months and develop coexisting, diverging communities (18, 23). Genes that are downstream targets of antibiotics have been mutated across different patients harboring the same pathogen, demonstrating the development of antibiotic resistance in realtime (18,24,25). With shotgun metagenomic sequencing, the relative abundances of different bacterial sublineages harbored in a single patient can be measured by determining the relative SNP frequencies in the total population. In patients intestinally colonized with *Bacteroides fragilis*, two evolutionary patterns emerged from the inferred population dynamics – one of clonal interference between two subclades, and a "sweep" in which a nonsynonymous mutation in a polysaccharide importer that became fixed in one of the lineages (26). Such dynamic events *in vivo* suggest that within-host genetic changes drive adaptation to the host within relatively short time scales. However, the within-patient evolution of VRE, a prevalent hospital-associated pathogen that can intestinally colonize patients for months, has not been well characterized. Understanding within-host VRE diversification can help inform how drug resistance develops, how and when patients acquire VRE in the GI tract, and provide potential treatment targets of genes important for long-term persistence.

1.3. THE BACTERIAL INTERACTIONS THAT UNDERPIN COLONIZATION RESISTANCE

1.3.1. Colonization resistance is mediated by the intestinal microbiota.

The intestinal microbiota prevents enteric pathogens such as Clostridium difficile and VRE from colonizing the gut through a process known as colonization resistance (15,27-30). Antibiotic treatment abrogates colonization resistance by depleting large communities of intestinal commensal microorganisms, particularly anaerobic bacteria, that mediate this defense (27,31-33). Repopulating the GI tract with a defined community of commensal microbes can effectively eliminate pathogens from the GI tract (34,35).

Commensal microbes facilitate clearance of enteric pathogens by various means (36-38). Broadly, commensals employ a variety of mechanisms to prevent infection: (i) indirect elimination that relies on activating the innate mucosal immunity or continual maintenance of mucosal barrier integrity, and (ii) direct antagonism through competition for nutrients or the production of inhibitory molecules.

1.3.2. Indirect inhibition involves activation of innate host immune defenses and maintenance of the mucosal barrier.

Intestinal microbes can stimulate innate receptors on immune cells and induce the production of antimicrobial peptides in other intestinal cell types. Paneth cells and intestinal epithelial cells produce RegIIIγ, a C-type lectin driven by Toll-like receptor (TLR) signaling with bactericidal activity against gram-positive bacteria (39-41). Secreted RegIIIγ kills bacteria by binding to peptidoglycans of the bacterial cell wall and forming pores (42). Antibiotic treatment reduces expression of RegIIIγ and, in mice, increases susceptibility to VRE colonization and bacteremia (43). Oral administration of lipopolysaccharide mimics commensal microbial signals and restores RegIIIγ production, thereby increasing resistance to VRE (43). A signaling pathway driving RegIIIγ expression was delineated by administration of the bacterial TLR5 ligand, flagellin. Flagellin administered intravenously stimulates the CD103+ CD11b+ subset of dendritic cells to produce interleukin-23, which drives the interleukin-22-mediated production of RegIIIγ by intestinal epithelial cells (44,45).

Intestinal microbes are separated from the mucosal epithelium and its distal lamina propria by mucus that coats the epithelial surface. The colonic epithelium is covered by a dense 50-μm-thick inner mucin layer composed primarily of Muc2 and a less dense outer stratum (46). Maintenance of a healthy epithelial barrier and intact gut physiology, such as gastric acid production, inhibits bacterial colonization of the GI tract (47). Goblet cells

produce mucin, and secretion is stimulated by commensal bacteria in a MyD88-dependent manner (48-50). Following antibiotic treatment, the mucin layer thins; without a robust physical barrier, intestinal microbes can directly access and potentially breach the epithelium (51). Both the density and composition of the mucus layers limit bacterial invasion. RegIIIγ is associated with mucin and reduces the density of intestinal bacteria near epithelial cells (52-54). Intact mucin production limits the invasive potential of intestinal enterococci (55). VRE is spatially segregated from the intestinal mucus layer and adjacent epithelium even after antibiotic treatment with its notable mucin reduction (55). Conversely, *K. pneumonaie* can reside in the inner mucus layer and translocate into the mesenteric lymph nodes following intestinal colonization. Co-colonization of mice with VRE and *K. pneumoniae*, which can more deeply penetrate the mucus coating, enables VRE to gain access to the mesenteric lymph nodes, possibly by *K. pneumoniae*-induced alterations to the mucin composition (55).

1.3.3. Direct inhibition involves competition for nutrients and the production of inhibitory molecules.

Commensals can outcompete pathogens for essential nutrients. Commensal *E. coli* clears *Citrobacter rodentium* from the gut by consuming the monosaccharides that both require for growth (56). Commensal E. coli can also outcompete a pathogenic E. coli strain through nutrient deprivation (57). Commensal microbes can inhibit pathogen colonization by producing toxic substances such as bacteriocins, which are small molecules with antimicrobial activity. Bacteriocin-coding genes are commonly harbored on plasmids in enterococci. Commensal *E. faecalis* strains that express a pheromone-responsive conjugative plasmid encoding bacteriocin bac-21 outcompeted VRE lacking it (58). *Lactococcus lactis* strains engineered to express bacteriocins significantly inhibited VRE growth *in vitro* (59). Oral administration of bacteriocin-producing *L. lactis* MM19 eliminated VRE at a faster rate from the gut of mice than mock treatment (60).

Intestinal commensals metabolize complex carbohydrates to short-chain fatty acids (acetate, propionate, and butyrate), which can have inhibitory effects on gram-negatives. Acetate directly inhibits the growth of *E. coli in vitro* through the accumulation of its anions in the cytoplasm which reduces the intracellular pH (pH-i) and thereby increases osmotic pressure (61). This effect is buffered by the amount of glutamate in the cell and recovery from acetate-induced pH-i is associated with synthesizing more glutamate (61). Additionally, the depletion of methionine and glycine contribute to the growth inhibition and can be restored with amino acid supplementation (62,63). This effect is due to intermediates in the amino acid biosynthetic pathways accumulating (63).

1.3.4. Evolved mechanisms of commensals to combat pathogens of same species.

Commensal enterococci have developed sophisticated mechanisms to eliminate exogenous enterococcal competitors from the gut. Recent studies have examined the colonization dynamics between enterococcal commensals and healthcare-related isolates in the GI tract. While resistant isolates outcompete sensitive enterococci in the context of antibiotic pressure, intestinal colonization in patients declines following discharge (64). In *in vivo* competition assays that compared the colonization ability of *E. faecium* strains in antibiotic-treated mice, commensal isolates outcompeted hospital-derived strains after 2 weeks (65).

As mentioned in the previous section, commensal *E. faecalis* that express bacteriocin bac-21 carried on the plasmid pPD1 that can target VRE, and this plasmid is quickly transferred to naive intestinal commensals by conjugation (58). Pheromones are secreted short lipoprotein signal peptide fragments that act as chemical messengers between bacteria and can mediate cell death. The multidrug-resistant *E. faecalis* isolate V583 harbors a plasmid called pTEF2 that renders it susceptible to a killing mechanism

induced by commensal-derived pheromone cOB1 (66). Bacteriophages, or phages, are viruses that selectively infect and kill microbes. Given their selective killing, phages could be used therapeutically as a narrow-spectrum antimicrobial. *E. faecalis* strains that contain the bacteriophage ϕV1/7 in their genetic repertoire possess a growth advantage over related bacteria that lack it through phage-mediated lysis of competitors (67). In a mouse model of VRE bacteremia, intraperitoneal injection of ENB6 phage protected all mice when administered shortly after lethal VRE challenge and half of the mice when administered after the mice were moribund (68).

1.4. THERAPEUTIC POTENTIAL OF MICROBIOTA TRANSPLANTATION

1.4.1. Current state of fecal microbial transplantation to clear intestinal antibiotic resistant *E. faecium* and *K. pneumoniae.*

Given the rise of antibiotic resistance, fecal microbiota transplantation (FMT) is an attractive alternative therapy to treat antibiotic-resistant pathogens and is an area of active research. FMT is remarkably successful at curing chronic, intractable *C. difficile* infection (69). A secondary analysis of a study involving patients with recurrent *C. difficile* infection showed that a human-derived FMT can reduce VRE colonization (70). However, the risk of unwittingly transmitting pathogenic microorganisms through FMTs is not insignificant, especially since many constituents of the microbiota have only recently been identified, if not characterized. This concern is particularly relevant to patients colonized with VRE, who are often immunocompromised. Researchers are actively exploring methods to perfect the acquisition of transferred bacteria and define critical members of FMTs that target infectious agents (71,72).

To date, clinical trials studying the impact of fecal bacteriotherapy on intestinal carriage of VRE and multi-drug resistant Enterobacteriaceae are limited. An FMT used to treat a

patient with recurrent urinary tract infections (UTIs) eliminated intestinal *P. aeruginosa* that was causing the bladder infection but failed to resolve E. coli colonization (73). In a trial of 20 immunocompromised patients, antibiotic-resistant *K. pneumoniae* was undetectable in 65% of colonized patients following FMT, with an 89% efficacy in those who did not receive concurrent antibiotics (74). A few studies demonstrate the efficacy of probiotic bacteriotherapy to clear VRE from the gut. In a randomized study of 21 renal patients harboring VRE in their GI tract, ingestion of a yogurt supplemented with *Lactobacillus rhamnosus* GG reduced VRE density to the limit of detection in all patients receiving the probiotic (75). VRE burden decreased during a 3-week oral supplementation with *L. rhamnosus* GG in a randomized clinical trial of 61 children (76). This effect was not seen with 5-week administration of *L. rhamnosus* Lcr35 in a randomized study of nine patients (77). A 2-week course of *L. rhamnosus* GG administration in 11 patients with comorbidities also did not affect VRE colonization (78). Studies of enterococcal probiotics have failed to demonstrate their potential to limit drug-resistant enterococci colonization. In a prospective cohort study with over 500 hospitalized patients, a 10-strain mixture that contained *E. faecium* and numerous *Lactobacillus* isolates did not prevent ampicillin-resistant *E. faecium* acquisition (79).

In the first study of its kind for VRE, a defined consortium of commensals was identified as capable of restoring colonization resistance in mice (30). Antibiotic-treated mice were orally administered diluted doses of fecal microbiota from a colony of mice that had received ampicillin for over 15 years. Bacterial isolates in low-dose fractions that conferred resistance to VRE were identified, cultured, and administered in discrete combinations to mice maintained on ampicillin. Through a series of leave-one-out adoptive transfers, a minimum of four anaerobic isoates were found to successfully prevent and clear VRE from the gut: *Blautia producta*, *Clostridium bolteae*, *Bacteroides sartorii*, and *Parabacteroides distasonis* (30). Of the four-commensal mixture, *B.*

producta was shown *ex vivo* as the member that directly inhibits VRE growth, although the exact mechanism remains unknown. An open question in the field is whether a precise mixture of commensal isolates can be identified and used to clear *K. pneumoniae* colonization as had been done for *C. difficile* and VRE.

1.5. THE HOST-MICROBE RELATIONSHIP

1.5.1. The intestinal microbiota promotes homeostasis and mucosal tolerance.

Microbial species from a variety of genera such as Bacteroides, Clostridium and Faecalibacterium can induce the expansion of T-regulatory cells and stimulate the production of anti-inflammatory cytokines. A 17-strain collection of Clostridia isolates from clusters IV, XIVa and XVIII increased the number of Foxp3+ Treg cells that accumulated in the colonic mucosa and improved survival in an OVA-induced intestinal allergic murine model (80). *Faecalibacterium prausnitzii* has been found in lower abundance in Crohn's disease patients, and oral inoculation into mice with acute TNBS-induced colitis minimized pathology (81). Polysaccharide A produced by *Bacteroides fragilis* stimulates Foxp3+ Treg cell proliferation and IL-10 cytokine production (82). In a large screen of mono-colonized gnotobiotic mice, Bacteroides strains were the most successful at inducing colonic Foxp3+ Treg accumulation (83). Short chain fatty acids (SCFAs), metabolic byproducts produced by commensal microbes such as members of 17-strain Clostridia consortium, boost the differentiation of peripheral Tregs (84).

1.5.2. The microbiota mediates the host response to drug treatment.

The immunomodulatory capacity of the microbiota extends to mediating the efficacy of drugs that target immune system, specifically of cancer drugs. In the case of anti-PD-L1 and anti-CTLA-4 blockade, as well as CpG-oligonucleotide immunotherapy and cyclophosphamide, therapeutic response is affected by the intestinal microbiota.

Bifidobacterium boosted antitumor immunity by increasing T cell numbers in the melanoma tumor microenvironment following PD-L1 checkpoint blockade (85). B. fragilis was correlated with reduced melanoma tumor burden following CTLA-4 checkpoint blockade, and this effect was abrogated by antibiotics (86). Commensal intestinal bacteria enhanced TNF and ROS production during CpG-oligonucleotide therapy that reduced solid tumor growth (87). Increased intestinal epithelial permeability caused by cyclophosphamide led to bacteria translocating to lymph nodes and thereby stimulating Th17 cell development that is required for the drug's antitumor effects (88). Three studies were published simultaneously in 2018 detailing the microbiota's role in mediating tumor responses to anti-PD-1 immunotherapy in cancer patients (89-91). An open question in the field was whether, like with treatment efficacy, the microbiome plays a role in the development of immune-mediated, new-onset colitis in patients and if the microbiota's composition can be used to predict toxicity.

1.6. SUMMARY AND CHAPTER OUTLINE

The overall aim of this thesis is to understand the role of the microbiota in modulating disease states (such as colitis and infection) and, after expansion following dysbiosis, how opportunistic pathogens evolve and adapt within the gut environment. In **Chapter 1**, we identify microbiome biomarkers that predict patient's risk of developing checkpoint-blockade-induced colitis. In **Chapter 2**, we correlate obligate anaerobes with resistance to Klebsiellsia pneumoniae colonization. In **Chapter 3**, we characterize the temporal dynamics of within-host VRE evolution.

* Adapted from: Dubin K, Pamer E. 2017. Microbiol Spec 5(6)

CHAPTER TWO

INTESTINAL MICROBIOME ANALYSES IDENTIFY MELANOMA PATIENTS AT RISK FOR CHECKPOINT-BLOCKADE-INDUCED COLITIS *

2.1. INTRODUCTION

Healthy individuals harbor distinct microbial populations in their intestinal tract that vary markedly in composition. The complexity and plasticity of the intestinal microbiota represent a significant challenge to the host's immune defenses, which must balance immune tolerance of beneficial microbes with inflammatory responses against pathogens. Certain bacterial species are essential for maintaining a tolerogenic state in the mucosa. Identifying the microbial species that promote homeostasis or drive inflammation has remained a challenge in the clinical context, in particular with chronic inflammatory conditions such as inflammatory bowel disease. Certain bacteria preferentially expand following inflammation, which alters the microbiota's composition (92-94). Thus, as most patients seek medical attention after inflammation has developed, it is difficult to define the microbiota composition that precedes the development of colitis. Ipilimumab, a monoclonal antibody that blocks the co-inhibitory molecule cytotoxic T-lymphocyte-associated antigen-4 (CTLA-4), is an immunomodulatory therapy that provides effective treatment against metastatic melanoma (95). Inhibition of CTLA-4 signaling dampens negative regulation of T cells, thereby enhancing anti-tumor responses. Within the first 16 weeks of treatment, roughly one-third of recipients develop intestinal inflammation as a result of mucosal immune dysregulation (96-98). The high incidence of colitis in patients receiving ipilimumab provides an opportunity to characterize the colonic microbiota

* Dubin K, et al. 2016. Nat Commun (7):10391. PMID: 26837003

before the development of intestinal inflammation.

Herein we use next-generation metagenomic sequencing to identify biomarkers that are associated with resistance to new-onset, immune-mediated colitis in the context of immune checkpoint-blockade therapy. Increased fecal abundance of the Bacteroidetes phylum and three of its families (Bacteroidaceae, Rikenellaceae and Barnesiellaceae), as well as microbial genetic pathways involved in polyamine transport and B vitamin biosynthesis, are correlated with resistance to the development of colitis following CTLA-4 blockade. This study provides a novel view of the intestinal microbiota before the development of colitis and offers insight into preventive treatments for patients at risk of adverse inflammatory events following immunologic checkpoint blockade.

2.2. RESULTS

2.2.1. Colitis development in patients following CTLA-4-blockade.

We analyzed the intestinal microbiota of 34 patients enrolled in a prospective study to correlate pre-colitis fecal composition with the subsequent development of checkpoint-blockade-induced colitis. The patients in this study ranged in age between 28 and 85 and were diagnosed with metastatic melanoma. In general, fecal samples were obtained from patients prior to the first dose of ipilimumab (30/34), although in 2 patients who subsequently developed inflammation and 2 patients who remained inflammation free, samples were obtained after initiation of ipilimumab, but before the onset of colitis. Of the 34 patients, 10 were diagnosed with gastrointestinal inflammation between 13 and 57 days after initiation of ipilimumab (**Fig. 2.1a**). Patients who did not develop gastrointestinal inflammation following CTLA-4 blockade are herein referred to as Colitis-Free (C-F), and patients who experienced inflammatory complications after

CTLA-4 blockade are referred to as having Progressed to Colitis (PtC). Patients were assigned a colitis score by retrospective chart review, which ranged from no diarrhea (score 0) in C-F patients to severe colitis (score 4) in PtC patients (**Table 2.1**). There were no differences in age or gender between C-F and PtC patients (**Table 2.1**). Additionally, 40% of PtC patients and 50% of C-F patients were treated with systemic cancer therapy administered either prior to (14/16) or both before and during (2/16; both C-F) ipilimumab treatment course (**Table 2.1**).

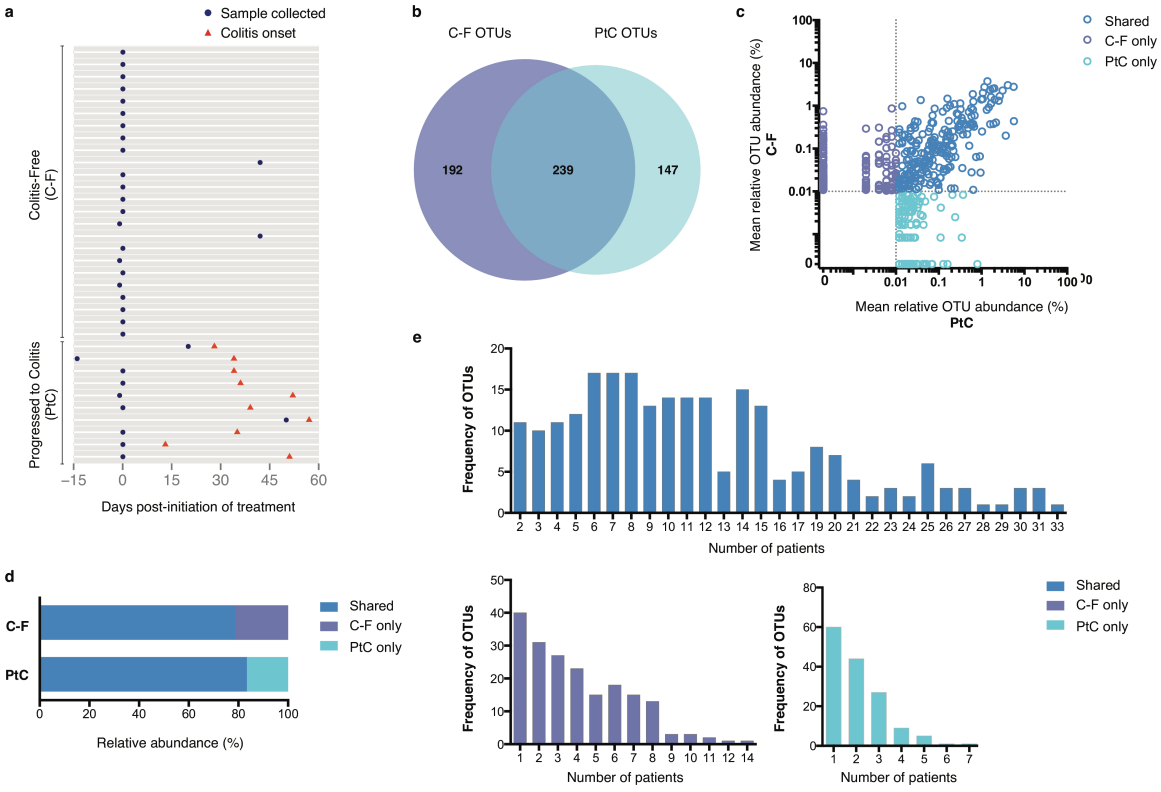

Figure 2.1 | Colitis-Free and Progressed to Colitis patients harbor distinct microbial populations. a) Fecal sample collection (blue circle) and the onset of colitis (red triangle) are shown at the indicated time-points during treatment with ipilimumab, a monoclonal antibody that blocks CTLA-4-signaling. Dates are relative to first dose of treatment. An average abundance >0.01% was used as the threshold for considering an OTU to be present within fecal samples in either patient group (OTUs, n=578); OTUs at an abundance of 0.01% were not considered to be present in the patients' microbiota. Using this definition, we calculated **b)** the number of OTUs present in C-F patients only (purple), PtC patients only (turquoise), or shared between the patient groups (blue) in a scaled Venn diagram. **c)** The mean relative abundance of OTUs, d) total abundance of OTUs, e) distribution of OTUs that are present in C-F patients only, PtC patients only or shared between the patient. C-F patients, n=24; PtC patients, n=10. OTUs, operational taxonomic units.

Table 2.1 | Patient characteristics and sample collection. Colitis score was determined by retrospective chart review using CTCAE, with scores ranging from 0 (no diarrhea) to 4 (severe colitis). Patient age was defined as of the first dose of ipilimumab and rounded down to the nearest integer. Patients' history of systemic cancer therapy was determined by retrospective chart review. A total of 16 patients received systemic cancer treatment, either prior to ipilimumab monotherapy (14/16) or both before and during ipilimumab treatment course (2/16). The symbol (+) indicates treatments that are given concurrently, while symbol (;) indicates treatments administered at different times. The symbol (*) indicates systemic cancer treatment administered both before and during ipilimumab therapy. C-F patients, n=24; PtC patients, n=10.

Patient group	Patient no.	Colitis Score	Sex	Age	Prior Systemic Cancer Treatment(s)
Colitis-Free	1	0	M	62	Tyrosinase DNA vaccine (in adjuvant setting)
Colitis-Free	2	0	F	50	Adjuvant Interferon
Colitis-Free	3	0	M	80	-
Colitis-Free	4	0	M	74	Vemurafenib
Colitis-Free	5	0	F	72	-
Colitis-Free	6	0	M	68	-
Colitis-Free	7	0	F	66	-
Colitis-Free	8	0	M	70	-
Colitis-Free	9	0	F	73	Anti-gp75 monoclonal antibody IMC-20D7S; AZD6244; vemurafenib
Colitis-Free	10	0	F	61	*Vemurafenib
Colitis-Free	11	0	M	63	-
Colitis-Free	12	0	M	60	-
Colitis-Free	13	0	M	69	-
Colitis-Free	14	0	F	53	Vemurafenib
Colitis-Free	15	0	F	28	*Vemurafenib
Colitis-Free	16	0	M	85	-
Colitis-Free	17	0	F	67	-
Colitis-Free	18	0	M	63	Cisplatin + vinblastine + temozolomide
Colitis-Free	19	0	M	42	Nivolumab (in clinical trial)
Colitis-Free	20	0	F	65	Cisplatin + vinblastine + temozolomide + R04929097; vinblastine
Colitis-Free	21	0	M	62	-
Colitis-Free	22	0	M	68	Temozolomide
Colitis-Free	23	0	F	65	-
Colitis-Free	24	0	M	81	Temozolomide; AZD6224
Progressed to Colitis	25	2	M	76	Vaccine, GD2L-KLH with OPT-821
Progressed to Colitis	26	3	F	66	-
Progressed to Colitis	27	3	M	60	Adjuvant Interferon
Progressed to Colitis	28	4	M	53	-
Progressed to Colitis	29	3	M	53	Vemurafenib
Progressed to Colitis	30	1	F	59	Temozolomide
Progressed to Colitis	31	1	M	73	-
Progressed to Colitis	32	1	F	66	-
Progressed to Colitis	33	1	M	73	-
Progressed to Colitis	34	2	F	64	-

2.2.2. Composition of the intestinal microbiota prior to colitis.

In order to characterize the intestinal microbial composition prior to immune-mediated colitis, fecal samples were submitted for bacterial microbiota profiling using 16S rRNA sequencing on the Illumina MiSeq platform. C-F and PtC patients harbored intestinal microbiota with similarly complex microbial populations and shared 239 of 578 operational taxonomic units (OTUs, defined at a 97% sequence similarity) (**Fig. 2.1b**). These 239 shared OTUs represent 79% and 83% of the total OTU abundance in the C-F and PtC patient groups, respectively (**Fig. 2.1c,d**), and many were present in 5 or more patients (**Fig. 2.1d**). In contrast, OTUs that were either associated with only C-F or PtC patients were generally detected in fewer than 5 patients (**Fig. 1e**). The OTUs that are shared between the two patient groups are more evenly distributed. Roughly 20% of shared OTUs are found in over half of all patients (**Fig. 2.1e**). These differences in the distribution of OTUs among the patient groups did not significantly impact the overall biodiversity (**Fig. 2.2a,b**). Microbial richness, reflecting the number of unique phylotypes within a given sample, was found to be similar between patients who developed CTLA-4 blockade-induced colitis or remained colitis-free (**Fig. 2.2c,d**).

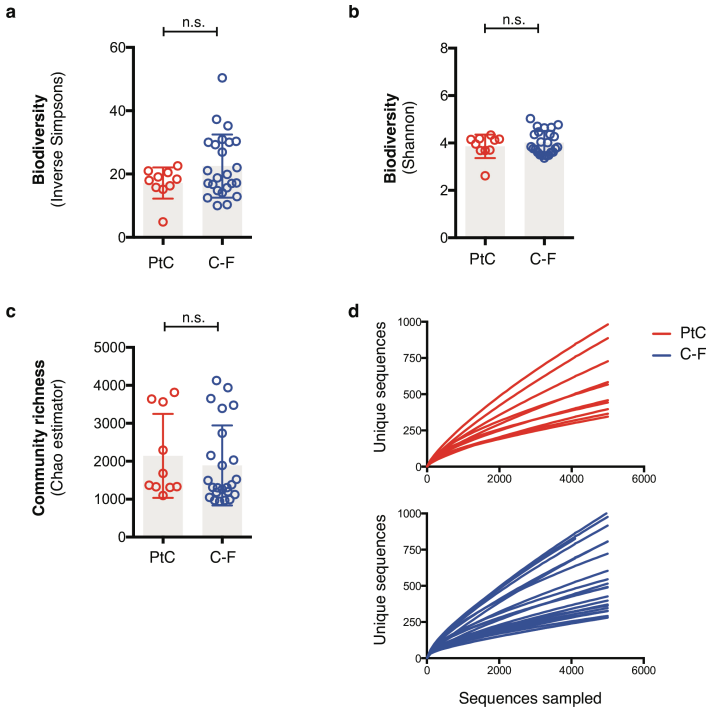

Figure 2.2 | Colitis-Free and Progressed to Colitis patients have similar levels of intestinal microbial diversity. Biodiversity is estimated by **a)** the Inverse Simpson index and **b)** the Shannon index for each patient sample. Richness is measured by **c)** the Chao estimator and **d)** rarefaction curves. Mann-Whitney tests were used to compare microbial diversity parameters between the patient groups. Height of bar represents the mean, error bars represent standard deviation. C-F, Colitis-Free; PtC, Progressed to Colitis. C-F patients, n=24; PtC patients, n=10. n.s., not significant.

To examine the intestinal microbiota structure between patient groups, we plotted the relative frequencies of bacterial phylotypes at the taxonomic level of family for each patient. Although C-F and PtC patients shared many bacterial taxa that belong to the Firmicutes phylum, C-F patients harbor a greater proportion of microbes within the Bacteroidaceae family (**Fig. 2.3a**). Our taxonomic classifications based on 16S sequencing data were similar to those found when applying MetaPhlAn to shotgun metagenomic sequencing data on a subset of this patient cohort, although the proportions of some bacterial phyla vary between the two methods (**Fig. 2.4**). To illustrate the microbiota composition with finer resolution, we plotted the relative abundances of 146 OTUs at 0.1% or greater mean abundance. While broad swaths of the microbiota are

found at similar frequencies between patients, microbes within the Bacteroidetes phylum are underrepresented in the patients who developed new-onset, immune-mediated colitis (**Fig. 2.3b**).

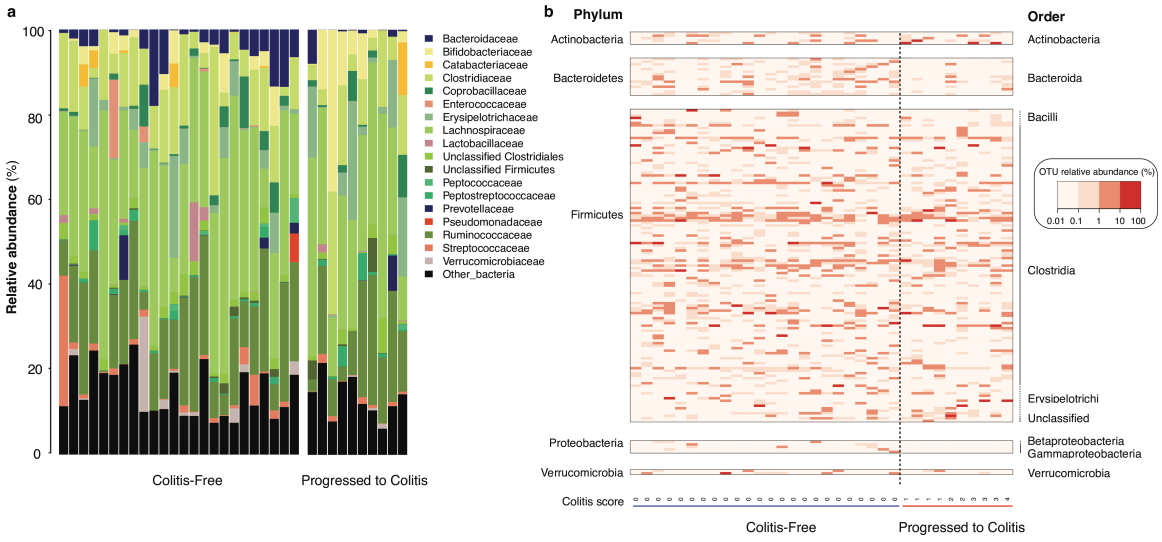

Figure 2.3 | Composition of the intestinal microbiota between C-F and PtC patients. a) OTUs with an average abundance >0.01% within either patient group were classified at the family taxonomic level. Families with an average abundance of 2.5% or maximum abundance of 5% are plotted. Each bar represents the fecal microbial composition of one patient. **b)** The relative abundances of the 146 bacterial OTUs in C-F and PtC patients represented in a heat map. OTUs plotted were present at a mean abundance of >0.1%. Patients are ordered by CTCAE-based colitis score. C-F patients, n=24; PtC patients, n=10. OTUs, operational taxonomic units. Actino, Actinobacteria; Bact, Bacteroidetes; Firm, Firmicutes; Proteo, Proteobacteria; Verr, Verrucomicrobia.

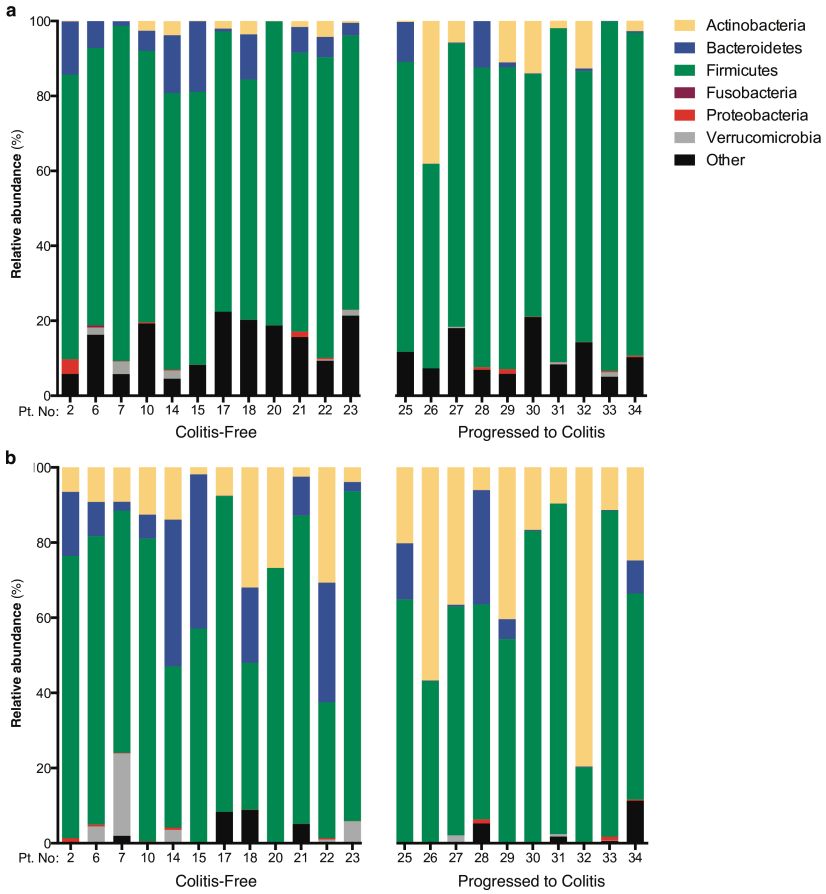

Figure 2.4 | Accuracy of bacterial taxonomic classification. a) 16s sequencing reads were clustered into OTUs by 97% sequencing homology. Relative abundances of OTUs that met our defined threshold (of an average abundance >0.01% in either patient group) were plotted by phylum. Bar plots were constructed only for those patients whose samples were subjected to shotgun metagenomic sequencing. **b)** Relative abundances of shotgun metagenomic sequencing reads were calculated using MetaPhlAn and plotted by phylum. OTUs, operational taxonomic units. C-F patients, n=12; PtC patients, n=10.

2.2.3. Members of Bacteroidetes phylum are associated with resistance.

To further explore the relationship between specific bacterial members of the intestinal microbiota and development of CTLA-4 blockade-induced colitis, we stratified patients by the severity of inflammation and performed a Spearman rank correlation test on the relative abundances of bacterial species grouped at different taxonomic levels. This analysis revealed that taxa within the Bacteroidetes phylum are more prevalent in C-F patient samples (**Fig. 2.5a**). The relative abundance of OTUs classified as Bacteroidetes, as well as the number of OTUs assigned to the phylum, were significantly higher in C-F

patients (Mann-Whitney test, p<0.05) (**Fig. 2.5b,c**). Within the Bacteroidetes phylum, the prevalence of Bacteroidaceae, Rikenellaceae, and Barnesiellaceae is significantly more abundant in patients resistant to Ipilimumab-induced colitis (Mann-Whitney test, p<0.01, p<0.05, p<0.05, respectively) (**Fig. 2.5d,e,f**). While the composition of the intestinal microbiota can vary over the lifetime of an individual, there was no association between patients' age and the abundance of Bacteroidetes (**Fig. 2.6**).

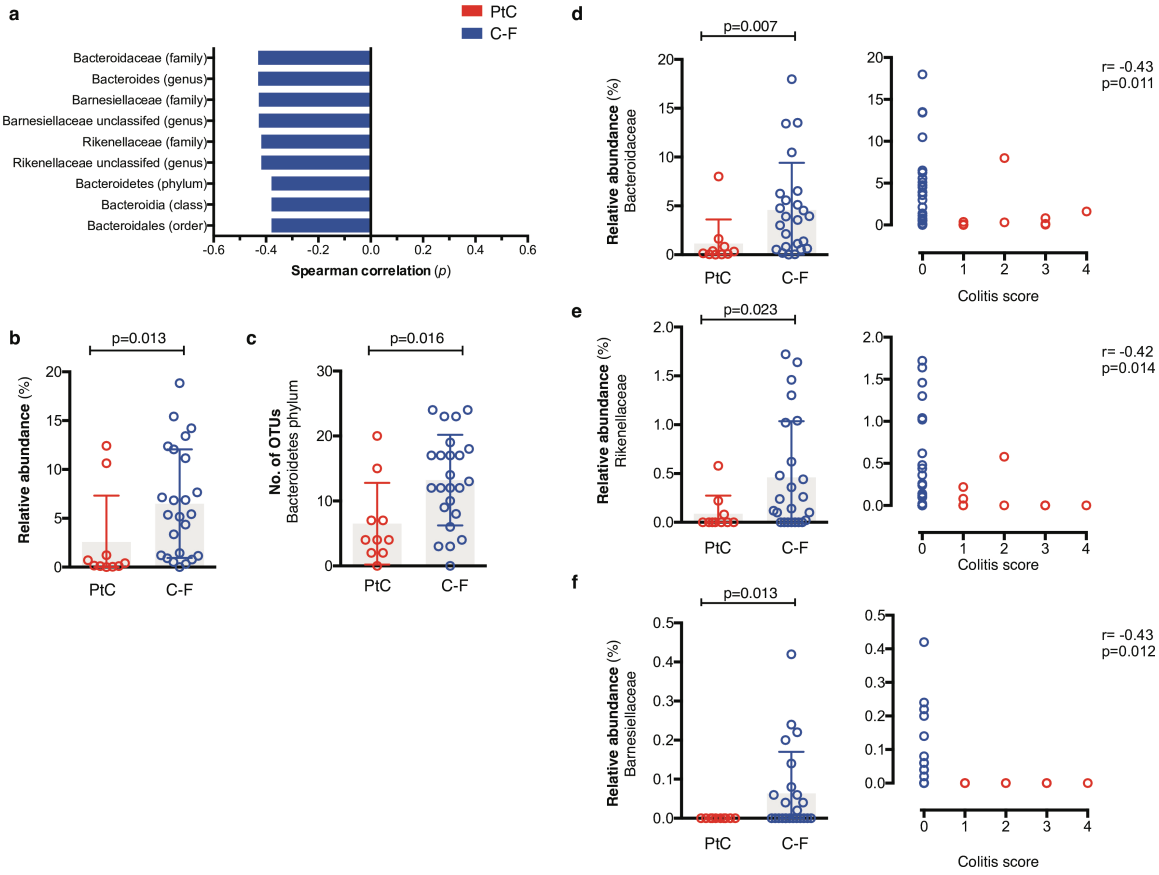

Figure 2.5 | Increased abundance of the Bacteroidetes phylum and select families correlates with protection from colitis. OTUs with an average abundance greater than 0.01% within either patient group were binned at different levels of taxonomic classification (phylum, class, order, family, genus). **a)** Correlation of bacterial phylotypes to CTCAE-based colitis score by Spearman analysis. Taxa with p-values <0.05 are plotted. **b)** Relative abundance of the phylum Bacteriodetes in PtC and C-F patients. **c)** The number of OTUs assigned to the Bacteroidetes phylum in each patient group. Relative abundances of the families **d)** Bacteroidaceae, **e)** Rikenellaceae, **f)** Barnesiellaceae within the Bacteroidetes phylum in PtC and C-F patients. P-values were determined by Mann-Whitney test. Height of bar represents the mean, error bars represent standard deviation. C-F patients, n=24; PtC patients, n=10. r, Rho coefficient; p, p-value; OTUs, Operational Taxonomic Units.

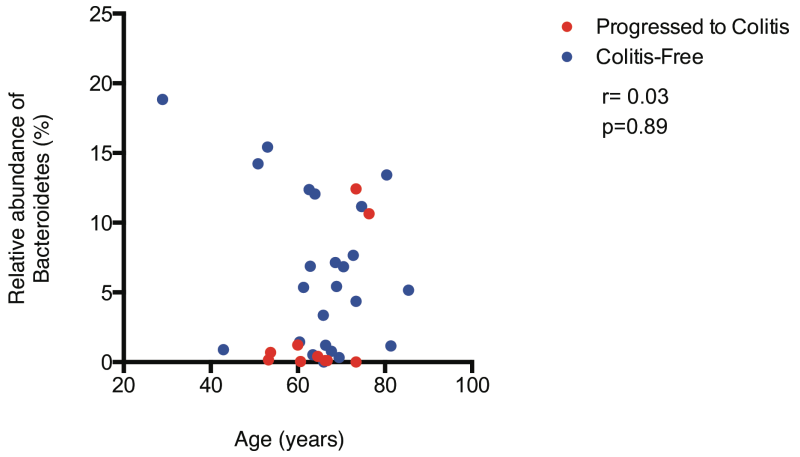

Figure 2.6 | Correlation between patient age and relative abundance of Bacteroidetes phylum. Patient age was defined as of the first dose of ipilimumab. OTUs with an average abundance >0.01% within either patient group were grouped by phylum. Spearman correlation test was performed on age and Bacterodietes abundance. r, Rho coefficient; *p*, p-value; OTUs, operational taxonomic units. C-F patients, n=24; PtC patients, n=10.

2.2.4. Specific microbial modules are associated with protection.

To evaluate the genetic pathways that may play a role in the development of immune-mediated colitis, we performed shotgun metagenomic sequencing on the 10 PtC and 12 C-F patient fecal samples. Sequencing reads were processed using HUMAnN and assigned to KEGG (Kyoto Encyclopedia of Genes and Genomes) modules. The microbial modules that comprised patients' intestinal microbiota were broadly similar between C-F and PtC patients (**Fig. 2.7a**). We conducted a univariate test for associations between colitis status and the 102 microbial modules using linear discriminant analysis effect size (LEfSe). We found that the spermidine/putrescine polyamine transport system and three modules involved in the biosynthesis of B vitamins (riboflavin (B2), pantothenate (B5) and thiamine (B1)) were more abundant in C-F patients (**Fig. 2.7b**). After stratifying samples by colitis status, Spearman analysis identified the polyamine transport system and thiamine (B1) modules as correlated with resistance to the development of colitis (**Fig. 2.7c**). The relative abundances of the aforementioned pathways are significantly

enriched in C-F patient samples (Mann-Whitney test, $p<0.05$ for all modules) (**Fig. 2.7d**). In addition, an additional module involved in the biosynthesis of the biotin (vitamin B7) was found in greater abundance in C-F patients (Mann-Whitney test, $p<0.05$).

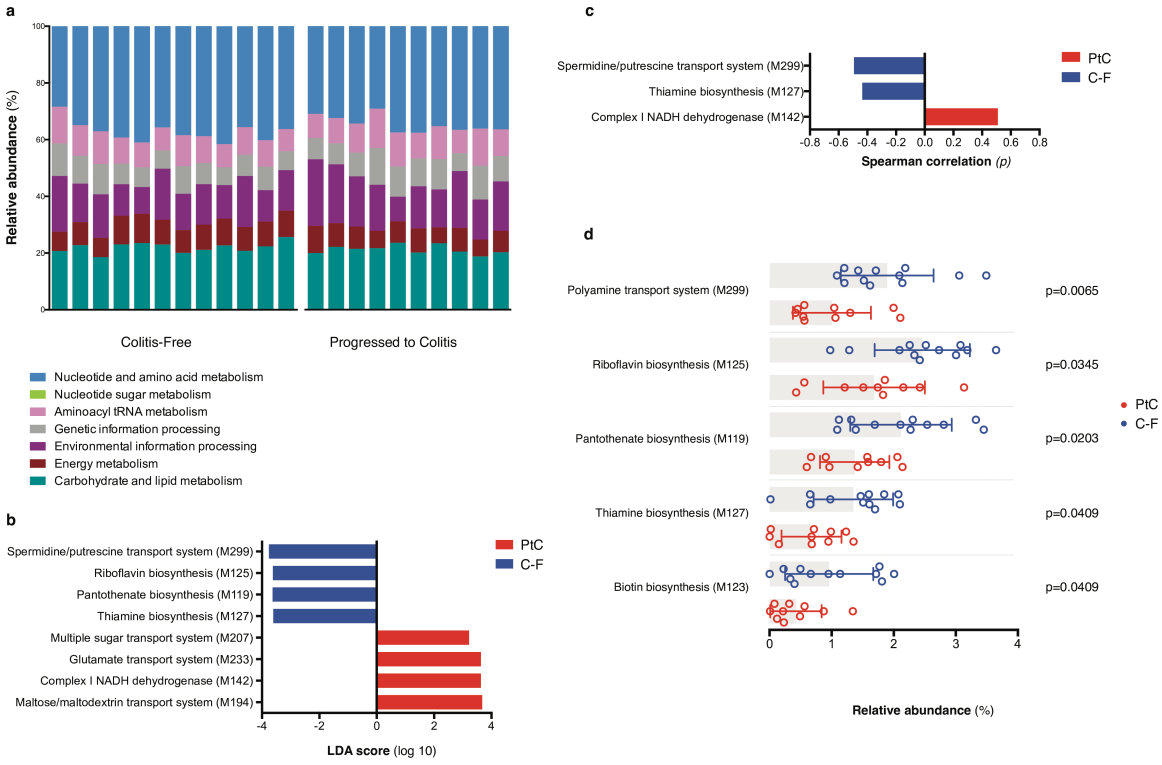

Figure 2.7 | Bacterial modules involved in polyamine transport and vitamin B synthesis are associated with resistance to colitis. a) Relative abundance of 102 microbial KEGG modules in C-F and PtC patients. **b)** Association of genetic modules with colitis status by linear discriminant analysis effect size (LEfSe) analysis. Modules with LDA score >3 are plotted. **c)** Correlation of genetic modules to colitis score by Spearman analysis. Modules with p-values <0.05 are plotted. d) Relative abundances of modules associated with C-F patients. P-values were determined by Mann-Whitney test. Height of bar represents mean, error bars represent standard deviation. C-F patients, n=12; PtC patients, n=10.

2.2.5. Select bacterial modules can identify colitis patients.

We next sought to assess the predictive accuracy of these microbial modules in determining a patient's risk for colitis. Utilizing the recursive partitioning machine-learning algorithm to form a classification tree based on the 102 modules, samples were

successfully classified as from either PtC or C-F patients using the relative abundance of polyamine transport system module alone (**Fig. 2.8a**). Samples with greater than 1% relative abundance of the polyamine transport system were binned as Colitis-Free (**Fig. 2.9)**. Of the PtC patients, 7 samples were appropriately identified while 3 samples were misclassified as C-F, resulting in a sensitivity of 70% and specificity of 100% (**Fig. 2.8a**). Performing a leave-one-out cross-validation of the probit regression analysis based on 4 of the modules associated with C-F patients, we correctly predicted the colitis status for 10 out of 12 C-F patients and 7 out of 10 PtC patients, at a probability threshold of 50% (**Fig. 2.8b)**. This model results in a sensitivity of 70% and specificity of 83%. For this regression analysis, we selected the 4 modules associated with resistance to colitis that were identified in the Spearman and LEfSe analyses, which include the polyamine transport system module and modules involved in the biosynthesis of vitamins riboflavin (B2), pantothenate (B5) and thiamine (B1). These modules performed better in combination than any individual module (**Fig. 2.8c)**. Taken together, our 4-module analysis predicts colitis risk with good accuracy as demonstrated by Receiver Operating Characteristic (ROC) curve, for which there are no other known biomarkers presented in the literature to use for comparison (**Fig. 2.8d)** (12, 15). In all, these analytical models identify bacterial pathways that may confer resistance to colitis and serve as biomarkers for patients at high risk of developing CTLA-4 blockade-induced colitis.

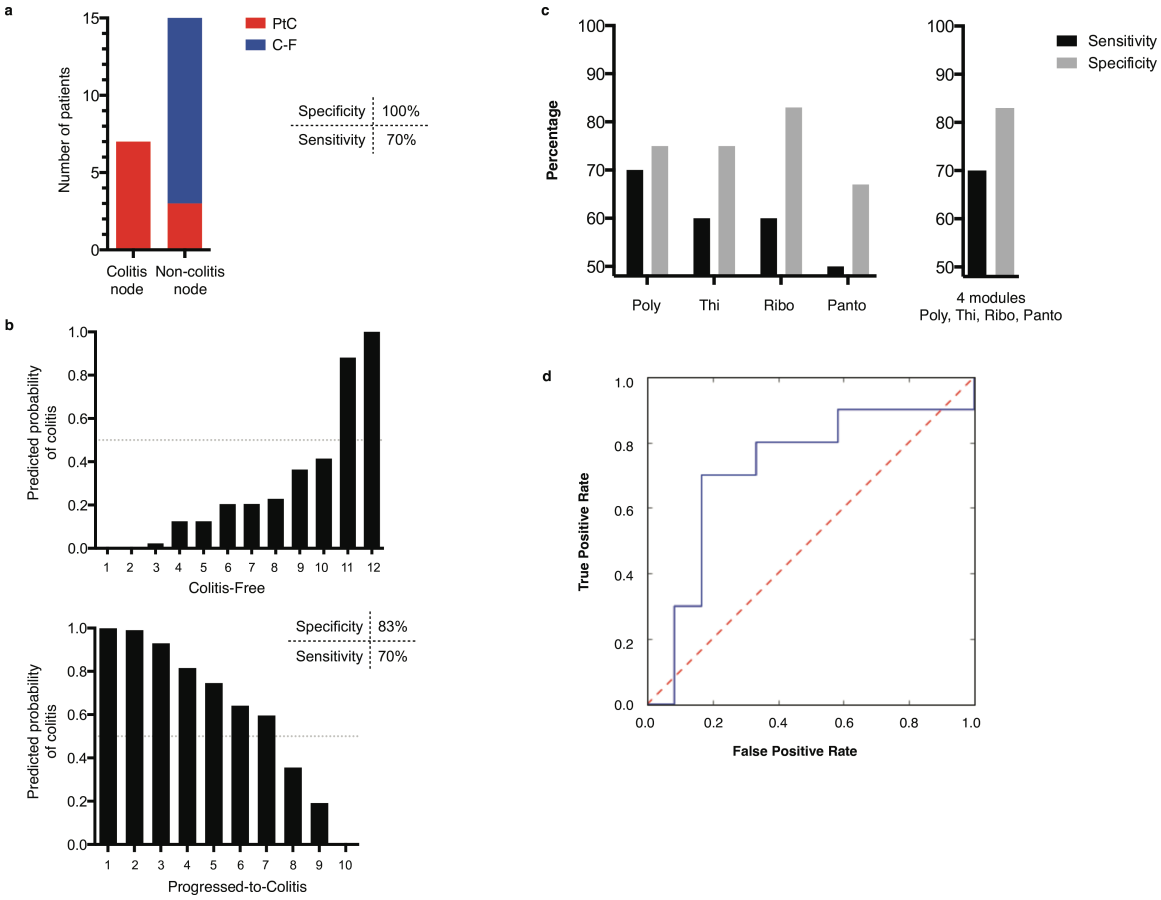

Figure 2.8 | Predictive accuracy of bacterial modules to identify patients who develop colitis. a) The recursive partitioning algorithm was utilized to construct a classification tree, based on the abundance of the polyamine transport module. **b)** Leave-one-out cross-validation of the probit regression analysis predicts the probability of colitis using four modules associated with colitis resistance: polyamine transport system, thiamine biosynthesis, riboflavin biosynthesis, and pantothenate biosynthesis. One patient is represented per column. Specificity and sensitivity calculated based on a probability threshold of 50%. **c)** The sensitivity and specificity of each module to predict patients' colitis status by their fecal microbial samples was determined using a probability threshold of 50%, as compared to the four-module model. **d)** Receiver Operating Characteristic (ROC) curve of the four-module model predicting colitis risk. ROC curve was created by calculating the True Positive Rate and False Positive Rate for 10,000 thresholds of the predicted probability of colitis between 0 and 1. True Positive Rate represents the test sensitivity, calculated by: True Positives / (True Positives + False Negatives). False Positive Rate, which is given by 1 minus the test specificity, is calculated by: False Positives / (False Positives + True Negatives). Poly, polyamine transport system; Thi, thiamine biosynthesis; Ribo, riboflavin biosynthesis; Panto, pantothenate biosynthesis. C-F patients, n=12; PtC patients, n=10.

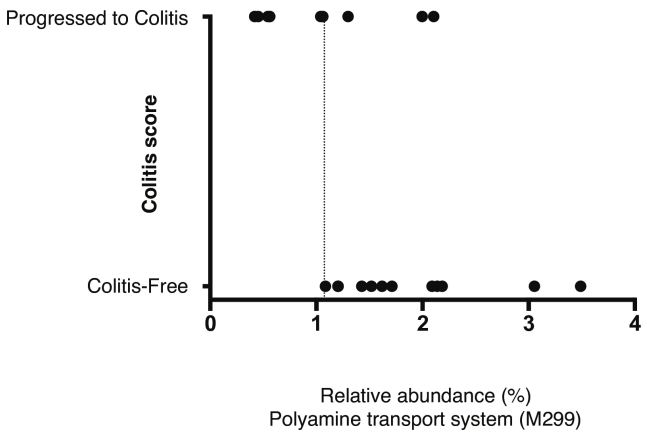

Figure 2.9 | Module abundance of the polyamine transport system. The recursive partitioning algorithm estimated colitis status of patient samples based on polyamine transport system abundance alone. Samples with a module abundance of >1% were classified as Colitis-Free by this algorithm. C-F patients, n=12; PtC patients, n=10.

2.4. DISCUSSION

Our study is the first to characterize the intestinal microbiota of patients before the development of intestinal inflammation and has identified microbiota-associated biomarkers that correlate with protection against CTLA-4 blockade-associated colitis. Our finding that members of the Bacteroidetes phylum are enriched in colitis-resistant patients is consistent with a proposed immunomodulatory role of these commensal bacteria. Bacteroidetes represents one of the major phyla of the human colonic microbiota and its members can limit inflammation by stimulating T-regulatory cell differentiation (82,83). Following the publication of our work, a second group independently verified our finding that higher abundances of Bacteroidetes prior to ipilimumab treatment are associated with lower risk of colitis in a French cohort of metastatic melanoma patients (99).

In addition, we show that the presence of microbiota-associated modules for bacterial polyamine transport system and the biosynthesis of thiamine, riboflavin and pantothenate

can accurately assess a patient's risk of developing colitis following CTLA-4 blockade. The microbiota plays an important role in the endogenous synthesis of water-soluble B vitamins and amines which can contribute to mucosal tolerance (100-102). Thiamine and riboflavin concentrations are significantly reduced in the blood of patients with Crohn's disease and the levels of bound pantothenate in the colonic mucosa decrease with the progression of inflammatory bowel disease (1003,104). An innate-like T-cell population known as mucosal-associated invariant T cells are activated in vitro by riboflavin metabolites (105,106). These cells accumulate in the inflamed mucosa of Crohn's Disease patients, although it is not yet known if their IL-17-skewed cytokine expression exacerbates or limits inflammation. Polyamines, which are small cationic amines that can be exported from bacteria cells through the spermidine and putrescine transport system (potA, B, C, and D), play an anti-inflammatory role by promoting colonic epithelial cell (CEC) proliferation to maintain the epithelial barrier (107). In patients with active colitis, levels of orthinine decarboxylase (ODC), the enzyme involved in polyamine synthesis, are lower than in control patients, but it remains unclear whether reduced polyamine levels contribute to colitis development or progression (108,109). Additional studies are required to further explore whether a reduced capacity for microbe-mediated production of B vitamins and polyamine transport lowers the threshold for initiation of immune-mediated colitis.

As with treatment efficacy, the microbiota may play a role in the development of immune-mediated, new-onset colitis in the context of other immunotherapies. Identification of biomarkers that predict the risk of developing colitis may help identify patients that are particularly susceptible to distinct forms of immunotherapy-induced inflammation, such as with CTLA-4 blockade, and may facilitate preemptive treatments.

2.4. METHODS

2.4.1. Study patients and specimen collection. 34 adults analyzed in our study were diagnosed with metastatic melanoma and received ipilimumab at Memorial Sloan-Kettering Cancer Center (MSKCC). Subjects had no previous history of colitis and bowel resection and had not received antibiotic treatment in the preceding 2 months. Patients were excluded from analysis if the first fecal sample was collected after the onset of colitis, if the patient did not receive ipilimumab, or if colitis status was unknown. Ipilimumab monotherapy was administered at a dose of 3mg/kg every 3 weeks for up to 4 doses, with three exceptions. Patients #10 and #15 received vemurafenib before and during ipilimumab treatment as part of a clinical trial. Patient #13 was part of a blinded clinical trial and received ipilimumab at either 3 mg/kg or 10 mg/kg. A small number of patients (Progressed to Colitis, n=2; Colitis-Free, n=3) received additional doses of ipilimumab either as part of maintenance treatment (every 3 months) on a clinical study or as part of a second course of ipilimumab; however, the colitis cases documented here occurred before this additional dosing was administered. Systemic cancer treatment administered prior to (n=14) or both before and during (n=2) ipilimumab therapy was determined retrospectively upon chart review by a single investigator (MKC). For 30 patients, fecal samples were collected from each participant prior to the first administration of ipilimumab; for 2 patients who developed gastrointestinal inflammation and 2 patients who remained inflammation free, samples were collected after the initiation of CTLA-4 blockade, but before onset of colitis. Toxicities were graded retrospectively by a single investigator (MKC) based upon chart review using CTCAE, version 4.0 and grading on the terms diarrhea and colitis. Patients were assigned a colitis score based upon the following: no diarrhea (score 0), grade 1 diarrhea (score 1), grade 2 diarrhea (score 2), grade 2 diarrhea and/or grade 2 colitis (all 3 cases had both grade 2 diarrhea and grade 2 colitis) (score 3), grade 3 diarrhea and/or grade 3 colitis (1 case with both grade 3 diarrhea and grade 3 colitis) (score 4). All participants provided written

consent for specimen collection and analysis under the study protocol approved by the MSKCC Institutional Review Board.

2.4.2. DNA extraction. Each fecal sample was immediately snap-frozen at -80C and subsequently subjected to bead beating and phenol chloroform extraction for DNA purification. Samples were resuspended in 500 µl of an extraction buffer (200 mM Tris, pH 8.0/200 mM NaCl/20 mM EDTA), 200 µl of 20% SDS, 500 µl of phenol:chloroform:isoamyl alcohol (24:24:1), and 500 µl of 0.1-mm diameter zirconia/ silica beads (BioSpec Products). For 2 min, cells were lysed by mechanical disruption using a bead beater. DNA was extracted in a phenol/chloroform/isoamyl solution twice and precipitated with ethanol and sodium acetate. DNA was resuspended in 200 µl of TE buffer containing 100ug/ml RNase and further purified using QIAmp Mini Spin Columns (Qiagen). After eluting the sample in 100 µl of distilled water, double-stranded DNA was quantified.

2.4.3. 16S rRNA gene amplification and multiparallel sequencing. The V4-V5 region of the 16S rRNA gene was amplified and sequenced on the llumina MiSeq platform. For each fecal sample, replicate PCR reactions were performed using modified universal bacterial primers designed to amplify the V4-V5 16S rRNA region: 563F (59-nnnnnnnn-NNNNNNNNNNN-AYTGGGYDTAAAGN G-39) and 926R (59- nnnnnnnn-NNNNNNNNNNN-CCGTCAATTYHTTTR AGT-39). Each reaction contained 50 ng of purified DNA, 0.2 mM dNTPs, 1.5 uM MgCl2, 1.25 U Platinum TaqDNA poly-merase, 2.5 µl of 10x PCR buffer, and 0.2 µM of each primer. A unique 12-base Golay barcode (Ns) preceded the primers for sample identification after pooling amplicons. One to eight additional nucleotides were added before the barcode to offset the sequencing of the primers. Cycling conditions were the following: 94 °C for 3 min, followed by 27 cycles of 94 °C for 50 sec, 51 °C for 30 sec, and 72 °C for 1 min, where the final

elongation step was performed at 72 °C for 5 min. Replicate PCRs were combined and were subsequently purified using the Qiaquick PCR Purification Kit (Qiagen) and Qiagen MinElute PCR Purification Kit. Using the Illumina TruSeq Sample Preparation procedure, PCR products were quantified and pooled at equimolar amounts before Illumina barcodes and adaptors were ligated on. The completed library was sequenced on an Ilumina Miseq platform according to the Illumina recommended protocol.

2.4.4. Sequence analysis. Sequences were analyzed using mothur version 1.31.1. Sequences were aligned using the Silva reference alignment as a template and potentially chimeric sequences were eliminated using the UChime algorithm. 5000 sequences per patient were selected (mean, 4974; SD, 150) and sequences with a distance-based similarity of 97% or greater were grouped into operational taxonomic units (OTUs) using the furthest-neighbor algorithm. OTUs were classified using the Greengenes 16S rRNA reference database. OTU-based microbial diversity was estimated by calculating two diversity indexes, Shannon and Inverse Simpson. OTU-based richness was determined by calculating the Chao richness estimate and constructing rarefaction curves. OTUs were grouped at different levels of classification (phylum, class, order, family, genus); at each level, OTUs that did not have a classification were grouped together by the highest available resolution (e.g. at the genus level, an OTU classified as p__Bacteroidetes_c__Bacteroidia_ o__Bacteroidales_ f__Barnesiellaceae_unclassifed will be grouped as f__Barnesiellaceae_unclassifed). Feature selection of the intestinal microbia's composition was performed on OTUs with an average abundance greater than 0.01% in either patient group and grouped by phylotype.

2.4.5. Shotgun sequencing and metabolic pathway reconstruction. Stool samples from all 10 Progressed to Colitis (PtC) patients and 12 Colitis-Free (C-F) patients were subjected to shotgun sequencing. C-F patient samples were chosen so that the full

spectrum of Bacteroidetes phylum abundance was represented. Libraries were constructed with Illumina barcodes from the TruSeq DNA Sample Prep kit (Illumina) and reagents from KAPA Library Preparation kit (Kapa Biosystems), and then sequenced on an Illumina MiSeq platform using 2 × 250 nucleotide paired-end sequencing, according to the manufacturer's instructions. Sequencing reads were converted into relative abundances of microbial metabolic modules using HUMAnN, the Human Microbiome Project metabolic reconstruction pipeline, and mapped to the Kyoto Encyclopedia of Genes and Genomes (KEGG). Relative species abundances were calculated by the MetaPhlAn pipeline.

2.4.6. Statistics. Statistical analyses of intestinal microbiota samples were performed using R Statistical Language (v3.1.1) and GraphPad Prism (version 6.0e) software packages. Unpaired Mann-Whitney rank sum test (two-tailed) was used for comparisons of continuous variables between two groups. Bar plots were used to represent the data's mean at the center values, with error bars to indicate standard deviation. Spearman rank correlation tests (two-tailed) were used to find significant correlations between two continuous variables. Linear discriminant analysis effect size (LEfSe) was used to identify differentially abundant features between classes of samples. Recursive partitioning to form classification trees was performed in R using the packages rpart. Generalized linear model (using probit regression and the glm R-function) was constructed on all combinations of the following five modules associated with Colitis-Free patients: Polyamine transport system (M299), Riboflavin biosynthesis (M125), Pantothenate biosynthesis (M119), Thiamine biosynthesis (M127) and Biotin biosynthesis (M123). Leave-one-out cross-validation was used to compute model sensitivity and specificity. The reported model provided the best total sensitivity plus specificity. Unadjusted p-values less than 0.05 were considered to be significant for the Mann-Whitney rank sum test and Spearman rank correlation tests.

CHAPTER THREE

MICROBIOTA-MEDIATED PROTECTION AGAINST THE ANTIBIOTIC-RESISTANT GRAM-NEGATIVE PATHOGEN KLEBSIELLA PNEUMONIAE

3.1. INTRODUCTION

The rise of antibiotic resistance among bacterial pathogens poses a serious health threat (14,110,111). The decreasing number of effective antibiotic treatment options has limited our ability to control bacterial infections (112). Members of the family Enterobacteriaceae, such as *Klebsiella pneumoniae*, are among the most concerning pathogens, as a growing number produce extended spectrum β-lactamase (ESBLs) (113-116). ESBL-producers cause an estimated 26,000 infections and 1,700 deaths annually and are inhibited only by the carbapenem family of antimicrobials (117). As resistant infections require more expensive treatments and longer hospital stays, the total economic burden of antibiotic resistance exceeds $20 billion (117,118). This clinical picture necessitates the development of novel approaches to treat infectious disease. Fortunately, the commensal microbes that colonize the human gut are capable of preventing infection caused by antibiotic-resistant pathogens (119). Adoptively transferring commensal populations into susceptible hosts offers a promising alternative to antimicrobial treatment. However, we have limited knowledge of the precise microbial populations that are required to inhibit intestinal colonization by antibiotic-resistant proteobacteria.

Here, we sought to determine which intestinal bacteria provide resistance to the antibiotic-resistant gram-negative *K. pneumoniae* (Kp). We first treated mice with different classes of antibiotics to differentially deplete microbial communities from the

GI tract. Ampicillin had the longest-lived impact on susceptibility to Kp. The loss of Clostridia class members was correlated with higher Kp density. Colonization resistance was restored when reconstituting mice with bacteria cultured anaerobically from donors with ampicillin-resistant microbiota (ARM). *In vitro* studies demonstrate that only anaerobic bacteria limit Kp growth from ampicillin-sensitive microbiota donors. A consortium of human-derived anaerobes, largely of clostridial strains, can resolve Kp colonization by 2-4 logs. A human-derived isolate of *Blautia producta* prevents Kp growth *ex vivo* through acetate production. Further work in the Pamer lab has characterized this finding of short-chain fatty acid-induced Kp inhibition *in vivo*. A second commensal was found, *Klebsiella oxytoca*, that alone could resolve Kp infection in our mouse model, mediated through cell contact. Using statistical models, we found that certain clostridial OTUs can help predict if Kp colonization resolves over time.

3.2. RESULTS

3.2.1 Antibiotics abrogate colonization resistance to low inoculating doses of *K. pneumoniae.*

Two experimental designs were employed to investigate the role of the intestinal microbiota in resolving and preventing Kp colonization (**Fig. 3.1a,b**). 8-10 week-old naïve C57BL/6 mice were treated with oral ampicillin (0.5 g/L) for 3 days and then orally challenged with an ampicillin- and carbapenem-resistant Kp bloodstream isolate that belongs to the ST258 clade (120) (**Fig. 3.1a**). We hereby refer to our antibiotic resistant isolate as AR-Kp. To first test if the intestinal microbiota is required for colonization resistance, antibiotic-treated or untreated mice were inoculated with 10^5 CFU of AR-Kp by oral gavage. Treatment with ampicillin renders mice highly susceptible to AR-Kp (**Fig. 3.1c**). Intestinal expansion is achieved as early as 12 hours post-inoculation (**Fig. 3.1d**). Once colonized, AR-Kp dominates the intestinal tract for up to four weeks even in the absence of continued oral antibiotic treatment (**Fig. 3.1e**). Patients who become

dominated with AR-Kp are either asymptomatic carriers or acquired it from the hospital setting, likely in low numbers from hands of medical staff or surfaces. We therefore tested the limiting inoculum dose of AR-Kp that results in high intestinal AR-Kp density. AR-Kp expands to a large bacterial load in the GI tract after transferring as few as 10 CFUs (**Fig. 3.1f**). For future experiments, 100 CFUs was chosen as our inoculating dose. These data indicate that the ampicillin-sensitive component of the intestinal flora is necessary and sufficient for providing colonization resistance to small inocula.

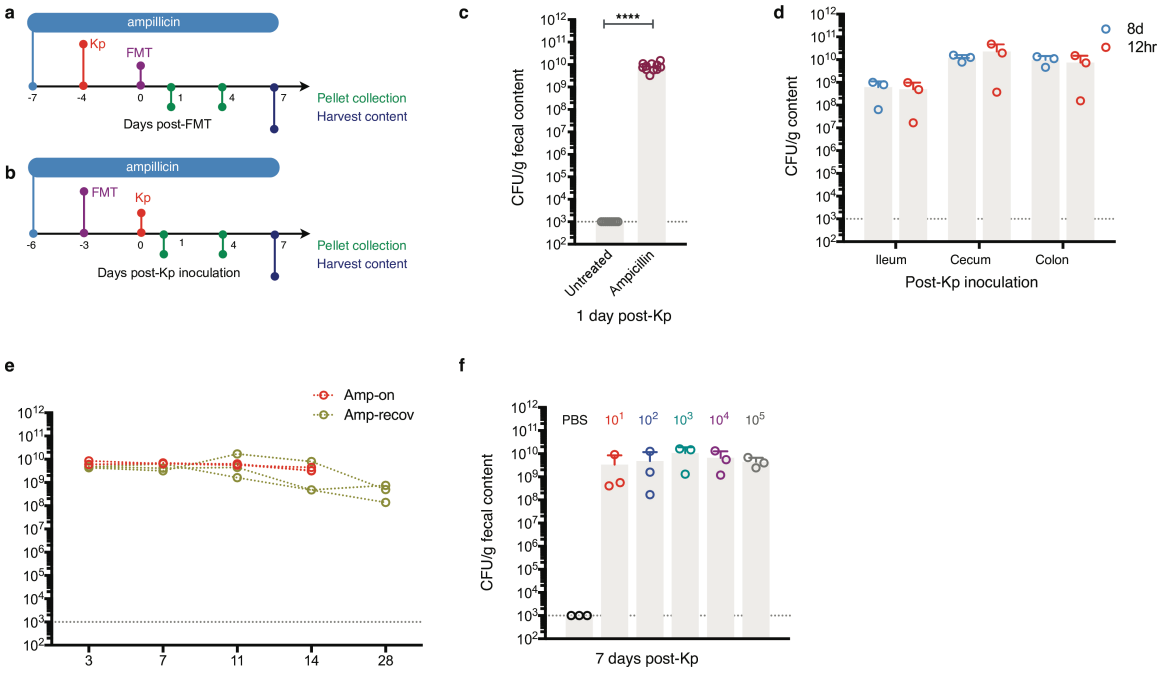

Figure 3.1 | Antibiotics disrupt colonization resistance to low-dose inocula of *K. pneumoniae*. a) Schematic for experiments that test the resolution of AR-Kp colonization. Mice were treated with ampicillin 0.5g/L in the drinking water for 3 days, then challenged with AR-Kp (100 CFU/ms unless otherwise noted) in 200ul/ms. Mice received a fecal microbiota transplant (FMT) 4 days after Kp challenge. If FMT consisted of ampicillin-sensitive bacteria, mice were taken off ampicillin following Kp inoculation. **b)** Schematic for experiments that test the prevention of AR-Kp colonization. Mice were pretreated with ampicillin for 3 days as stated in (a). If the FMT was ampicillin-resistant, mice were gavaged 3 days after antibiotic initiation. If the FMT was ampicillin-sensitive, an additional 4 rest days were given between antibiotic cessation and before FMT reconstitution. **c)** Untreated mice received no antibiotics; those on ampicillin were treated for 3 days. Results are compiled from 2 experiments. **d)** Mice were sacrificed either 12 hours or 8 days after ampicillin administration and CFUs per gram of intestinal content were measured by growing PBS-resuspended content on LB plates with 100ug/ml of carbenicillin and 50ug/ml neomycin; n=3 per group. **e)** After a 3-day treatment with ampicillin, mice were either continually treated with antibiotics (amp-on) or allowed to recover with untreated water (amp-recov); n=3 per group. **f)** Kp was grown to mid-log stage and serially diluted. Mice were orally gavaged at the indicated Kp dose in 200ul. ****, p<0.00001.

3.2.2. Fecal microbiota transplants (FMT) restore colonization resistance to *K. pneumoniae*.

To determine whether the reconstitution of a diverse intestinal flora restores colonization resistance, complex colonic ampicillin-resistant microbiota (ARM) was adoptively transferred to antibiotic-treated mice 3 days prior to AR-Kp inoculation (**Fig. 3.1a**). ARM was derived from a strain of immunocompromised mice in the Pamer lab colony that has been treated with amoxicillin for over 10 years. This strategy allows for continuous antibiotic treatment without any negative interactions between the antibiotics and microbioa. PBS was administered as an FMT control. ARM-recipient mice are fully protected from AR-Kp colonization (**Fig. 3.2a**). To determine whether transplantation of complex flora eliminates AR-Kp from the GI tract (**Fig. 3.1b**), ARM was orally gavaged into antibiotic-treated mice that have been colonized for 4 days with AR-Kp. After 4 weeks, ARM-recipients had nearly a five-log reduction in AR-Kp burden (**Fig. 3.2b**).

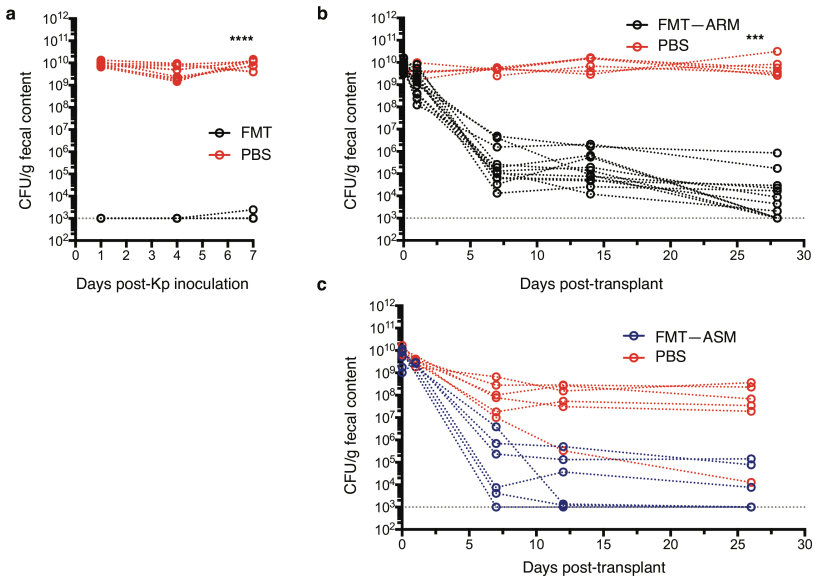

Figure 3.2 | Adoptive transfer of fecal microbiota restores colonization resistance to *K. pneumonaie* that was lost after antibiotic treatment. a) Kp density in fecal content (CFU/g) in mice that received an FMT or mock treatment (PBS) prior to challenge (100 CFUs). Results are compiled from 4 experiments. Kp density in mice that received an FMT or mock treatment (PBS) before Kp challenge (100 CFUs); in **b**), FMT was ampicillin-resistant (ARM); in **c)**, FMT was ampicillin-sensitive (ASM). Results are compiled from 2 experiments for b and c. $p<0.0001$, ****, $p<0.00001$.

Previous work in the Pamer lab has compared the composition of ARM maintained in our MyD88-/- mouse colony to naïve C57BL/6 mice and noted distinct though overlapping bacterial communities (30). We therefore tested the efficacy of an FMT from ampicillin-sensitive microbiota (ASM) derived from age-matched naïve C57BL/6 mice. For such experiments, we removed ampicillin pressure following AR-Kp inoculation. The kinetics of AR-Kp resolution were similar between the two FMT donors as both partially eliminate AR-Kp from the gut by day 7 (**Fig. 3.2c**). Taken together, these data indicate that intestinal microbiota protects against gram-negative colonization and restores resistance following fecal bacteriotherapy from unique donors.

3.2.3. Different classes of antibiotics induce distinct alternations to the intestinal microbiota composition that have lasting consequences for *K. pneumoniae* susceptibility.

Antimicrobials disrupt the intestinal microbiota in distinct ways by acting on different bacterial targets. The resulting changes to the microbiota's composition leaves patients at variable risk for AR-Kp expansion. We characterized the effect of short-term antibiotic treatment on the susceptibility to AR-Kp colonization. Mice were treated for 3 days with either ampicillin (**Fig. 3.3a**), metronidazole (**Fig. 3.3b**), or vancomycin (**Fig. 3.3c**) in the drinking water. Clindamycin was administered once via intraperitoneal injection (**Fig. 3.3d**). The microbiota was left to recover prior to AR-Kp challenge for various number of days post antibiotic cessation (indicated on the x-axis). Ampicillin had the most profound change, attenuating colonization resistance for up to 14 days. A similar long-lived effect was seen in clindamycin, a broad-spectrum antibiotic active against obligate anaerobes, but only in one mouse tested. Metronidazole and vancomycin had brief effects in our hands, although work from other Pamer lab members has shown AR-Kp susceptibility for longer durations with vancomycin (121). Given that ampicillin treatment resulted in the

most variance in resistance recovery, we compared the structure of the microbiota's composition prior to AR-Kp challenge from one experiment depicted in Fig. 3a. OTUs were grouped at the genus level and those genera with a mean abundance of >1% were plotted. The loss of Clostridium genus is associated with increased AR-Kp susceptibility (**Fig. 3.3e**). 3 of the 4 operational taxonomic units (OTUs) negatively correlated with AR-Kp levels by spearman were assigned to the Clostridium disporicum species ($\rho < -0.7$). Thus antibiotic-induced shifts in commensal microbial populations correspond to variable recovery of resistance.

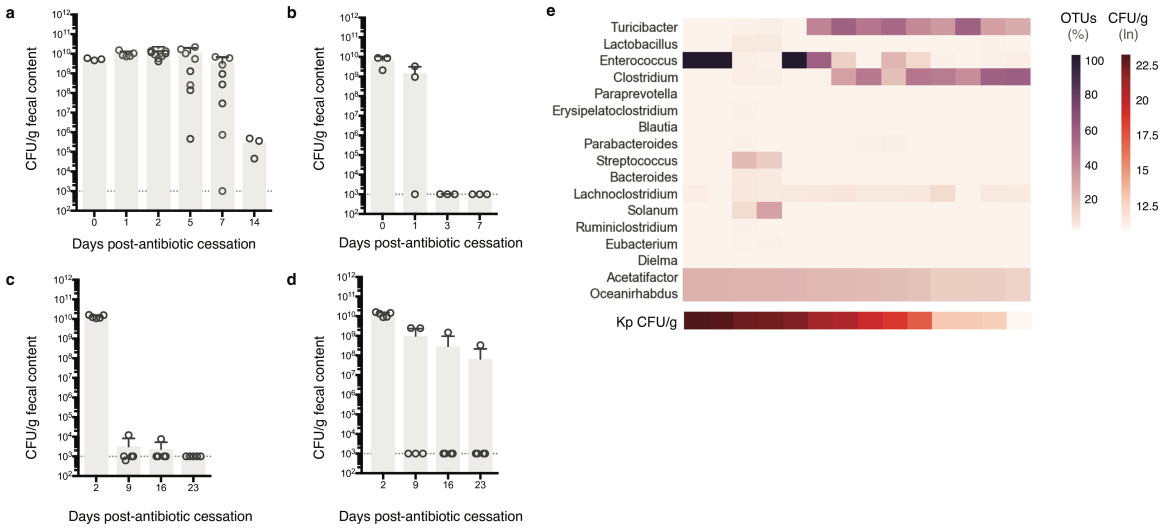

Figure 3.3 | Differential impact of antibiotics on intestinal *K. pneumonaie* susceptibility. Mice were treated with the indicated antibiotics for 3 days: **a)** ampicillin at 0.5g/L, **b)** metronidazole at 1g/L, and **c)** vancomycin at 0.5h/L. Results in a) are compiled from two experiments. **d)** Clindamycin was administered in one 200 µg dose via intraperitoneal injection. Mice were challenged with 100 Kp CFUs by oral gavage on the indicated days after antibiotic cessation. Kp burden was measured by plating fecal content collected 24 hours after challenge. **e)** OTUs on the day prior to Kp inoculation are plotted in mice that had been allowed to recover following ampicillin administration. OTUs with >10 reads total and an average relative abundance >0.02% (across multiple experiments) were binned at the genus level and genera with a mean >1% were plotted. Kp density in CFU/g content was measured 24hrs after challenge, and samples are ordered in the heatmap by Kp burden (converted to natural log). OTUs, operational taxonomic units.

3.2.4. Obligate anaerobes protect against intestinal *K. pneumoniae* infection.

In an alternative approach to determining which subsets of the complex intestinal microbiota are required for resistance, colonic ARM was cultured on blood-agar plates at 37 C in either aerobic or anaerobic conditions for 3 days. Colonies were resuspended in sterile PBS and transplanted into antibiotic-treated mice. A single transfer of the anaerobic and aerobic fraction of ARM protected against AR-Kp challenge (**Fig. 3.4a**). A complementary experiment was performed *ex vivo* by culturing AR-Kp in ASM cecal content anaerobically and aerobically. Only anaerobes prevented AR-Kp growth (**Fig. 3.4b**). We therefore focused on adoptively transferring smaller fractions of the anaerobic microbiota. We performed serial dilutions of anerobically-grown ARM as our bacterial consortium transplant (BCT) inoculum. We transferred roughly 1000, 100 and 10 isolates at 10^{-5}, 10^{-6}, 10^{-7} dilutions respectively. The 2 higher dilutions conferred a 3-4 log reduction in AR-Kp colonization, while the lowest failed to protect (**Fig. 3.4c**). These data suggested that a discrete set of bacterial species could recover colonization resistance via BCT. We then turned to a human-derived 17-strain collection of anaerobic Clostridia species (122,123). We spiked roughly 10^8 CFUs of midlog cultures of selected Clostridia isolates into antibiotic-treated cecal content with 100 CFU of AR-Kp. After 24-hr *ex vivo* co-culture, one isolate in our screen, *Blautia producta*, inhibited AR-Kp growth nearly as well as untreated cecal content (**Fig. 3.4d**).

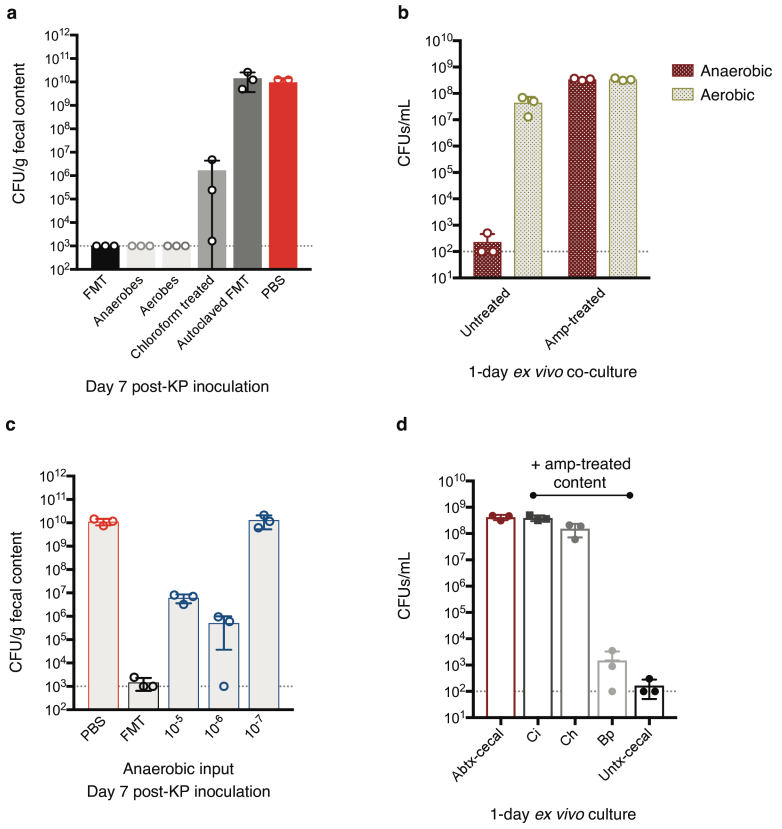

Figure 3.4 | Obligate anaerobes *in vivo* and *ex vivo* inhibit *K. pneumoniae* growth. a) Fecal pellets from an ARM donor were resuspended in either normal or reduced PBS to roughly 50mg/ml and cultured on blood agar plates (BAPs) for 3 days at 37C in either aerobic or anaerobic conditions, respectively. In a third condition, the resuspended content was treated in 3% solution of chloroform at 225 rpm for 1 hour and then plated on reduced BAPs. Bacterial lawns were collected by scraping each BAP and resuspended in PBS. Bacterial solutions were transplanted at 200ul per mouse. On the day of transplant, additional ARM pellets were resuspended in PBS – one aliquot of the fecal suspension was kept on ice as an FMT control, a second aliquot was autoclaved for 30min. n=3 mice per group. **b)** Cecal content from untreated and 3-day ampicillin-treated mice were resuspended in PBS to roughly 250mg/ml and 200ul/ well was added in a 96-well plate. 100 Kp CFUs were co-cultured per well (20ul). **c)** Fecal pellets were harvested as described in (a) and were serially plated on reduced BAPs. Indicated dilutions were transplanted in 200ul into pretreated mice that then received a 100-CFU Kp challenge. n=3 mice per group. **d)** 10^8 CFUs of anaerobic strains in midlog cultures were added to wells (100ul) with ~250mg/ml antibiotic-treated cecal content (100ul) and co-cultured with 100 Kp CFUs (20ul). *Ex vivo* conditions were cultured in triplicates. Ci, Clostridium indolis; Ch, Clostridium hathewayi; Bp, Blautia producta.

3.2.5. Short-chain fatty acids suppresses *K. pneumoniae* growth.

Over 10^7 CFU of *Blautia producta* is required to fully suppress AR-Kp growth *in vitro* (**Fig. 3.5a**). To determine if this inhibition was mediated by cell contact or a bacterial product, we grew AR-Kp in filtered culture media from an overnight culture of Blautia

producta (Bp-FCM). Bp-FCM inhibited AR-Kp growth, however this affect was diluted when adding more media than a 5:1 ratio of Bp-FCM to BHI (**Fig. 3.5b**). Bp-FCM is acidic at a pH 5.2. Reducing the neutral pH of BHI to 5.2 with HCl did not inhibit AR-Kp growth *in vitro* (**Fig. 3.5c**). Thus, the acidic environment of the Bp-FCM alone does not suppress AR-Kp. Normalizing the Bp-FCM pH to 7 with NaHCO3, however, abrogated its inhibitory effect (**Fig. 3.5c**). This pH-dependent growth inhibition suggested that *Blautia producta* operates through a weak acidic metabolite such as short-chain fatty acids. Of the isolates in the 17-strain collection, *Blautia producta* was the highest acetate producer (123). We found that 25mM of acetic acid impacts AR-Kp growth to the same degree as the Bp-FCM (**Fig. 3.5d**). This concentration is in range with the 50-100 mM physiological levels of total SCFAs in the colonic lumen of patients and rodents, with 60:20:20 ratio of acetate, butyrate, priopionate (124,125). We further demonstrated that the acetic acid, and not the anion acetate, mediates this suppression. Holding the concentration of acetate constant at 100mM, we changed the pH and thus acetic acid levels. A drop from 36mM to 5.75mM of acetic acid abolished its inhibitory effect (**Fig. 3.5e**). This finding fits with our knowledge that acetic acid in its protonated form can cross the hydrophobic cell membrane and then dissociate to drop the intracellular pH (61). Glycine was not able to rescue acetate-induced growth inhibition (5-50mM tested; data not shown). Additional work in the Pamer lab has extended this finding *in vivo* to show that ~20mM of commensal-derived acetate inhibits AR-Kp growth in the GI tract.

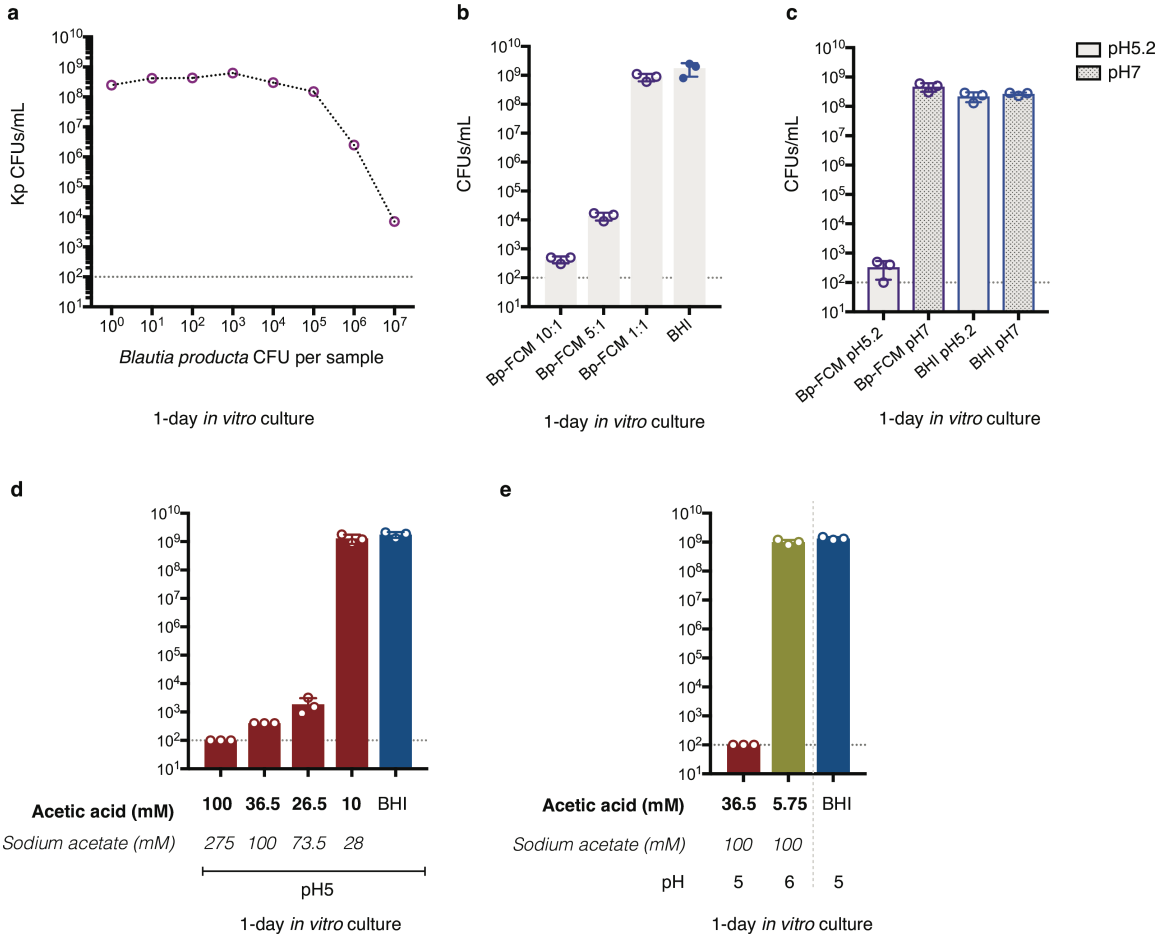

Figure 3.5 | *Blautia producta* suppresses *K. pneumoniae* growth *in vitro* through a metabolite that operates by a pH-dependent mechanism. a) A midlog culture of *Blautia producta* (5x10^8 CFU/ml) was serially diluted and co-cultured with 100 Kp CFUs in vitro (50ul of BHI in 220ul total). Filtered culture media (FCM) was obtained by filtering 4ml of an overnight midlog Blautia producta culture at 0.22um. BHI media was added to Bp-FCM at the ratios indicated in **b)** and in 10:1 (FCM:BHI) in **c)**. In both b) and c), the BHI control is 1:10 media in PBS; total volume is 200ul/well. 100 Kp CFUs was cultured in the indicated concentrations of acetic acid/acetate (mM) in **d)** and **e)** with BHI in 2ml total.

3.2.6. *Klebisella oxytoca*, a member of the enteric microbiota, inhibits *K. pneumoniae* colonization through a cell contact-mediated mechanism.

In our fractionation experiments, we found that the aerobic compartment of the ARM, but not ASM, could prevent AR-Kp colonization *in vivo*. Dilutions as low as 10^{-5} of ARM, which resulted in transplanting aerobic 14 colonies, rescued resistance post-antibiotic treatment *in vivo* (**Fig. 3.6a**). By Sanger-sequencing the full-length 16S rRNA gene, we

identified 13 isolates as *Enterococcus casseliflavus* and 1 that belonged to the Klebsiella genus, *K. oxytoca*. 2x10^8 CFUs of bacteria in total was adoptively transferred into ampicillin-treated mice for three inocula: the 13 *E. casseliflavus* isolates, 1 *K. oxytoca* strain or the 14 isolates together. Only the groups that received the *K. oxytoca* isolate resisted AR-Kp challenge (**Fig. 3.6b**). *In vivo* and *in vitro*, 10^8 CFUs of *K. oxytoca* inhibited AR-Kp growth (**Fig. 3.6c**). As with *Blautia producta*, we tested if this Klebsiella strain produced a metabolite that had inhibitory effect. AR-Kp grew as well in LB as *K. oxytoca*-FCM, even without the addition of fresh media (**Fig. 3.6d**). Thus, *K. oxytoca* does not deplete AR-Kp of its essential nutrients, making *in vivo* nutrient competition a less likely mechanism. Taken together, these data indicate that K. oxytoca suppresses AR-Kp growth in cell-contact dependent manner.

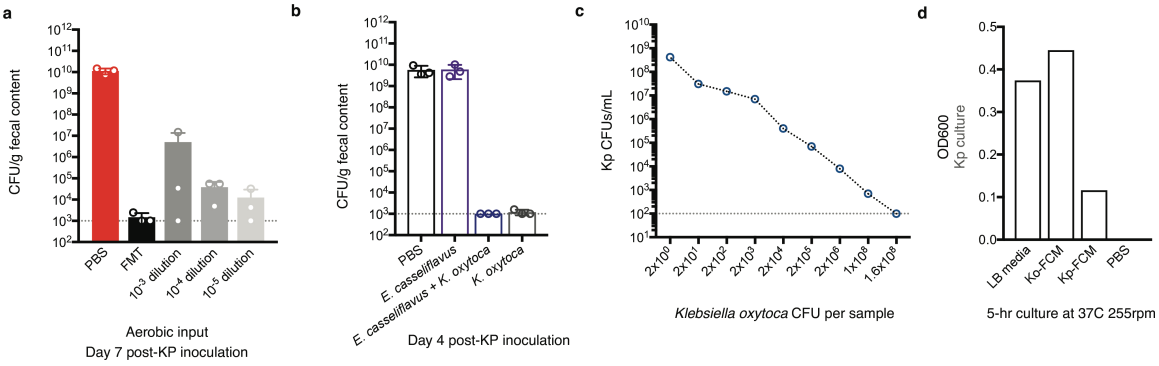

Figure 3.6 | A related species *Klebisella oxytoca* can eradicate *K. pneumoniae* from the GI tract. a) Fecal pellets were harvested from an ARM donor and were serially plated on BAPs grown at 37C aerobically. Indicated dilutions were transplanted in 200ul into pretreated mice, which then received a 100 Kp CFU challenge. n=3 mice per group. **b)** 14 aerobic strains were cultured in 6ml BHI for 5.5hrs to roughly 10^9 CFU/ml. 2x10^8 CFUs in 200ul per BCT were adoptively transferred to pretreated mice. **c)** A midlog culture of *K. oxytoca* (2x10^9 CFU/ml) was serially diluted and co-cultured with 100 Kp CFUs in vitro (50ul of BHI in 200ul total). **d)** 4ml of midlog cultures of either Kp or *K. oxytoca* were filtered at 0.22um. 100 CFUs of Kp was added to the 2ml of Kp-FCM and Ko-FCM and grown for 5hrs at 37C at 255rpm.

3.2.7. Clostridial species are associated with the prevention of *K. pneumoniae* colonization.

To identify commensals correlated with prevention of AR-Kp colonization, the intestinal microbiota of a total 318 mice were perturbed prior to AR-Kp challenge using a variety of experimental protocols, such as multi-drug antibiotic cocktails and different antibiotic doses with or without bacterial reconstitution. The heatmap depicts OTU relative abundances over time for these mice (**Fig. 3.7a**). The samples are ranked according to AR-Kp burden measured by the next sample collected for the same mouse, between 1-7 days later.

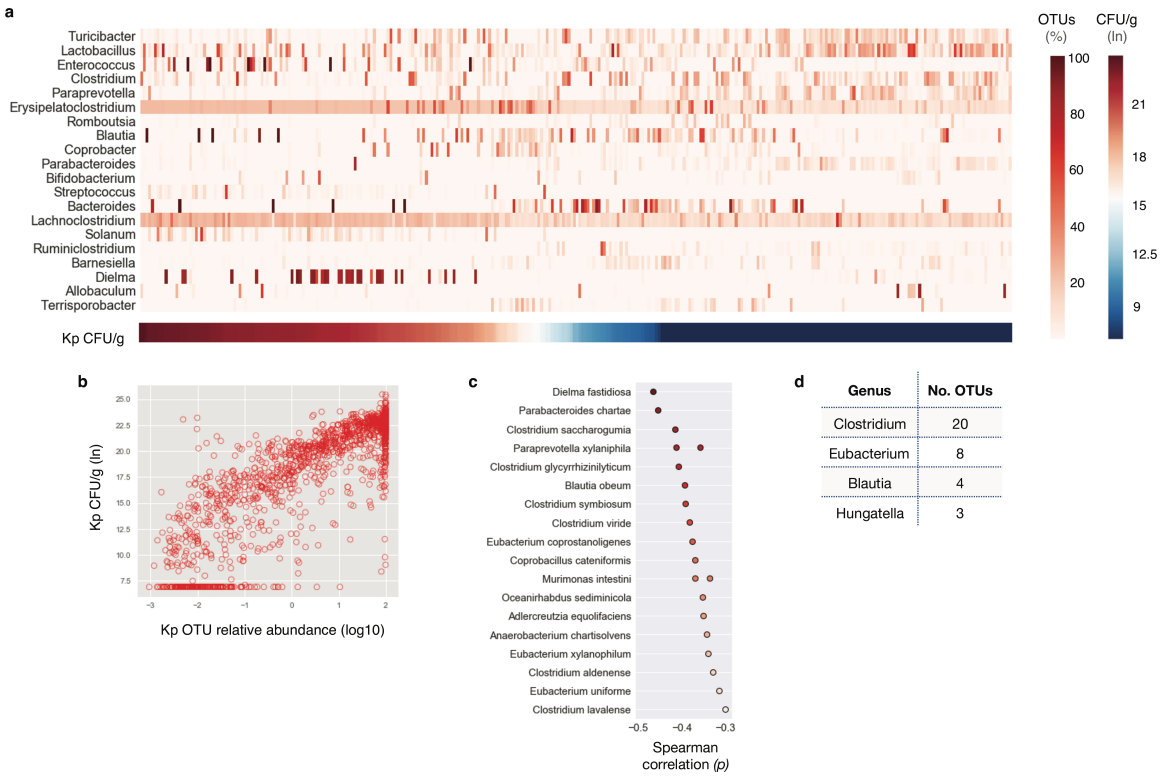

Figure 3.7 | Members of the Clostridia class are correlated with colonization resistance. A heatmap of 16S sequencing samples from mice (n=318) from prevention experiments. **a)** OTUs were grouped at the genus level, and samples were ordered by the Kp burden measured at the following timepoint (converted to natural log). Each column represents a mouse. Mice are ordered by Kp density 1-7days post-challenge. **b)** 16S relative abundances of the major OTU classified as *Klebsiella pneumonaie* is plotted against the Kp density within the same sample, measured in over 2000 samples across 24 experiments. **c)** The 20 of the most negatively correlated OTUs (/66 OTUs total) in the spearman analysis, with correlation of <-0.3, are plotted. **d)** Genera with 3 or more OTUs found significant in the spearman analysis are represented in the table.

The relative abundance of the major OTU classified as *K. pneumoniae* correlates well with the AR-Kp levels measured within that same sample, indicating that OTU relative abundances accurately reflect bacterial density in our experiments (**Fig. 3.7b**). Performing a spearman analysis on this dataset, we found 66 OTUs that were significantly negatively correlated with AR-Kp density (**Fig. 3.7c**). We grouped all significant OTUs at the genus level and found that Clostridium species were the most represented, with 20 OTUs (30%) assigned to the genus. Our data demonstrates that higher abundances of clostridial commensals are strongly correlated with suppressed growth states of AR-Kp *in vivo.*

3.2.8. Clostridial commensals are correlated with the rescue of colonization resistance.

We then asked if resolving high-density Klebsiella colonization requires a different, precise set of commensals that can flourish despite AR-Kp overgrowth. To address this, we first performed a series of resolution experiments (**Fig. 3.1b**) to test the reproducibility of our ASM-FMT findings with other *K. pneumoniae* strains. Using our MH258 AR-Kp strain as a control, we found similar kinetics of elimination with other carpanenamase-producing (CP) strains (**Fig. 3.8a**) and non-CP Kp isolates (**Fig. 3.8b**) of *K. pneumoniae*. We then transplanted the 17-strain human-derived Clostridia consortium into MH258 Kp-colonized mice, using *Lactobacillus johnonsii* as a BCT control. Although the dynamics were slowed, 2 out of the 4 Clostridia-only recipients eliminated AR-Kp as well as an FMT (**Fig. 3.8c**). We tested *K. oxytoca*'s capacity to resolve AR-Kp from the GI tract. While also delayed, the *K. oxytoca*-transferred mice has reached similar low densities of AR-Kp as the FMT recipients by day 28 (**Fig. 3.8d**).

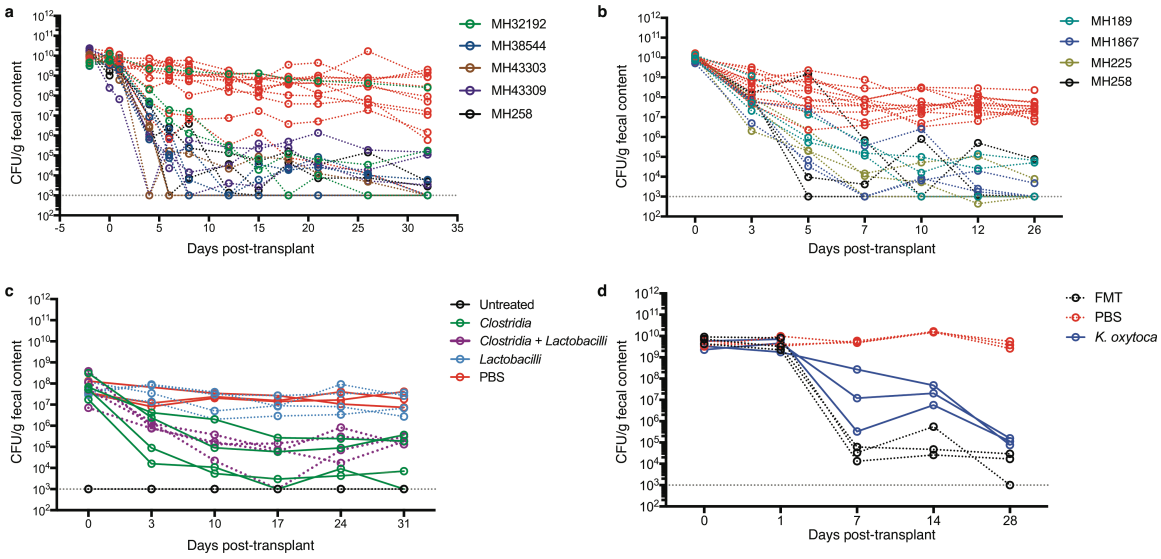

Figure 3.8 | The kinetics of *K. pneumoniae* clearance from the intestine. FMTs derived from ASM donors were transplanted into antibiotic-treated mice pre-colonized with either **a)** carpanenamase-producing (CP) or **b)** non-carpanenamase-producing (non-CP) strains. MLST, wzi and K typing for these isolates are provided in the Methods. 1 FMT dose was administered. **c)** 1-10x10^7 CFUs in total of 17 clostridial strains were adoptively transferred into Kp-colonized mice in 1 dose. 2x10^6 CFUs of lactobacillus johnsonii served as a BCT control. n=3-4 mice per group. **d)** Roughly 10^8 CFUs of K. oxytoca were gavaged into Kp-colonized mice. n=3 mice per group. Kp burden was monitored by plating fecal pellets on the indicated days post-transplant.

Using this 16S sequencing data, we leveraged the time-series nature of these resolution experiments and built models to determine which bacteria at earlier timepoints were predictive of AR-Kp density on the final experimental day (our target variable). In order to include 96 mice across 5 experiments in the same model, we grouped samples at a range of timepoints: i) day 0, ii) days 1-3 and ii) days 5-10 days relative to transplant (**Fig. 3.9a**). Since the mice had been pre-colonized with Klebsiella, we could measure AR-Kp levels (CFU/g) in each sample, which we multiplied by the relative abundance of the Kp OTU to determine the total bacterial density per sample. We then calculated absolute abundance of each OTU in the same sample, which we used in our model instead of relative abundances. The independent variables used were therefore the absolute abundances of OTUs on days prior to the last experiment timepoint (e.g. OTU1_day0, OTU1_day1, OTU2_day0, OTU2_day1). Given the smaller number of

observations (i.e. mice) relative the large extent of features (i.e. OTU absolute abundances per day), we performed 10-fold cross-validation to minimize overfitting. Lasso regression and random forest classification algorithms were employed. For the random forest model, mice were assigned to 1 of 3 groups based on their last measured AR-Kp density using k-means clustering (k=3). 3 clusters were selected by visually examining the AR-Kp CFU/g distribution. OTUs that were kept in the models were ranked by either their coefficient (lasso regression) or feature importance (random forest); all OTUs that remained in the models were considered significant.

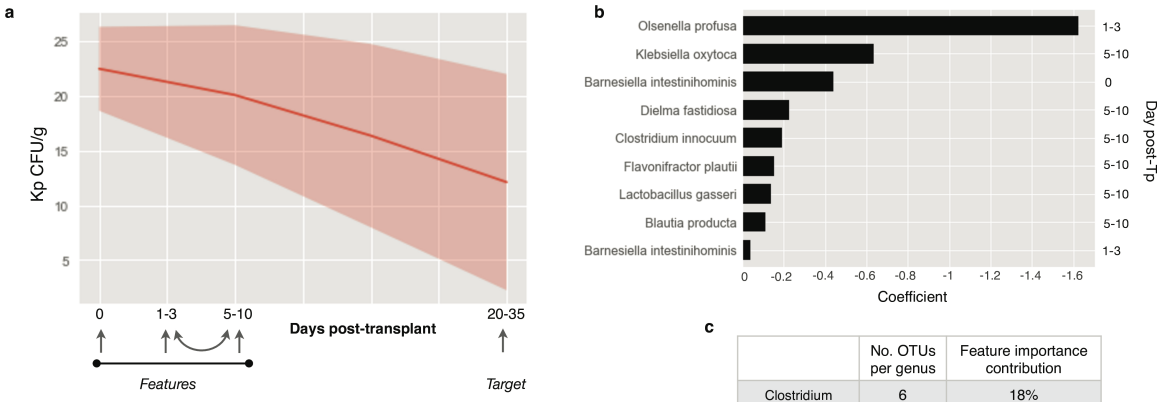

c

	No. OTUs per genus	Feature importance contribution
Clostridium	6	18%
Hungatella	3	9%
Parabacteroides	2	5%

Figure 3.9 | Select bacterial species are predicted to resolve *K. pneumoniae* infection. a) Mice (n=96) from 5 experiments were pre-colonized with Kp and transplanted with an FMT or bacterial consortium. The red line indicates the median Kp CFU/g while the shaded area represents 2 STDs. The absolute abundances of OTUs on days 0, 1-3 and 5-10 were used as independent features in our models (b, c). **b)** Significant features in lasso regression are plotted with respect to their coefficients. The right side of the figure indicates the day post-transplant that a given feature was significant at. **c)** OTUs that were significant in the random forest model were grouped at the genus level. Genera with 2 or more OTUs assigned are shown.

The density of AR-Kp in 96 reconstituted mice is plotted over time (**Fig. 3.9a**). The lasso regression analysis identified *K. oxtyoca* and *Blautia producta* as OTUs strongly associated with Kp clearance, complementing our *in vitro* experiments (**Fig. 3.9b**). The

most significant predictor of AR-Kp density, *Olsenella profusa*, could be detected by 1-3 days post-reconstitution. In the random forest model, 27 OTUs were important predictors, of which 6 were clostridial OTUs (*Clostridium scindens*, *lavalense*, *innocuum* and *algidixylanolyticum*), making the Clostridium genus the most represented. The Clostridium genus contributed 18% to the total feature importance of the random forest model.

3.2.9. Obligate anaerobes are predictive of changes in intestinal *K. pneumoniae* colonization density in allo-HSCT patients.

Allo-HSCT patients experience large shifts in their microbiota composition due to frequent antibiotic therapy given their immunocompromised status. Stool samples were collected over the course of their hospitalization and stored in a fecal biobank. The majority of patients had no detectable levels of Kp by 16S rRNA sequencing (**Fig. 3.10a**). Most patient samples were acquired within 7 days of each other, allowing us to characterize short-term compositional dynamics (**Fig. 3.10b**). Most patients did not experience large shifts in rate of Kp (**Fig. 3.10c**). A PCA on the first sample per patient collected did not reveal obvious groupings of patients susceptible to high density Kp colonization (**Fig. 3.10d**). We therefore applied our time-series random forest model to identify intestinal bacterial species that may be implicated in Kp resistance in human hosts. The log change in Kp levels per day between pairs of consecutive patient samples collected in a 7-day or shorter timeframe were used as our dependent variable. Target variables were binned into 2 levels for the random forest classifier and coded 1 if there was a ≥0 log change between samples per day and a 0 was assigned to targets with <0 log change. The model's features were the relative abundances of OTUs measured on the first sample of the pair. The model determined that the initial levels of Kp as well as Clostridia, Blautia producta, and Faecalibacterium prausnitzii were important predictors of the change in intestinal Kp density seen in allo-HSCT patients (**Fig. 3.10e**).

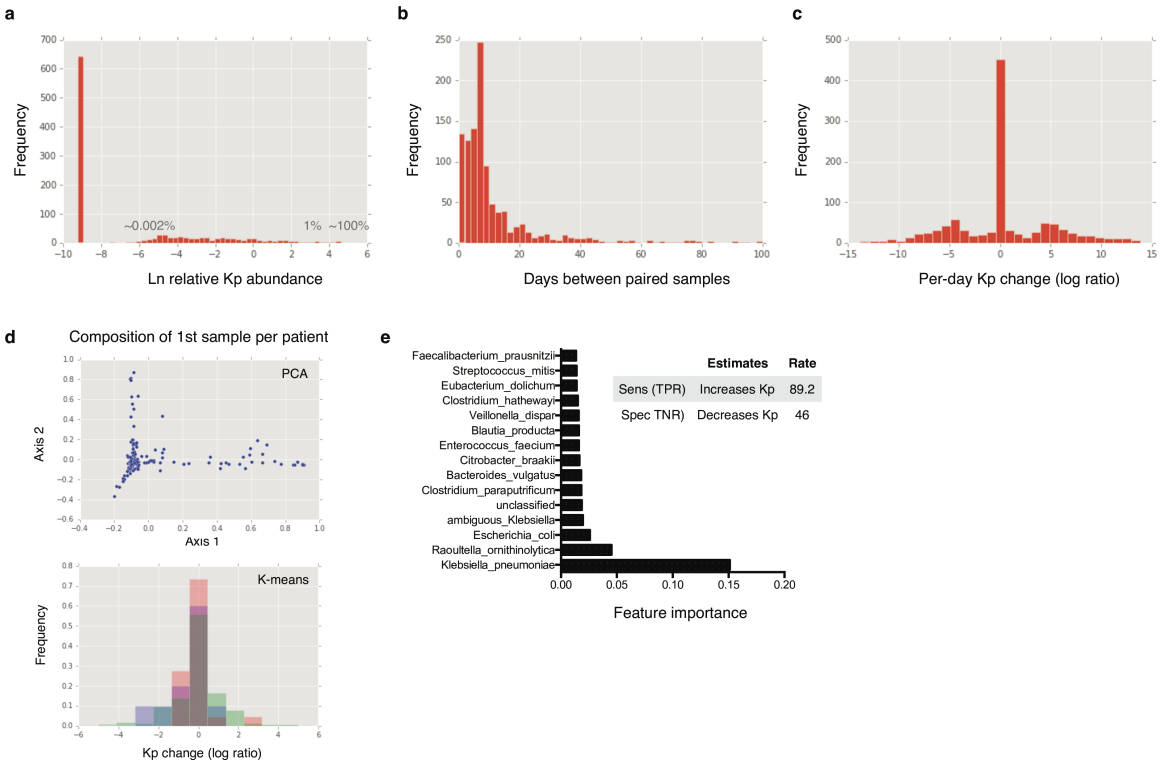

Figure 3.10 | Modeling Kp resolution in allo-HSCT patients. Paired samples (n=650) taken from allo-HSCT patients were compared. **a)** The distribution of Kp relative abundances in 389 allo-HSCT patients was plotted in natural log. **b)** The days between all possible pairs of samples are shown. Paired samples used in the model had to be collected within <7 days of each other. **c)** The relative abundances of OTUs from the earlier sample were used as features to predict the log Kp change per day (target variable). The distribution of the log change in Kp per day is plotted. **d)** PCA was performed on the first sample from each patient. 3 clusters were detected. The distribution of the log change in Kp (relative to the second sample from each patient) were broken down by the 3 clusters (k-means clustering, n=3). **e)** A random forest model was constructed using the OTU relative abundances on the first sample of the pair to predict the level of Kp log change. Target variables were binned into 2 levels for the classifier and coded 1 if 0 log change between samples per day (a 0 was assigned to targets with <0 log change).

3.3. DISCUSSION.

Microbiome research utilizes deep 16S rRNA gene sequencing to profile bacterial communities of the gut and to predict candidate commensals that confer colonization resistance in time-series microbiota-reconstitution experiments. Ecological modeling of the microbiota using 16S sequencing data has accurately predicted fluctuations in the

composition of the microbiota following clindamycin administration and *C. difficile* challenge, and identified commensal bacteria that could inhibit *C. difficile* colonization (72,126). Here, we employed high throughput sequencing and *in vivo* adoptive transfer experiments to demonstrate the efficacy of bacteriotherapy in clearing intestinal K. pneumonaie colonization and to correlate obligate anaerobic commensals from the Clostridia class with resistance.

How these findings are best translated to treating at-risk patients has yet to be determined. In a promising phase 1b trial, orally administered capsules of 50 human-derived live *Firmicutes* spores prevented recurrent *C. difficile* infection, while the phase II clinical study found no efficacy (127,128). A key question facing the translation of optimal bacterial combinations into patient therapy is what is required for a high transplantation efficacy. The study that defined a minimal consortium for VRE in mice highlights this challenge (30). Successful colonization of *B. producta* in ampicillin-treated mice required the adoptive transfer of three additional commensals. *B. sartorii* and *P. distasonis* inactivate ampicillin through the production of beta-lactamase, which was critical for ampicillin-sensitive isolates' survival in the GI tract, while *C. bolteae* supported *B. producta*'s engraftment through an unknown mechanism (30). Modulating the local gut environment through drug inactivation with probiotics is of particular importance for preventing VRE colonization in patients currently receiving antibiotics (129). Probiotic commensals can limit pathogen colonization in the gut by mitigating the disruptive effects of antibiotics to begin with. A *Bacteroides thetaiotaomicron* strain that produces a cephalosporinase has been shown to prevent intestinal VRE outgrowth by inactivating ceftriaxone and thus minimizing any significant changes to the microbiota (130). Further work is therefore required to identify the precise combination of isolates using *in vivo* mouse models that can successfully engraft and broadly confer resistance to *K. pneumoniae*-infected hosts.

Another open question is whether a protective microbial consortium should be tailored to individual patients, and if so, how to scale such a design. Given the falling costs of deep sequencing, profiling patients' microbiota may occur regularly in clinical practice. Patients with different degrees of immune system impairment and treatment histories may benefit from personalized alterations to the minimally defined protective consortium. For example, patients who recently received antibiotics may be deficient in nutrients that resistance-mediating bacteria require to survive in the gut, necessitating additional isolates to support successful engraftment. Mouse models would not be a scalable approach to test these individual modifications. In this era of deep sequencing, we can potentially integrate diet, treatment regimens, and gut microbiome data to build algorithms that can assess a patient's risk of colonization by antibiotic-resistant pathogens and can optimize probiotic combinations. Incorporating information on microbiome composition and function improved predictions of individuals' glycemic response following a meal and helped design dietary interventions for better glycemic control (131). Such data-driven approaches may help tailor preclinical findings to individual patients at scale to successfully mitigate their susceptibility to pathogen colonization.

3.4. MATERIALS AND METHODS.

3.4.1. Mouse husbandry and *in vivo* challenge experiments. *in vivo* experiments were performed in compliance with Memorial Sloan Kettering's institutional guidelines and were approved by its Institutional Animal Care and Use Committee. 8-10 week old wild-type female C57BL/6 mice were purchased from the Jackson Laboratories and housed in sterile cages with irradiated feed and acidified water. Mice were treated with ampicillin 0.5g/L in the drinking water for 3 days before Kp challenge and were singly housed at the time of inoculation. Kp density was quantified by resuspending fecal pellets in 1ml PBS

and plating serial dilutions on Luria-Bertani (LB) agar plates supplemented with 50 μg/ml neomycin (Sigma-Aldrich) and 100 μg/ml carbenicillin (LabScientific). Plates were incubated aerobically for at 37°C. Mice were maintained on ampicillin water for the duration of the experiment; if an ampicillin-sensitive FMT or BCT was gavaged, mice were taken off ampicillin and rested for 4 days before transplant.

3.4.2. K. pneumoniae isolates and culture. 5ml LB media was inoculated with frozen stock of the MH258 isolate overnight and the next day a 1:20ml diluted culture was grown for 2.5hr at 225rpm at 37°C to midlog phase (~OD 0.6 at ~$5x10^8$ CFU/ml). Kp was serially diluted in PBS to $5x10^2$ CFU/ml to inoculate mice with 100 colony-forming units (CFUs) in 200ul/ms by oral gavage. A concentration of $5x10^3$ CFU/ml was obtained in order to add 100 CFUs to 96-wells for *in vitro* and *ex vivo* co-culture. The table below details the MLST, *wzi* and K type for each K. pneumomiae strain used (116).

Isolate	**Figures**	**Carpanenamase**	**MLST**	***wzi* type**	**K type**
MH258	All	+	ST258	wzi-54	ST258 cps2
43309	3.8a	+	ST11	wzi-177	non-K-type
43303	3.8a	+	ST11		K24
32192	3.8a	+	ST258		cps1 K41
38544	3.8a	+	ST258		cps3 K57
MH189	3.8b	-	ST189	wzi-99	K31
MH1867	3.8b	-	ST11	wzi-177	non-K-type
MH225	3.8b	-	ST225	wzi-59	K3

3.4.3. Bacterial culture and isolation. Fecal pellets from MyD88-/- donor mice were resuspended in reduced PBS at 20-50mg/ml to serve as ARM-FMTs. ASM-FMTs were derived from the cecal content of naïve untreated wild-type female C57BL/6 mice. A

single 200ul dose was adoptively transferred in Kp-colonized or ampicillin-pretreated mice with the exception of one experiment (which tested the efficacy of 1, 2 and 3 sequential FMT doses to clear Kp). To prepare bacterial inocula from diluted intestinal content, fecal pellets were resuspended in PBS and aliquoted onto reduced BAPs for anaerobic culture and nonreduced BAPs to aerobic growth. Dilution cultures were incubated for 3 days at 37°C and scraped into PBS prior to transplant. 15% glycerol cultures were stored at -80°C. Individual colonies were restreaked and the16S rRNA gene was amplified for each isolate by colony PCR. The resulting PCR product was Sanger sequenced with primers that spanned the full 16S gene and classified by BLAST. To culture anaerobic isolates for *ex vivo* co-culture or transplant, 5ml of reduced BHI supplemented with 5g of yeast-5g and 1% cysteine (BHI+) was inoculated with frozen stocks of anaerobic isolates and grown statically overnight at 37°C. The next day, a 1:20 diluted culture was incubated statically for 6 hours and 150-200ul were added to 96wells for co-culture with Kp. 4ml of the midlog Blautia producta (Bp) liquid culture was filtered at 0.22um and added to 96well plates at different ratios with BHI+.

3.4.4. *in vivo* and *ex vivo* growth inhibition assays. Fecal content was resuspended in PBS to 50mg/ml and 100-300mg/ml for cecal content. Roughly 10^8 CFUs of individual isolate were added to 96well plates with antibiotic-treated cecal content. Kp growth was measured 24hrs after co-culture by plating on selective media. To test growth suppression by acetate, stocks were made in 25ml for glacial acetic acid (1M, 0.364M) and sodium acetate (anhydrous) (2.75M, 1M). For 1M acetic acid, 1ml sodium acetate (2.75M) and 1ml glacial acetic acid (1M) was added to 8ml BHI+ to obtain pH 5.2 and serial dilutions performed. For 1M sodium acetate, 1ml sodium acetate (1M) and 1ml glacial acetic acid (0.364M) was added to 8ml BHI+ to obtain pH 5.2 and serial dilutions performed. *In vitro* cultures with acetate were performed in total 2ml.

3.4.5. DNA extraction and 16s rRNA gene sequencing. DNA from intestinal content was extracted using the phenol-chloroform extraction method with with bead beating and purified with a Qiagen QiaAmp kit. The V4-V5 region of the 16S rRNA gene was amplified and PCR products were quantified and pooled at equimolar amounts before Illumina barcodes and adaptors were ligated on using the Illumina TruSeq Sample Preparation protocol. The completed library was sequenced on an Illumina Miseq platform by 2x250bp paired-end reads following the Illumina recommended procedures. The 16S paired-end reads were merged and demultiplexed. The UPARSE pipeline was used to perform error filtering, using maximum expected error (Emax = 1), group sequences into operational taxonomic units (OTUs) of 97% distance-based similarity and identify and remove potential chimeric sequences, using both de novo and reference-based methods. OTUs were classified by BLAST.

3.4.6. Sequence-based analyses. Sequences were analyzed using a custom Python script to convert OTU reads to relative abundances and convert samples to panel data for each experiment. Samples had an average of 25500 reads. OTUs with an average relative abundance >0.02% (across multiple experiments) met our thresholds. Spearman analyses were performed using the stats module in the scipy package and p-values were corrected for multiple hypothesis by the Bonferroni-Hochberg procedure. Lasso, ridge and elastic net regressions were performed with the sklearn linear model module and the random forest classifier with the sklearn ensemble module. The cluster module and decomposition modules in sklearn package were used for kmeans clustering and PCA.

CHAPTER FOUR

THE EVOLUTION OF VANCOMYCIN-RESISTANT ENTEROCOCCUS FAECIUM WITHIN THE GASTROINTESTINAL TRACT

4.1. INTRODUCTION

Enterococci are an intestinal commensal as well as leading nosocomial pathogen, particularly in the immunocompromised. Vancomycin-resistant Enterococci (VRE) can colonize and rapidly expand in patients whose intestinal microbiota has been perturbed by antibiotics. Intestinal VRE colonization greatly increases a patient's risk for bloodstream infection, during which VRE can acquire resistance *in vivo* to antibiotic therapy (16,132). Increasingly, epidemiological studies have used single nucleotide polymorphisms (SNPs) to track antibiotic-resistant infections in the hospital. However, the rapidity of SNP accumulation and its stability over time have not been carefully characterized in VRE as it expands the GI tract. Bacterial evolution has generally been studied *in vitro*, documenting a rapid rate of mutations (133). By characterizing the temporal dynamics of intestinal VRE evolution, we can shed light on within-host VRE diversity and complexity that may confound epidemiological studies.

Here, we seek to characterize how VRE adapts and diversifies in the GI tract of a colonized patient in response to selective pressures from antibiotics and inflammation in the gut. We first employed a culture-dependent, longitudinal approach by isolating individual VRE colonies at multiple timepoints from five colonized patients. Using high-throughput whole-genome sequencing, we identify single nucleotide polymorphisms (SNPs) to determine the clonal relatedness of VRE in the gut of individual patients over

time. We have found that patients can harbor enterococci from multiple sequence types, and that there is variability in the number of SNPs per isolate found at any timepoint within individual patients. To understand how an individual bacterium evolves in the gut from the onset of colonization, we inoculated a mouse with a single VRE CFU and found a linear rate of *de novo* SNP accumulation in our isolates. Combining metagenomic shotgun data to our analysis, we obtained a better estimate of the number of mutations acquired in a complex bacterial population. We detect hundreds of SNPs that evolve rapidly at around three weeks post-colonization. After this rapid evolution, we estimated that four subclades of *E. faecium* exist in stable proportions. A nonsynomous SNP in the catalytic domain of the penicillin-binding protein 5 (pbp5) persists at 100% frequency. Reperforming this low-inoculum experiment with a different E. faecium strain, we detected 3 nonsynomous pbp5 SNPs that changed their frequencies within the intestinal VRE population in a pattern that indicates clonal interference. Our results indicate that VRE can rapidly adapt within the GI tract in response to selective antibiotic pressure and that such diversity is preserved over time.

4.2. RESULTS

4.2.1. Genomic diversity of *E. faecium* in the gut of an individual patient.

We first characterized the cross-sectional diversity of vancomycin-resistant *E. faecium* (VREfm) in an allo-HSCT patient, herein identified as pt110 (**Fig. 4.1a**). The patient was initially colonized at <10% relative abundance six days prior to bone marrow transplantation, after which VREfm expanded and remained in the gut at high densities. A single isolate was cultured from three samples taken at day -6, 1, and 8. VREfm isolates were subjected to whole-genome sequencing and aligned using *breseq* to a reference built from an isolate isolated from this same patient to call SNPs. Surprisingly, unique SNP patterns were seen at each day examined (**Fig. 4.1b**).

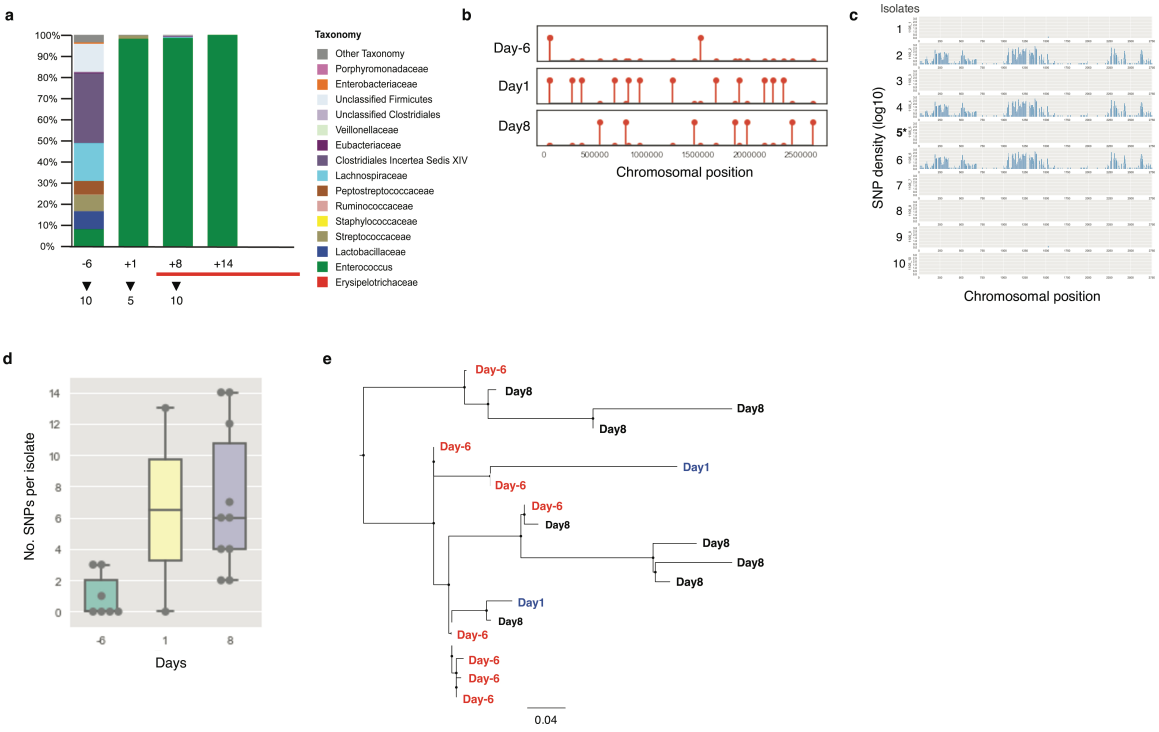

Figure 4.1 | Within-host diversity of a single allo-HSCT patient at MSKCC within and across time. a) The relative abundances of OTUs measured by 16S rRNA sequencing and grouped at the order level are shown for 4 stool samples collected. Days are relative to BMT. **b)** Lollipops indicate the presence of a SNP along the chromosome for 3 VREfm isolates taken on day -6, 1 and 8. **c)** The SNP densities for 10 isolates cultured from day -6 are plotted. SNPs are grouped at 1000-bp intervals along the chromosomal and number of SNPs per bin are reported in log-based 10. **d)** Barplots of the number of SNPs per isolate on days -6, 1 and 8. Boxes represent the interquartile range and the stems denote the minimum and maximum. **e)** A maximum-likelihood tree of the MLST 412 isolates cultured across day -6, 1 and 8 based on SNPs in the core genomes using the ASC GTR-GAMMA model in RAxML (optimized for <50 genomes). Branch length values are the mean expected rates of substitution per site

To clarify the relatedness of these VREfm strains, we deeply sampled the initial day -6 timepoint by culturing 10 isolates. Two coexisting lineages were found (**Fig. 4.1c**), revealing even greater diversity than what was observed with the three analyzed genomes (**Fig. 4.1b**). Each bar represents an isolate, where the x-axis indicates the position along the chromosome and the y-axis represents the number of SNPs detected (log-based 10) at 1000-bp intervals against the reference (typed MLST 412) (**Fig. 1c**). Isolates 2, 4, and 6 are over 6000 SNP differences from the reference and were typed as MLST 736.

We then looked at timepoints following the expansion of VREfm within the gut of this patient. At day 8, when VREfm reached over 99% of the intestinal abundance, we cultured a set of 10 isolates in total and found a slight increase in the number of SNPs accumulated over time (**Fig. 4.1d**). However, variants detected in earliest timepoint were still present. A maximum likelihood tree of the MLST 412 sublineage isolates, based on SNPs that appeared in the core genome, reveals that this diversity did not respect time (**Fig. 4.1e**).

4.2.2. Genomic diversity of *E. faecium* within GI tract over time.

We broadened our analysis by characterizing the pattern of within-patient VREfm diversity in four additional patients, identified as pt139, pt1325, pt151 and pt843 (**Fig. 4.2a**). References were built for each patient using an isolate cultured at the earliest timepoint that we sampled and subjected it to Illumina Miseq and MinION high throughput sequencing. All patients other than pt110 were colonized by a single MLST. We examined the level of variation for each patient, splitting up our analysis for pt110 by the two sublineages. Over the course of VREfm colonization, we found that all patients harbor at least 2 unique genotypes based on SNP patterns at any timepoint investigated (**Fig. 4.2a**). The heatmap is scaled from 0 to 15 SNPs per isolate.

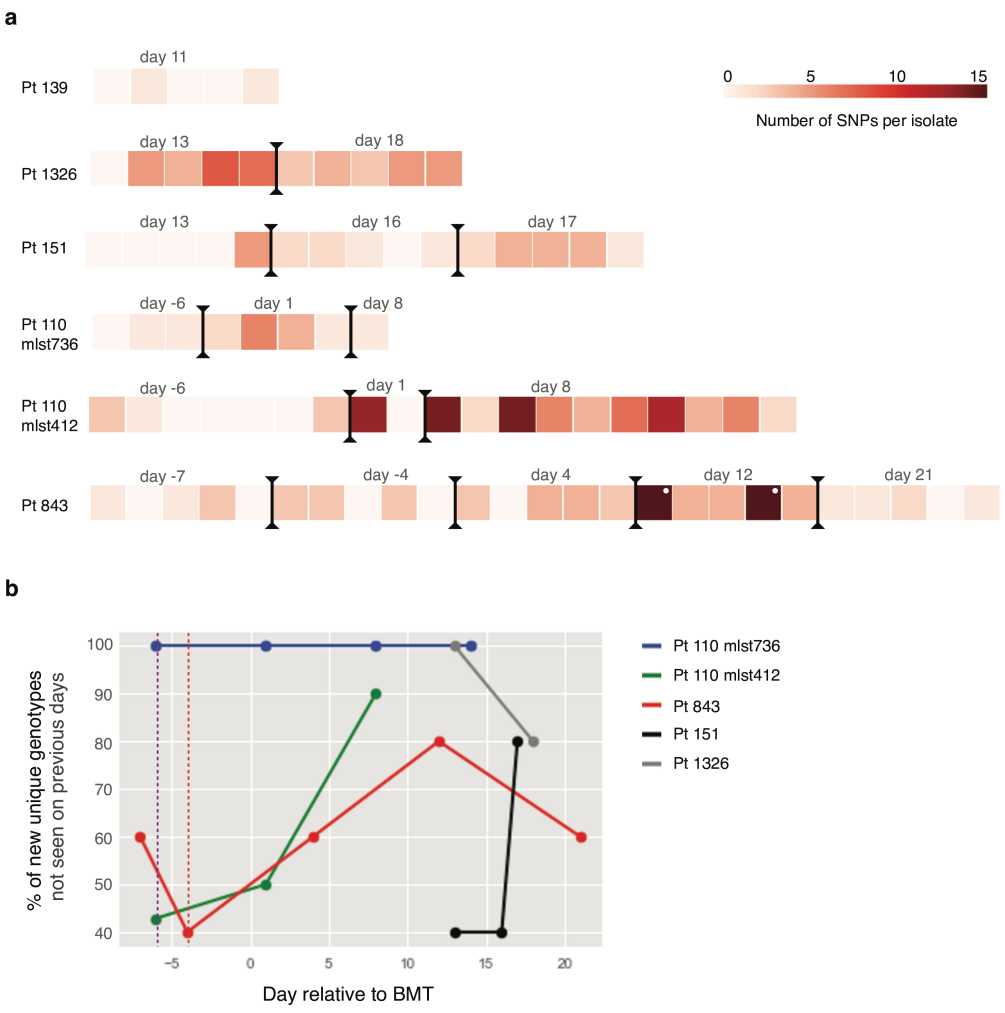

Figure 4.2 | Unique SNP patterns are detected on each day for 5 VREfm-colonized allo-HSCT patients and are acquired at variable rates. a) One isolate per patient was cultured and sequenced by both Illumina Miseq and Nanopore MinION platforms. A hybrid assembly was created with Unicyler and SNPs were called and corrected with *breseq* and bcftools. Reads for all patient isolates were aligned to their own reference and *breseq* was used to detect SNPs. A heatmap with a range of 0 to 15 SNPs was plotted, with one row per patient. Vertical lines separate each day timepoint. 2 isolates from pt843, #1 and #4 from day 12 (indicated by a white circle within the square), had 51 and 49 SNPs respectively that fell in a 757bp region in scaffold 5. Therefore, a maximum of 15 SNPs was plotted for these isolates in order to maintain a readable scale for the other VREfm strains. **b)** The proportion of new unique genotypes per day were plotted at each day sampled for the 4 out of 5 patients who were sampled on multiple timepoints. Dashed lines indicate the last day prior to VREfm expansion in the gut.

Given our longitudinal sampling of each patient, we next looked at the rate of VRE diversification over time. We hereafter use the term genotype to refer to isolates that share the same SNPs. Any SNP differences in another isolate would be considered a different genotype by this definition (thereby ignoring phylogenetic relationships of how one isolate evolves from another). For each patient, we plotted the proportion of unique

genotypes seen for the first time at each timepoint, which we refer to as new genotypes (**Fig. 4.2b**). For example, if we consider the isolates from MLST 412 from our first patient pt110 (4th row in Fig. 2a, green line in Fig. 2b), we found on day -6 that 3 out of the 7 VREfm isolates had acquired SNPs, 2 of which shared the same SNP pattern, while 4 VREfm strains were identical to the reference. The proportion of unique genotypes on day -6 is therefore 42% (3/7). On day 1, 1 isolate was identical to the reference while the second VREfm strain had 13 SNPs in a previously unseen pattern, yielding a 50% (1/2) ratio. This comparison allows us to track the amount of diversity acquired over time. For rapidly evolving VREfm, we would expect to see 100% novel genotypes at each timepoint sampled. Instead, we do not detect a consistent trend among the patient samples, suggesting that the dynamics of VREfm diversification in the gut are variable. The dashed lines indicate the last timepoint at which VREfm occupied less than <10% of the microbiota for pt843 (red line) and pt110 (purple line), after which VREfm expanded to >99% relative abundance. For pt843 and pt110 sublineage 412, there is an increase in proportion of new genotypes detected post-expansion (**Fig. 4.2b**).

4.2.3. Putting the heterogeneity of MSKCC patient-derived VRE in a global context

To compare how related the VREfm isolates are across our MSKCC patients, we constructed a maximum-likelihood tree based on the core genome after *de novo* assembling each fecal isolates' Illumina reads (**Fig. 4.3a**). For a subset of patients analyzed, each patient's strains cluster together, grouped by their MLST. Additional bloodstream Efm isolates cultured at MSKCC are included in the tree. To expand our interpretation of VREfm in-host diversity from our patients, we put them in a global context by replicating the work recently published on 289 VREfm bloodstream colonies isolated across the UK (134). Reads were aligned to Efm reference Aus0004 and a consensus sequence was obtained for each isolate. Regions of recombination were removed using Gubbins in the original analysis by Raven *et al.,*; however, at the time of

this writing, Gubbins was unable to run for the nearly 400 total isolates. MSKCC isolates are distributed within the tree, indicating that our patients are members of the hospital-associated clade A1 (**Fig. 4.3b**). We find no geographic signature in our isolate dataset.

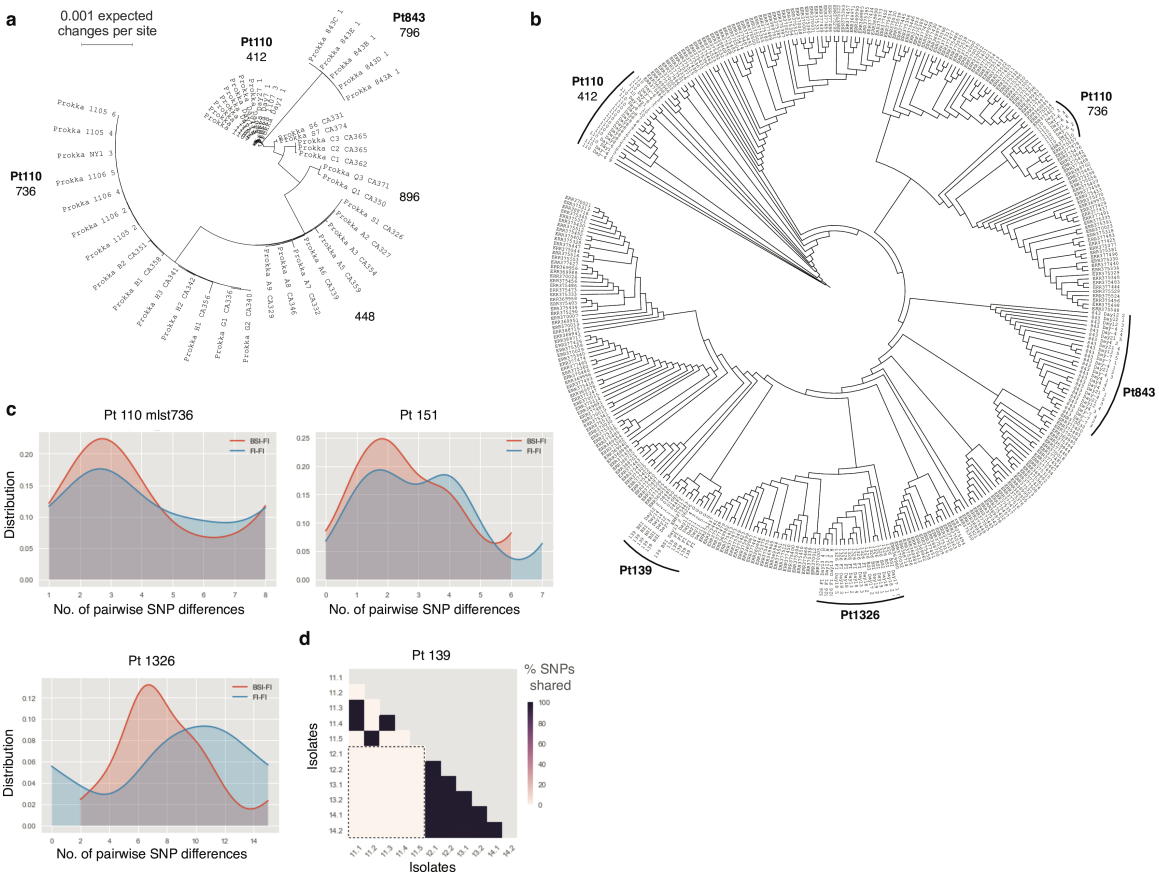

Figure 4.3 | VREfm isolates from MSKCC reside within an international collection of hospital-associated clade A strains and cluster by patient. a) *de novo* assemblies were constructed from Illumina reads using Spades. Core genome alignments were obtained using Roary, and a maximum-likelihood tree was created using RAxML's GTR-GAMMA model. **b)** Illumina reads were aligned to a published reference Aus0004 using SMALT and a consensus sequence was created by replacing SNPs and unmapped regions with the called variants and dashes respectively. RAxML was called to construct trees with using the GTR-CAT -V model. Trees were visualized in iTol. **c)** Pairwise SNP distances were calculated between BSI and fecal isolates (FI) and within FIs. A probability distribution for both sets of distances (BSI-FI; FI-FI) were plotted using a kernel density estimate, showing the probability of finding a given number of SNP differences between any 2 isolates. **d)** A similarity matrix shows in each square the percentage of SNPs shared by 2 isolates out of the total number of SNPs harbored by both strains.

Four patients in this study acquired bloodstream infections (BSI) following VREfm domination. The fecal samples chosen for these patients were the closest to the onset of bacteremia (**Fig. 4.2a**). For three out of the four patients, the bloodstream and fecal isolates cluster together amongst the UK blood isolate collection (**Fig. 4.3b**). Pairwise SNP distances between blood and fecal isolates (BSI-FI), compared to distances amongst fecal isolates alone (FI-FI), were calculated **(Fig. 4.3c**). Each graph indicates the probability of measuring a given number of SNP differences between two isolates. The red plot represents the pairwise distances for BSI-FI comparisons, and the blue for FI-FI. For three out of the four patients (pt110 MLST736, pt1326 and pt151), the probability distributions overlap significantly between the BSI-FI and FI-FI sets with <15 SNP differences, indicating that the GI tract seeded the BSI (**Fig. 4.3c**). For the 4th patient pt139, the BSIs and FIs were >1000 SNP differences apart and isolates from the same source are highly related to each other (**Fig. 4.3d**). A similarity matrix for pt139 depicts the percentage of SNPs shared by two isolates, and all pairwise comparisons are calculated. The dashed square represents the region of the matrix comparing bloodstream isolates (y-axis) to fecal (x-axis), showing that no SNPs are harbored in common. The top triangle displays the FI-FI comparisons; the binary aspect of this subplot is due to the fact that there are 2 genotypes found, one identical to the reference (n=3 isolates) and one with a single acquired SNP (n=2 isolates).

4.2.4. A single nonsynonymous penicillin-binding protein 5 mutation confers a fitness advantage in an *in vivo* model of VRE colonization.

Given the heterogeneity of VREfm found in colonized patients at any single timepoint, we sought to determine when such diversity develops during colonization. Since we lack information on how long patients had harbored VREfm in the gut in our time-series data, we were limited in our ability to quantify the evolutionary dynamics in patients. Therefore, we chose to model the expansion and diversification of VREfm in a mouse

model. 8-10 week old naïve C57BL/6J mice were treated with 0.5 g/L ampicillin in their drinking water for two days, and colonized with low-dose inoculums of VRE derived from our first patient (**Fig. 4.4a**). We colonized a single mouse with 1-2 CFUs of VREfm. During the 133-day course of the experiment, we cultured 4 isolates at 11 different timepoints from this single mouse which received continuous ampicillin treatment (**Fig. 4.4b**). Whole genome sequencing of the 44 isolates revealed 25 mutations in the chromosome. The first SNP mutation appeared at day 15 in a single isolate, and eight SNPs were seen only once prior to day 133 (**Fig. 4.4c**). To estimate the rate of *in vivo* diversity, we plotted the number of SNPs in the four isolates derived from each day and found that mutations accumulated at a linear rate (**Fig. 4.4d**). By day 27, a SNP in the penicillin-binding protein 5 (pbp5) appeared and was fixed in the population (**Fig. 4.4c**). A heatmap depicts the number of isolates (0-4) that carry a given SNP at each measured day. All isolates cultured post-day 27 harbored the pbp5 mutation, making it the most frequent SNP detected (**Fig. 4.4e**). 22 unique genotypes were found based on the chromosomal SNP pattern, and 16 out of the 22 subclones carried the pbp5 mutation, as demonstrated in the phylogenic tree, indicating a strong selective advantage (**Fig. 4.4f**). This nonsynomous pbp5 mutation occurred in 434th codon, which changes the negatively-charged aspartate to a nonpolar alanine within the transpeptidase domain of PBP5.

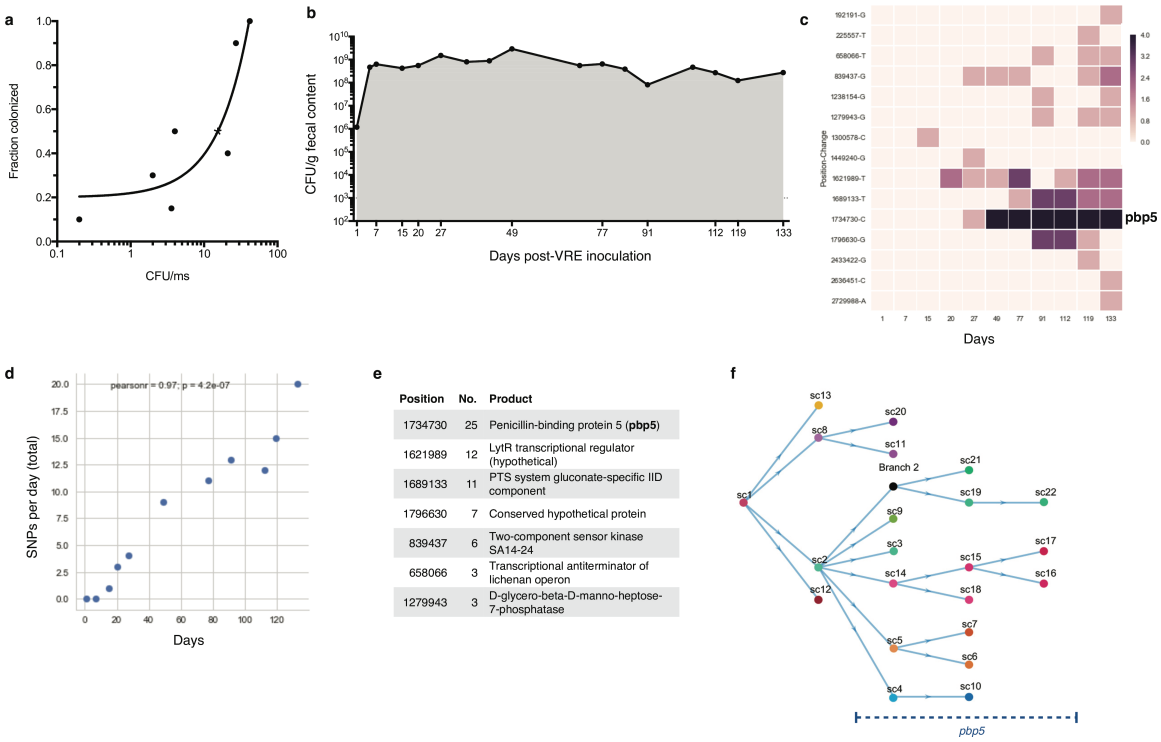

Figure 4.4 | VREfm rapidly evolves in the GI tract after acquiring a nonsynonymous mutation in the gene encoding penicillin binding protein 5 (pbp5). a) Low inocula of VREfm (CFU/ms) are plotted relative to the number of mice that were successfully colonized in the inoculated group; n=5 or 10 per experimental group. The dose of 0.2 CFUs/ms, which is equivalent to 2 CFUs/ml, infected 1 mouse out of 10 and **b)** this individual mouse was followed for a total of 133 days. The density of VREfm was measured by plating fecal pellets on selective media. 4 isolates were cultured from fecal content obtained at the 11 timepoints indicated. **c)** A heatmap of the 25 SNPs acquired in chromosome across the 44 isolates. The pbp5 SNP is indicated. **d)** The total number of SNPs found among the four isolates at each day are indicated over time. **e)** A table of SNPs mutated in 3 or more isolates. The second column indicates the number of isolates that carry that mutation. **f)** A phylogenetic tree based on the 22 unique genotypes found amongst the 44 isolates. The branch of isolates that evolved harboring the pbp5 mutation are indicated by the dashed line.

4.2.5. Metagenomic shotgun data reveals rapid intestinal VRE adaptation that occurred weeks post-colonization.

To track the dynamics of VREfm diversification in the total intestinal population, we performed metagenomic sequencing on 6 fecal samples taken from days 1, 27, 49, 77, 112 and 133. 219 chromosomal SNPs were detected at ≥5% frequency in the VREfm-dominated intestinal microbiota (**Fig. 4.5a**). The nonsynomous pbp5 achieved 100%

frequency by day 49 and persisted, fitting the pattern of positive selection seen in our isolates. During this same timeframe, we observed a rapid evolution of the majority of SNPs, only a subset of which were picked up in our isolate screen. While metagenomic sequencing provides greater sampling depth, it remains a challenge to determine which SNPs co-occur in unique genomes. Therefore, to further characterize the pattern of *in vivo* VREfm evolution over time, we combined our culture-based and deep sequencing approaches. We compared the relative abundances of our 22 subclades in the complex microbiota by estimating their proportions based on the SNP frequencies from the shotgun data (**Fig. 4.5b**, bottom panel). These refined frequency estimations clarified the lineage structure of VREfm over time, demonstrating that four subclades stably coexist for months after day 49 (**Fig. 4.5c**, bottom panel). By day 27, evolved strains outcompeted the ancestor, and the four coexisting subclades were derived from the pbp5 mutant. This phylogenetic pattern was not apparent from the isolate data alone (**Fig. 4.5c**, top panel). Taken together, our data indicates that a strong selective advantage conferred by the pbp5 mutation.

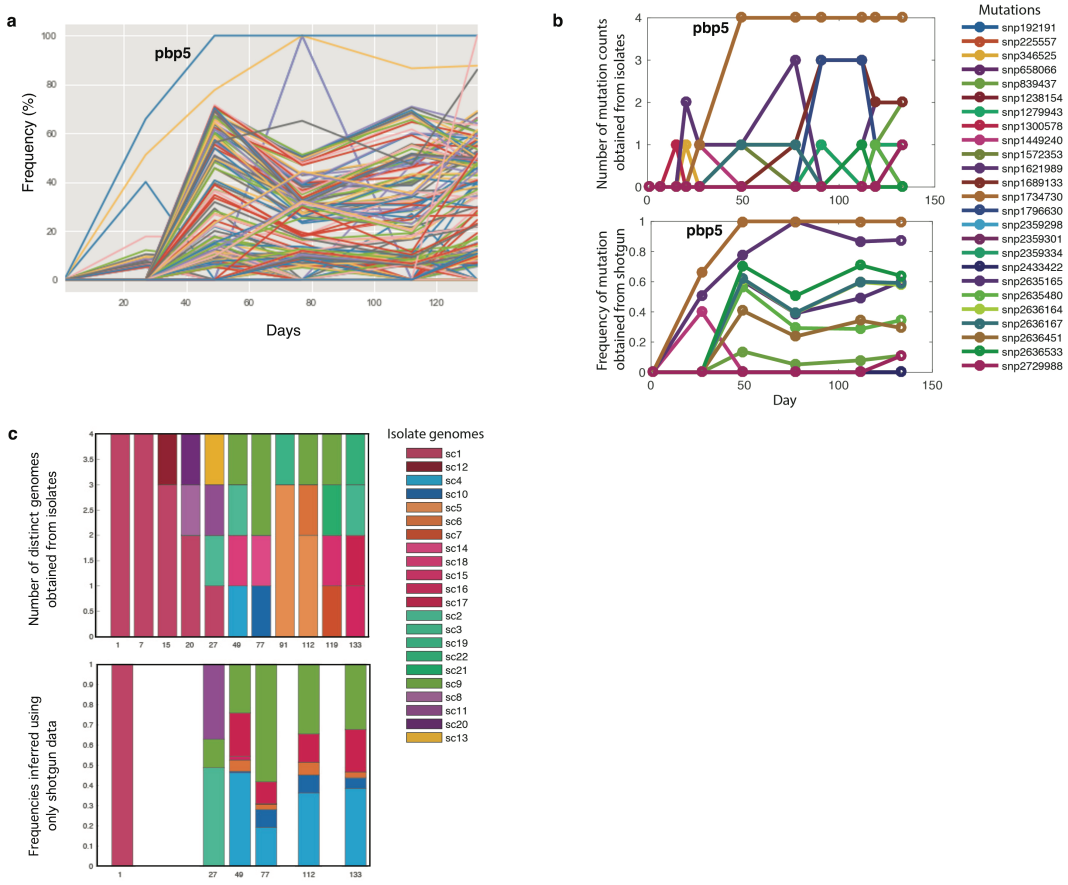

Figure 4.5 | Sublineages coexist after rapid diversification in which the pbp5 mutation becomes fixed in the total intestinal VREfm population. a) Frequency traces are shown for the 219 chromosomal SNP picked up by shotgun sequencing of fecal pellets from a single colonized mouse. **b)** Comparisons of the frequency estimates are shown for each SNP found in the isolate collection. The top graph depicts the number of isolates that carry a given SNP on each day; the bottom graph shows the percentage of reads that had a given SNP as determined from HiSeq metagenomic sequencing data. **c)** After refining the frequency estimates of the 25 isolate-derived chromosomal SNPs by shotgun sequencing, the proportions of related strains (as determined in Fig. 4.4f) are plotted over time. Related isolates are grouped into colored bins.

4.2.6. Parallel evolution and clonal interference characterize the *in vivo* population dynamics of a second VRE isolate.

To further characterize the dynamic nature of within-host VREfm evolution, we reperformed our low-inoculum experiment with a second E. faecium isolate, the ATCC 700221 strain. We cultured 28 isolates over 7 timepoints during the 62-day course of the experiment (**Fig. 4.6a**). The lab strain acquired 8 chromosomal mutations, 3 of which

were nonsynonmous mutations in the pbp5 gene (**Fig. 4.6a,b**). No isolate harbored more than 1 pbp5 SNP (**Fig. 4.6a**). 8 unique genomes were represented in our isolates (**Fig. 4.6c**). Applying the same approach of combining the two sequencing datasets, we tracked the dynamics of SNPs identified in the isolates over time based on their shotgun-derived frequencies. Interestingly, we see the 2 of the 3 pbp5-mutated subclades change frequencies relative to each other (**Fig. 4.6d**). As strains harboring pbp5-1 drift to lower frequencies, those bearing the pbp5-2 mutation rise, which suggests clonal interference among the lineages (**Fig. 4.6d,e**). All three mutations arose in the PBP5 C-terminal transpeptidase domain, as was the case in the first VREfm colonizing isolate. Thus, experimental evolution highlights the position selection of the pbp5 loci through a different pattern of within-host adaptation.

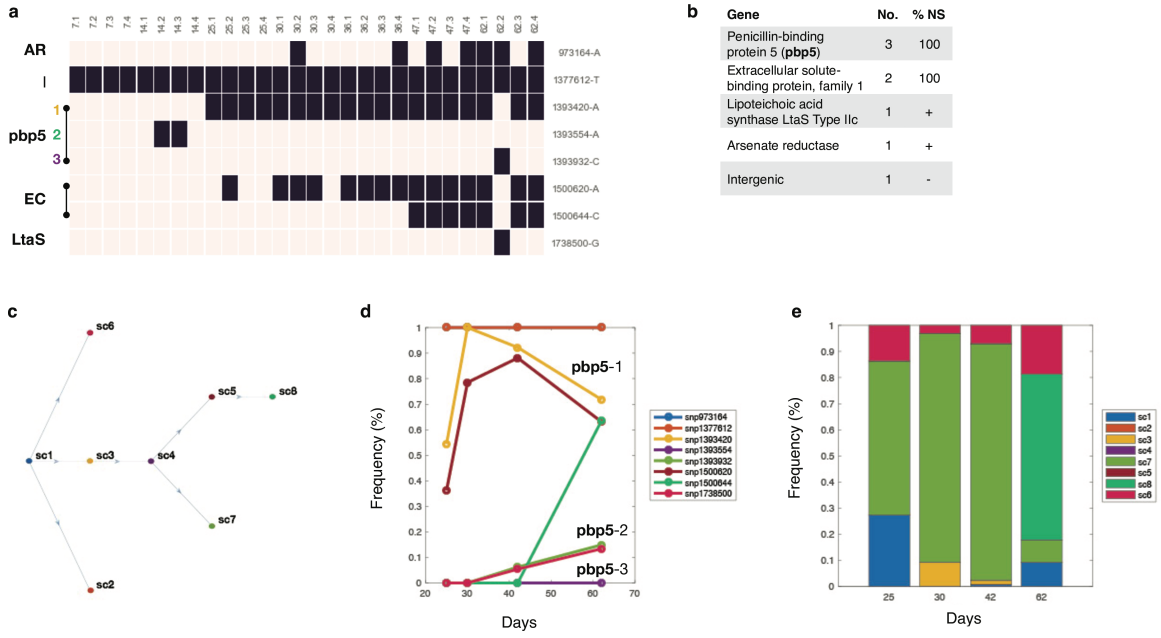

Figure 4.6 | A second, unrelated VREfm isolate colonizing the GI tract independently evolves nonsynonymous mutations in the pbp5 genes. a) 28 isolates from the indicated timepoints (x-axis; from day 7 to 62) were cultured over the course of *in vivo* colonization by ATCC E.fm strain in a single mouse. 8 SNPs were picked up along the chromosome. **b)** 7 out of the 8 SNPs were nonsynonymous, 3 of which appeared in the pbp5 gene. For the 2 genes that harbored only 1 SNP, a + was indicated if the mutation was nonsynonymous. **c)** A phylogenetic tree inferred from the SNP patterns displayed in a). **d)** The relative frequencies of the 8 unique genotypes fluctuate over time.

4.34. DISCUSSION

There is considerable genomic diversity among enterococcal strains, with genome sizes ranging from 2.7 to 3.6 Mb (135-137). Laterally transferred genetic elements make up 25% of the genome in some isolates (138) and this variation has likely aided hospital adaptation of enterococci (139-141). Compared to commensal enterococcal strains, multidrug-resistant clinical isolates possess larger genomes through the acquisition of foreign genetic material (137). Large-scale phylogenomic studies of Enterococci have estimated mutation rates of 7 SNPs per genome per year (134). The rate at which enterococci continues to evolve in the hospital environment is of particular clinical concern given its morbidity among the critically ill. Recent work has demonstrated that individuals can be colonized with multiple enterococcal clones simultaneously, and isolates collected at a given day are more similar than those across timepoints within a patient (142). How selective forces drive within-host diversification, and what this evolutionary pattern looks like, are not well known.

Herein, we surveyed intra-patient intestinal diversity by culturing isolates at various timepoints during VREfm colonization. We assessed the degree of VRE diversification in our patients by deeply sampling multiple timepoints, providing cross-sectional and longitudinal data. We found at least 2 genotypes amongst the patient isolates at every timepoint measured and this diversity did not respect time. Combining single-isolate whole-genome comparisons with deep metagenomic sequencing, we characterized the rapid adaptive dynamics in an *in vivo* evolution experiment. Our patient-derived isolate acquired a high degree of diversity over 133 days. In both *in vivo* experiments, evolved isolates successfully outcompeted the ancestral strain. Strong selective pressure acting on intestinal enterococci was observed by the parallel mutation of the penicillin-binding protein 5 (pbp5) gene between the two experiments. The pbp5 mutation shaped the

adaptive dynamics of VRE evolving in the GI tract, providing evidence of rapid adaptation to antibiotic pressure as a result of positive selection in real-time.

Enterococci are of particular clinical concern due to their growing resistance to antibiotics. Beta-lactams, such as ampicillin, inhibit bacterial growth by modifying and thereby inactivating penicillin-binding proteins (PBPs) required for cell wall synthesis. Enterococcal strains harbor some intrinsic resistance to beta-lactams by producing PBP5, which is chromosomally encoded (143,144). The acquisition of pbp5 gene mutations contributed to the high-level ampicillin resistance that healthcare-related E. faecium isolates developed in the late 1970s and 1980s (145-147). Increased resistance to ampicillin is associated with mutations to the PBP5-encoding gene that further reduce the protein's affinity for beta-lactam antibiotics, such as mutations that result in amino acid substitutions near the active site in its transpeptidase domain (148-151). Resistance is amplified when multiple mutations are present in the pbp5 gene (151). Here, we document the positive fitness advantage conferred *in vivo* by mutations in the pbp5 gene, acquired by intestinal enterococci in as few as two weeks, during continuous ampicillin treatment. This data has demonstrates the rapidity in which bacterial pathogens evolve under antibiotic pressure.

4.4. MATERIALS AND METHODS

4.4.1. VREfm isolate collection and culturing. Stool samples were collected from allo-HSCT patients in an ongoing IRB-approved study and stored in 2ml freezer vials at -80°C. Stored content was thawed and streaked with an inoculating loop onto selective Difco Enterococcosel agar supplemented with 10ug/ml vancomycin (EAPv). Fecal pellets collected from mice were immediately kept on ice after harvesting and plated the same day on EAPv. Plates were incubated aerobically for 48hrs at 37°C and 4-10 colonies were

selected and restreaked. Stocks were made by growing a restreaked colony in 5ml Brain Heart Infusion liquid media (BHI) overnight and growing in 1:20ml dilution in 20ml BHI for 6hrs at 225pm at 37°C. 800ml of the culture was resuspended in 200ml of 75% glycerol to obtain 4 15% glycerol stocks per isolate, stored at -80°C. Bloodstream isolates were stored by the MSKCC microbiology laboratory and restreaked on EAPv as described for fecal isolates.

4.4.2. Mouse husbandry and *in vivo* VREfm colonization. *in vivo* experiments were performed in compliance with Memorial Sloan Kettering's institutional guidelines and were approved by its Institutional Animal Care and Use Committee. 8-10 week old wild-type female C57BL/6 mice were purchased from the Jackson Laboratories. Mice were housed in sterile cages with irradiated feed and acidified water. 5ml BHI was inoculated with frozen stock overnight and the next day a 1:20ml dilution was incubated for 2.5hrs at 225pm at 37°C to obtain a midlog culture of ~$6x10^8$ CFU/ml. Serial dilutions were performed in PBS. Inocula were plated to determine the CFU input per mouse. Mice were pretreated with ampicillin at 0.5g/L for 2 days in the drinking water to abrogate colonization resistance, and orally gavaged in 200ul per mouse. Mice were individually housed at the time of inoculation. The number of mice per group that were colonized (out of 5 or 10 mice total) was assessed on day 1 and day 5 post-challenge by serially diluting fecal pellets in PBS and plating on EAPv. Mice in the group that received the lowest inocula dose were kept to monitor VREfm and maintained on ampicillin-treated water. VREfm density was measured as described every other week henceforth.

4.4.3. Whole genome sequencing, reference assembly and annotation. Isolates grown in BHI until early stationary phase and centrifuged. DNA was extracted using phenol-chloroform extraction with bead beating and purified with a Qiagen QiaAmp kit. Purified DNA was sheared using a Covaris ultrasonicator and prepared for Illumina MiSeq

sequencing with a Kapa library preparation kit with Illumina TruSeq adaptors to create 2x300bp paired-end reads. Fecal pellets sent for shotgun metagenomics were sequenced with Illumina HiSeq by 2x100bp paired-end reads. Reads were processed using a custom bash shell script. Trimmomatic was used to quality filter raw sequence reads (version 0.36). Read quality was assessed by FastQC (version 0.11.5).

For pt110, PacBio reads were assembled with HGAP and iteratively corrected using Pilon with Illumina MiSeq reads from the same isolate. A consensus sequence was constructed for an isolate from day -6 using *breseq* SNP and INDEL calls to correct the PacBio reference. For all other patients, a hybdrid assembly was constructed with Oxford Nanopore MinION and MiSeq reads with Unicycler and iteratively corrected with *breseq* (version 0.31.1). Quality assessment of finished assemblies was performed using QUAST (version v4.5). References were annotated using the PATRIC web portal

4.4.4. Variant detection. Trimmed quality-filtered Illumina reads were aligned to our in-house references and variants called using *breseq*. For isolates, the consensus mode was used. Shotgun metagenomes were run in the polymorphism mode with default settings, which called SNPs at ≥5% frequency. *breseq*'s annotated output files were parsed and analyzed in a custom Python script. A custom bash script was used to determine the number of mapped reads for each SNP detected in our isolate dataset within the shotgun metagenomic sequencing data. Genotypes were determined based on SNP patterns in a custom script written in matlab.

4.4.5. Construction of phylogenetic trees. Trimmed reads were assembled into contigs using the short-read genome assembler SPAdes (version 3.11.1) and annotated with PROKKA (version 1.12). Strains were typed by MLST using mlst (version 2.8). Core genomes and accessory genes were identified by Roary (version 3.8.2). Maximum-

likilihood trees were constructed on core genome alignments with RAxML using the model GTRCAT if >50 genomes were analyzed or GTRGAMMA if fewer. For large core genome alignments, SNPs were called with SNP-sites (version 2.3.2). Maximum-likelihood trees based on SNPs in the core genomes were created with RAxML using ASC-GTRCAT if >50 genomes were analyzed or ASC-GTRGAMMA if fewer.

For the UK BSI isolates collected by Raven *et al.*, fastq files hosted on the European Nucleotide Archive were downloaded by their accession numbers (130). A custom bash script was written to replicate this study's findings. In brief, reads were trimmed and aligned to the published genome Aus0004 by SMALT as described (130). For each isolate, consensus sequences were obtained by editing the SNPs and unmapped regions with the called variants and dashes respectively with vcftools and bcftools. Gubbins was used to remove regions of recombination in the original study and failed to run in our hands.

CHAPTER 5

CONCLUSIONS AND FUTURE DIRECTIONS

The intestinal microbiota plays a key role in keeping infection and inflammation at bay. Tolerogenic microbes from genera such as Bacteroides and Clostridium are important for maintaining homeostasis in the intestinal mucosa, and select bacterial species are essential for providing colonization resistance to pathogens. When the intestinal microbiota is perturbed by antibiotics, resistant bacteria can colonize the GI tract and rapidly reach high densities. Without an intervention to restore the intestinal microbiota, pathogens stably persist in the gut for months and the risk of developing bloodstream infections increases. In the hospital setting, antibiotic-resistant pathogens can spread between patients, acquiring new mutations as bacteria evolve. Using next-generation metagenomic sequencing, we characterized the intestinal microbial dynamics that impact 1) the development of colitis, 2) susceptibility to hospital-associated gram-negative pathogens, and 3) intra-species diversity following colonization.

In Chapter 2, we aimed to determine which specific components of the microbiota promote resistance to immunotherapy-associated colitis. We found that members of the Bacteroidetes phylum and three of its families are correlated with resistance to the development of colitis following CTLA-4 blockade. We also found that a lack of genetic pathways involved in polyamine transport and B vitamin biosynthesis is associated with an increased risk of colitis. Whether or not B vitamins play a direct role in the modulating colitis risk or are a signature of a healthy microbiota remains to be determined.

In Chapter 3, we asked which intestinal bacteria provide resistance to the antibiotic-resistant gram-negative *Klebsiella pneumonia* (Kp). We used an *in vivo* mouse model to differentially alter intestinal microbial communities using antibiotic treatment and bacterial adoptive transfers. Colonization resistance was restored when reconstituting mice with bacteria cultured anaerobically. We found that higher abundances of Clostridia class members is correlated with lower Kp density. Using statistical models on our time-series sequencing data, we also found that the certain clostridial OTUs can help predict whether Kp colonization resolves over time. A major challenge in constructing bacterial consortium to resolve infection is identifying the right combination of isolates, as the microbes must both engraft in the host and eliminate the colonizing pathogen. The modeling analyses presented here have identified a select number of isolates that should tested further in *in vivo* adoptive transfer experiments. Ideally, future studies would test these candidates from a bank of human-derived bacterial isolates. Additionally, further studies are required to understand how such a consortium resolves *K. pneumonia* colonization. The work presented in this thesis suggests that short-chain fatty acids might play a role, as *c*lostridial species are known producers in the colon, through a direct mechanism of inhibition.

In Chapter 4, we sought to characterize the temporal dynamics of how *E. faecium*, which exists as a commensal and a pathogen in patients, evolves within the host as it colonizes the gut. Using a culture-based approach, we found multiple genotypes per timepoint in VRE-colonized allo-HSCT patients. To understand the rate that VRE acquires this diversity, we followed the expansion and colonization of a single CFU of *E. faecium* inoculated into an antibiotic-treated mouse. We found many mutations that evolve rapidly at roughly three weeks post-colonization, and estimated that four subclades remain in stable proportions following this rapid evolution. In two independent mouse experiments, we detected nonsynomous SNPs in the transpeptidase-encoding region of the penicillin-

binding protein 5 (pbp5) gene, which is known to accumulate mutations in clinical isolates and confers ampicillin resistance. Our results indicate that VRE can rapidly adapt within the GI tract in response to selective antibiotic pressure. Whether or not the evolutionary pattern of VRE in our mouse experiment is stochastic can be answered by inoculating additional mice with the same VRE isolate. Work has currently been undertaken to formally describe the mutation rate and fitness costs observed in our *in vivo* experiments. The mathematical modeling used here to analyze the population dynamics of VRE can also be applied to high-throughput shotgun data of patient samples. The Pamer lab has deeply sequenced fecal content taken serially from a number of allo-HSCT patients who have been colonized by VRE. With this dataset, we can identify all mutations acquired in VRE in the gut to further understand how rapidly VRE diversifies in patients and if multiple lineages coexist and compete.

REFERENCES

1. Whitman WB, Coleman DC, Wiebe WJ. Prokaryotes: The unseen majority. Proceedings of the National Academy of Sciences 1998;95(12):6578-83.

2. Hooper LV, Littman DR, Macpherson AJ. Interactions between the microbiota and the immune system. Science 2012, Jun 8;336(6086):1268-73.

3. Eckburg PB, Bik EM, Bernstein CN, Purdom E, Dethlefsen L, Sargent M, et al. Diversity of the human intestinal microbial flora. Science 2005, Jun 10;308(5728): 1635-8.

4. Turnbaugh PJ, Ley RE, Hamady M, Fraser-Liggett CM, Knight R, Gordon JI. The human microbiome project. Nature 2007, Oct 18;449(7164):804-10.

5. Human Microbiome Project Consortium. Structure, function and diversity of the healthy human microbiome. Nature 2012, Jun 14;486(7402):207-14.

6. Arumugam M, Raes J, Pelletier E, Le Paslier D, Yamada T, Mende DR, et al. Enterotypes of the human gut microbiome. Nature 2011, May 12;473(7346):174-80.

7. Koren O, Knights D, Gonzalez A, Waldron L, Segata N, Knight R, et al. A guide to enterotypes across the human body: Meta-analysis of microbial community structures in human microbiome datasets. PLoS Comput Biol 2013;9(1):e1002863.

8. Ding T, Schloss PD. Dynamics and associations of microbial community types across the human body. Nature 2014, May 15;509(7500):357-60.

9. Turnbaugh PJ, Hamady M, Yatsunenko T, Cantarel BL, Duncan A, Ley RE, et al. A core gut microbiome in obese and lean twins. Nature 2009, Jan 22;457(7228):480-4.

10. Scher JU, Sczesnak A, Longman RS, Segata N, Ubeda C, Bielski C, et al. Expansion of intestinal Prevotella copri correlates with enhanced susceptibility to arthritis. Elife 2013;2:e01202.

11. Sampson TR, Debelius JW, Thron T, Janssen S, Shastri GG, Ilhan ZE, et al. Gut microbiota regulate motor deficits and neuroinflammation in a model of Parkinson's disease. Cell 2016, Dec 1;167(6):1469-1480.e12.

12. Zheng P, Zeng B, Zhou C, Liu M, Fang Z, Xu X, et al. Gut microbiome remodeling induces depressive-like behaviors through a pathway mediated by the host's metabolism. Mol Psychiatry 2016;21(6):786-96.

13. Zitvogel L, Daillère R, Roberti MP, Routy B, Kroemer G. Anticancer effects of the microbiome and its products. Nat Rev Microbiol 2017, Aug;15(8):465-78.

14. Donskey CJ, Chowdhry TK, Hecker MT, Hoyen CK, Hanrahan JA, Hujer AM, et al. Effect of antibiotic therapy on the density of vancomycin-resistant enterococci in the stool of colonized patients. N Engl J Med 2000, Dec 28;343(26):1925-32.

15. Ubeda C, Taur Y, Jenq RR, Equinda MJ, Son T, Samstein M, et al. Vancomycin-resistant Enterococcus domination of intestinal microbiota is enabled by antibiotic treatment in mice and precedes bloodstream invasion in humans. J Clin Invest 2010, Dec; 120(12):4332-41.

16. Taur Y, Xavier JB, Lipuma L, Ubeda C, Goldberg J, Gobourne A, et al. Intestinal domination and the risk of bacteremia in patients undergoing allogeneic hematopoietic stem cell transplantation. Clin Infect Dis 2012, Oct;55(7):905-14.

17. Donskey CJ, Hanrahan JA, Hutton RA, Rice LB. Effect of parenteral antibiotic administration on persistence of vancomycin-resistant Enterococcus faecium in the mouse gastrointestinal tract. J Infect Dis 1999, Aug;180(2):384-90.

18. Lieberman TD, Flett KB, Yelin I, Martin TR, McAdam AJ, Priebe GP, Kishony R. Genetic variation of a bacterial pathogen within individuals with cystic fibrosis provides a record of selective pressures. Nat Genet 2014, Jan;46(1):82-7.

19. Snitkin ES, Zelazny AM, Thomas PJ, Stock F, Henderson DK, Palmore TN, Segre JA. Tracking a hospital outbreak of carbapenem-resistant Klebsiella pneumoniae with whole-genome sequencing. Sci Transl Med 2012, Aug 22;4(148):148ra116.

20. Chin CS, Sorenson J, Harris JB, Robins WP, Charles RC, Jean-Charles RR, et al. The origin of the Haitian cholera outbreak strain. N Engl J Med 2011, Jan 6;364(1):33-42.

21. Gardy JL, Johnston JC, Ho Sui SJ, Cook VJ, Shah L, Brodkin E, et al. Whole-genome sequencing and social-network analysis of a tuberculosis outbreak. N Engl J Med 2011, Feb 24;364(8):730-9.

22. Rasko DA, Webster DR, Sahl JW, Bashir A, Boisen N, Scheutz F, et al. Origins of the E. coli strain causing an outbreak of hemolytic-uremic syndrome in Germany. N Engl J Med 2011, Aug 25;365(8):709-17.

23. Zdziarski J, Brzuszkiewicz E, Wullt B, Liesegang H, Biran D, Voigt B, et al. Host imprints on bacterial genomes--rapid, divergent evolution in individual patients. PLoS Pathog 2010, Aug 26;6(8):e1001078.

24. Lieberman TD, Michel JB, Aingaran M, Potter-Bynoe G, Roux D, Davis MR, et al. Parallel bacterial evolution within multiple patients identifies candidate pathogenicity genes. Nat Genet 2011, Dec;43(12):1275-80.

25. Lellek H, Franke GC, Ruckert C, Wolters M, Wolschke C, Christner M, et al. Emergence of daptomycin non-susceptibility in colonizing vancomycin-resistant Enterococcus faecium isolates during daptomycin therapy. Int J Med Microbiol 2015, Sep 12.

26. Zhao S, Lieberman TD, Poyet M, Groussin M, Gibbons SM, Xavier RJ, Alm EJ. Adaptive evolution within the gut microbiome of individual people. BioRxiv 2017, Oct: 208009.

27. Vollaard J, Clasener A. Colonization resistance. Antimicrob Agents Chemother 1994, Mar 1;38(3):409-14.

28. van der Waaij D, Berghuis-de Vries JM, Lekkerkerk Lekkerkerk-v. Colonization resistance of the digestive tract in conventional and antibiotic-treated mice. J Hyg (Lond) 1971, Sep;69(3):405-11.

29. Buffie CG, Jarchum I, Equinda M, Lipuma L, Gobourne A, Viale A, et al. Profound alterations of intestinal microbiota following a single dose of clindamycin results in sustained susceptibility to clostridium difficile-induced colitis. Infect Immun 2012, Jan; 80(1):62-73.

30. Caballero S, Kim S, Carter RA, Leiner IM, Sušac B, Miller L, et al. Cooperating commensals restore colonization resistance to vancomycin-resistant Enterococcus faecium. Cell Host Microbe 2017, May 10;21(5):592-602.e4.

31. Freter R. The fatal enteric cholera infection in the guinea pig, achieved by inhibition of normal enteric flora. J Infect Dis 1955;97(1):57-65.

32. Bohnhoff M, Miller CP, Martin WR. Resistance of the mouse's intestinal tract to experimental Salmonella infection. J Exp Med 1964;120(5):817-28.

33. Ubeda C, Bucci V, Caballero S, Djukovic A, Toussaint NC, Equinda M, et al. Intestinal microbiota containing Barnesiella species cures vancomycin-resistant Enterococcus faecium colonization. Infect Immun 2013, Mar;81(3):965-73.

34. Lawley TD, Clare S, Walker AW, Stares MD, Connor TR, Raisen C, et al. Targeted restoration of the intestinal microbiota with a simple, defined bacteriotherapy resolves relapsing Clostridium difficile disease in mice. PLoS Pathog 2012;8(10):e1002995.

35. Reeves AE, Koenigsknecht MJ, Bergin IL, Young VB. Suppression of Clostridium difficile in the gastrointestinal tracts of germfree mice inoculated with a murine isolate from the family Lachnospiraceae. Infect Immun 2012, Nov;80(11):3786-94.

36. van der Waaij D, Berghuis-de Vries JM, Lekkerkerk Lekkerkerk-v. Colonization resistance of the digestive tract in conventional and antibiotic-treated mice. J Hyg (Lond) 1971, Sep;69(3):405-11.

37. Berg RD, Owens WE. Inhibition of translocation of viable Escherichia coli from the gastrointestinal tract of mice by bacterial antagonism. Infection and Immunity 1979;25(3):820-7.

38. Buffie CG, Pamer EG. Microbiota-mediated colonization resistance against intestinal pathogens. Nat Rev Immunol 2013, Nov;13(11):790-801.

39. Cash HL, Whitham CV, Behrendt CL, Hooper LV. Symbiotic bacteria direct expression of an intestinal bactericidal lectin. Science 2006, Aug 25;313(5790):1126-30.

40. Brandl K, Plitas G, Schnabl B, DeMatteo RP, Pamer EG. MyD88-mediated signals induce the bactericidal lectin RegIIIγ and protect mice against intestinal Listeria monocytogenes infection. J Exp Med 2007, Aug;204(8):1891-900.

41. Vaishnava S, Behrendt CL, Ismail AS, Eckmann L, Hooper LV. Paneth cells directly sense gut commensals and maintain homeostasis at the intestinal host-microbial interface. Proc Natl Acad Sci U S A 2008, Dec 30;105(52):20858-63.

42. Mukherjee S, Zheng H, Derebe MG, Callenberg KM, Partch CL, Rollins D, et al. Antibacterial membrane attack by a pore-forming intestinal c-type lectin. Nature 2013, Nov 20.

43. Brandl K, Plitas G, Mihu CN, Ubeda C, Jia T, Fleisher M, et al. Vancomycin-resistant enterococci exploit antibiotic-induced innate immune deficits. Nature 2008, Oct 9;455(7214):804-7.

44. Kinnebrew MA, Ubeda C, Zenewicz LA, Smith N, Flavell RA, Pamer EG. Bacterial flagellin stimulates toll-like receptor 5-dependent defense against vancomycin-resistant enterococcus infection. J Infect Dis 2010, Feb;201(4):534-43.

45. Kinnebrew MA, Buffie CG, Diehl GE, Zenewicz LA, Leiner I, Hohl TM, et al. Interleukin 23 production by intestinal CD103(+)cd11b(+) dendritic cells in response to bacterial flagellin enhances mucosal innate immune defense. Immunity 2012, Feb 24;36(2):276-87.

46. Godl K, Johansson ME, Lidell ME, Mörgelin M, Karlsson H, Olson FJ, et al. The N terminus of the MUC2 mucin forms trimers that are held together within a trypsin-resistant core fragment. J Biol Chem 2002, Dec 6;277(49):47248-56.

47. Donskey CJ. The role of the intestinal tract as a reservoir and source for transmission of nosocomial pathogens. Clin Infect Dis 2004, Jul 15;39(2):219-26.

48. Johansson ME, Jakobsson HE, Holmén-Larsson J, Schütte A, Ermund A, Rodríguez-Piñeiro AM, et al. Normalization of host intestinal mucus layers requires long-term microbial colonization. Cell Host Microbe 2015, Nov 11;18(5):582-92.

49. Petersson J, Schreiber O, Hansson GC, Gendler SJ, Velcich A, Lundberg JO, et al. Importance and regulation of the colonic mucus barrier in a mouse model of colitis. Am J Physiol Gastrointest Liver Physiol 2011, Feb;300(2):G327-33.

50. Frantz AL, Rogier EW, Weber CR, Shen L, Cohen DA, Fenton LA, et al. Targeted deletion of MyD88 in intestinal epithelial cells results in compromised antibacterial immunity associated with downregulation of polymeric immunoglobulin receptor, mucin-2, and antibacterial peptides. Mucosal Immunol 2012, Sep;5(5):501-12.

51. Wlodarska M, Willing B, Keeney KM, Menendez A, Bergstrom KS, Gill N, et al. Antibiotic treatment alters the colonic mucus layer and predisposes the host to exacerbated Citrobacter rodentium-induced colitis. Infect Immun 2011, Apr;79(4): 1536-45.

52. Johansson ME, Phillipson M, Petersson J, Velcich A, Holm L, Hansson GC. The inner of the two muc2 mucin-dependent mucus layers in colon is devoid of bacteria. Proc Natl Acad Sci U S A 2008, Sep 30;105(39):15064-9.

53. Vaishnava S, Yamamoto M, Severson KM, Ruhn KA, Yu X, Koren O, et al. The antibacterial lectin RegIIIγ promotes the spatial segregation of microbiota and host in the intestine. Science 2011, Oct 14;334(6053):255-8.

54. Loonen LM, Stolte EH, Jaklofsky MT, Meijerink M, Dekker J, van Baarlen P, Wells JM. Reg3γ-deficient mice have altered mucus distribution and increased mucosal inflammatory responses to the microbiota and enteric pathogens in the ileum. Mucosal Immunol 2014, Jul;7(4):939-47.

55. Caballero S, Carter R, Ke X, Susac B, Leiner IM, Kim GJ, et al. Distinct but spatially overlapping intestinal niches for vancomycin-resistant Enterococcus faecium and carbapenem-resistant Klebsiella pneumoniae. PLoS Pathog 2015, Sep;11(9):e1005132.

56. Kamada N, Kim YG, Sham HP, Vallance BA, Puente JL, Martens EC, Nunez G. Regulated virulence controls the ability of a pathogen to compete with the gut microbiota. Science 2012, Jun 8;336(6086):1325-9.

57. Maltby R, Leatham-Jensen MP, Gibson T, Cohen PS, Conway T. Nutritional basis for colonization resistance by human commensal Escherichia coli strains HS and nissle 1917 against E. Coli O157:H7 in the mouse intestine. PLoS One 2013;8(1):e53957.

58. Kommineni S, Bretl DJ, Lam V, Chakraborty R, Hayward M, Simpson P, et al. Bacteriocin production augments niche competition by enterococci in the mammalian gastrointestinal tract. Nature 2015, Oct 29;526(7575):719-22.

59. Borrero J, Chen Y, Dunny GM, Kaznessis YN. Modified lactic acid bacteria detect and inhibit multiresistant Enterococci. ACS Synth Biol 2015, Mar 20;4(3):299-306.

60. Millette M, Cornut G, Dupont C, Shareck F, Archambault D, Lacroix M. Capacity of human nisin- and pediocin-producing lactic acid bacteria to reduce intestinal colonization by vancomycin-resistant enterococci. Appl Environ Microbiol 2008, Apr;74(7): 1997-2003.

61. Roe AJ, McLaggan D, Davidson I, O'Byrne C, Booth IR. Perturbation of anion balance during inhibition of growth of Escherichia coli by weak acids. J Bacteriol 1998, Feb;180(4):767-72.

62. Han K, Hong J, Lim HC. Relieving effects of glycine and methionine from acetic acid inhibition in Escherichia coli fermentation. Biotechnol Bioeng 1993, Feb 5;41(3):316-24.

63. Roe AJ, O'Byrne C, McLaggan D, Booth IR. Inhibition of Escherichia coli growth by acetic acid: A problem with methionine biosynthesis and homocysteine toxicity. Microbiology 2002, Jul;148(Pt 7):2215-22.

64. Weisser M, Oostdijk EA, Willems RJ, Bonten MJ, Frei R, Elzi L, et al. Dynamics of ampicillin-resistant Enterococcus faecium clones colonizing hospitalized patients: Data from a prospective observational study. BMC Infect Dis 2012;12:68.

65. Montealegre MC, Singh KV, Murray BE. Gastrointestinal tract colonization dynamics by different Enterococcus faecium clades. J Infect Dis 2016, Jun 15;213(12):1914-22.

66. Gilmore MS, Rauch M, Ramsey MM, Himes PR, Varahan S, Manson JM, et al. Pheromone killing of multidrug-resistant Enterococcus faecalis V583 by native commensal strains. Proc Natl Acad Sci U S A 2015, Jun 9;112(23):7273-8.

67. Duerkop BA, Clements CV, Rollins D, Rodrigues JL, Hooper LV. A composite bacteriophage alters colonization by an intestinal commensal bacterium. Proc Natl Acad Sci U S A 2012, Oct 23;109(43):17621-6.

68. Biswas B. Bacteriophage therapy rescues mice bacteremic from a clinical isolate of vancomycin-resistant Enterococcus faecium. Infection and Immunity 2002, Jan 1;70(1): 204-10.

69. van Nood E, Vrieze A, Nieuwdorp M, Fuentes S, Zoetendal EG, de Vos WM, et al. Duodenal infusion of donor feces for recurrent Clostridium difficile. N Engl J Med 2013, Jan 31;368(5):407-15.

70. Dubberke ER, Mullane KM, Gerding DN, Lee CH, Louie TJ, Guthertz H, Jones C. Clearance of vancomycin-resistant Enterococcus concomitant with administration of a

microbiota-based drug targeted at recurrent Clostridium difficile infection. Open Forum Infect Dis 2016, Sep;3(3):ofw133.

71. Lahti L, Salojärvi J, Salonen A, Scheffer M, de Vos WM. Tipping elements in the human intestinal ecosystem. Nat Commun 2014;5:4344.

72. Buffie CG, Bucci V, Stein RR, McKenney PT, Ling L, Gobourne A, et al. Precision microbiome reconstitution restores bile acid mediated resistance to Clostridium difficile. Nature 2014, Oct 22.

73. Stalenhoef JE, Terveer EM, Knetsch CW, Van't Hof PJ, Vlasveld IN, Keller JJ, et al. Fecal microbiota transfer for multidrug-resistant gram-negatives: A clinical success combined with microbiological failure. Open Forum Infect Dis 2017;4(2):ofx047.

74. Bilinski J, Grzesiowski P, Sorensen N, Madry K, Muszynski J, Robak K, et al. Fecal microbiota transplantation in patients with blood disorders inhibits gut colonization with antibiotic-resistant bacteria: Results of a prospective, single-center study. Clin Infect Dis 2017, Aug 1;65(3):364-70.

75. Manley KJ, Fraenkel MB, Mayall BC, Power DA. Probiotic treatment of vancomycin-resistant Enterococci: A randomised controlled trial. Med J Aust 2007, May 7;186(9):454-7.

76. Szachta P, Ignyś I, Cichy W. An evaluation of the ability of the probiotic strain Lactobacillus rhamnosus GG to eliminate the gastrointestinal carrier state of vancomycin-resistant Enterococci in colonized children. J Clin Gastroenterol 2011;45(10):872-7.

77. Vidal M, Forestier C, Charbonnel N, Henard S, Rabaud C, Lesens O. Probiotics and intestinal colonization by vancomycin-resistant enterococci in mice and humans. J Clin Microbiol 2010, Jul;48(7):2595-8.

78. Doron S, Hibberd PL, Goldin B, Thorpe C, McDermott L, Snydman DR. Effect of Lactobacillus rhamnosus GG administration on vancomycin-resistant Enterococcus colonization in adults with comorbidities. Antimicrob Agents Chemother 2015, Aug; 59(8):4593-9.

79. de Regt MJ, Willems RJ, Hené RJ, Siersema PD, Verhaar HJ, Hopmans TE, Bonten MJ. Effects of probiotics on acquisition and spread of multiresistant Enterococci. Antimicrob Agents Chemother 2010, Jul;54(7):2801-5.

80. Atarashi K, Tanoue T, Oshima K, Suda W, Nagano Y, Nishikawa H, et al. Treg induction by a rationally selected mixture of Clostridia strains from the human microbiota. Nature 2013, Aug 8;500(7461):232-6.

81. Sokol H, Pigneur B, Watterlot L, Lakhdari O, Bermúdez-Humarán LG, Gratadoux J-J, et al. Faecalibacterium prausnitzii is an anti-inflammatory commensal bacterium identified by gut microbiota analysis of Crohn disease patients. Proceedings of the National Academy of Sciences 2008;105(43):16731-6.

82. Round JL, Mazmanian SK. Inducible Foxp3+ regulatory t-cell development by a commensal bacterium of the intestinal microbiota. Proc Natl Acad Sci U S A 2010, Jul 6;107(27):12204-9.

83. Faith JJ, Ahern PP, Ridaura VK, Cheng J, Gordon JI. Identifying gut microbe-host phenotype relationships using combinatorial communities in gnotobiotic mice. Sci Transl Med 2014, Jan 22;6(220):220ra11.

84. Arpaia N, Campbell C, Fan X, Dikiy S, van der Veeken J, Deroos P, et al. Metabolites produced by commensal bacteria promote peripheral regulatory t-cell generation. Nature 2013, Nov 13.

85. Sivan A, Corrales L, Hubert N, Williams JB, Aquino-Michaels K, Earley ZM, et al. Commensal Bifidobacterium promotes antitumor immunity and facilitates anti-pd-l1 efficacy. Science 2015, Nov 5.

86. Vétizou M, Pitt JM, Daillère R, Lepage P, Waldschmitt N, Flament C, et al. Anticancer immunotherapy by CTLA-4 blockade relies on the gut microbiota. Science 2015, Nov 5.

87. Iida N, Dzutsev A, Stewart CA, Smith L, Bouladoux N, Weingarten RA, et al. Commensal bacteria control cancer response to therapy by modulating the tumor microenvironment. Science 2013, Nov 22;342(6161):967-70.

88. Viaud S, Saccheri F, Mignot G, Yamazaki T, Daillère R, Hannani D, et al. The intestinal microbiota modulates the anticancer immune effects of cyclophosphamide. Science 2013, Nov 22;342(6161):971-6.

89. Routy B, Le Chatelier E, Derosa L, Duong CPM, Alou MT, Daillère R, et al. Gut microbiome influences efficacy of PD-1-based immunotherapy against epithelial tumors. Science 2018;359(6371):91-7.

90. Gopalakrishnan V, Spencer CN, Nezi L, Reuben A, Andrews MC, Karpinets TV, et al. Gut microbiome modulates response to anti-PD-1 immunotherapy in melanoma patients. Science 2018;359(6371):97-103.

91. Matson V, Fessler J, Bao R, Chongsuwat T, Zha Y, Alegre ML, et al. The commensal microbiome is associated with anti-PD-1 efficacy in metastatic melanoma patients. Science 2018;359(6371):104-8.

92. Lupp C, Robertson ML, Wickham ME, Sekirov I, Champion OL, Gaynor EC, Finlay BB. Host-mediated inflammation disrupts the intestinal microbiota and promotes the overgrowth of Enterobacteriaceae. Cell Host Microbe 2007, Aug 16;2(2):119-29.

93. Stecher B, Robbiani R, Walker AW, Westendorf AM, Barthel M, Kremer M, et al. Salmonella enterica serovar Typhimurium exploits inflammation to compete with the intestinal microbiota. PLoS Biol 2007, Oct;5(10):2177-89.

94. Winter SE, Winter MG, Xavier MN, Thiennimitr P, Poon V, Keestra AM, et al. Host-derived nitrate boosts growth of E. coli in the inflamed gut. Science 2013, Feb 8;339(6120):708-11.

95. Hodi FS, O'Day SJ, McDermott DF, Weber RW, Sosman JA, Haanen JB, et al. Improved survival with ipilimumab in patients with metastatic melanoma. New England Journal of Medicine 2010;363(8):711-23.

96. Berman D, Parker SM, Siegel J, Chasalow SD, Weber J, Galbraith S, et al. Blockade of cytotoxic T-lymphocyte antigen-4 by ipilimumab results in dysregulation of gastrointestinal immunity in patients with advanced melanoma. Cancer Immun 2010;10:11.

97. Weber JS, Dummer R, de Pril V, Lebbé C, Hodi FS, MDX010-20 Investigators. Patterns of onset and resolution of immune-related adverse events of special interest with ipilimumab: Detailed safety analysis from a phase 3 trial in patients with advanced melanoma. Cancer 2013, May 1;119(9):1675-82.

98. Lord JD, Hackman RC, Moklebust A, Thompson JA, Higano CS, Chielens D, et al. Refractory colitis following anti-CTLA4 antibody therapy: Analysis of mucosal Foxp3+ T cells. Dig Dis Sci 2010, May;55(5):1396-405.

99. Chaput N, Lepage P, Coutzac C, Soularue E, Le Roux K, Monot C, et al. Baseline gut microbiota predicts clinical response and colitis in metastatic melanoma patients treated with ipilimumab. Ann Oncol 2017, Jun 1;28(6):1368-79.

100. Hill MJ. Intestinal flora and endogenous vitamin synthesis. Eur J Cancer Prev 1997, Mar;6 Suppl 1:S43-5.

101. Gill SR, Pop M, Deboy RT, Eckburg PB, Turnbaugh PJ, Samuel BS, et al. Metagenomic analysis of the human distal gut microbiome. Science 2006, Jun 2;312(5778):1355-9.

102. Coates ME, Ford JE, Harrison GF. Intestinal synthesis of vitamins of the B complex in chicks. British Journal of Nutrition 1968;22(03):493-500.

103. Kuroki F, Iida M, Tominaga M, Matsumoto T, Hirakawa K, Sugiyama S, Fujishima M. Multiple vitamin status in Crohn's disease. Dig Dis Sci 1993;38(9):1614-8.

104. Ellestad-Sayed JJ, Nelson RA, Adson MA, Palmer WM, Soule EH. Pantothenic acid, coenzyme A, and human chronic ulcerative and granulomatous colitis. The American Journal of Clinical Nutrition 1976;29(12):1333-8.

105. Kjer-Nielsen L, Patel O, Corbett AJ, Le Nours J, Meehan B, Liu L, et al. MR1 presents microbial vitamin B metabolites to MAIT cells. Nature 2012, Nov 29;491(7426):717-23.

106. Serriari NE, Eoche M, Lamotte L, Lion J, Fumery M, Marcelo P, et al. Innate mucosal-associated invariant T (MAIT) cells are activated in inflammatory bowel diseases. Clin Exp Immunol 2014, May;176(2):266-74.

107. Furuchi T, Kashiwagi K, Kobayashi H, Igarashi K. Characteristics of the gene for a spermidine and putrescine transport system that maps at 15 min on the Escherichia coli chromosome. Journal of Biological Chemistry 1991;266(31):20928-33.

108. Ricci G, Stabellini G, Bersani G, Marangoni G, Fabbri P, Gentili G, Alvisi V. Ornithine decarboxylase in colonic mucosa from patients with moderate or severe Crohn's disease and Ulcerative Colitis. Eur J Gastroenterol Hepatol 1999, Aug;11(8): 903-4.

109. Weiss TS, Herfarth H, Obermeier F, Ouart J, Vogl D, Schölmerich J, et al. Intracellular polyamine levels of intestinal epithelial cells in inflammatory bowel disease. Inflamm Bowel Dis 2004, Sep;10(5):529-35.

110. Donskey CJ. Antibiotic regimens and intestinal colonization with antibiotic-resistant gram-negative bacilli. Clin Infect Dis 2006, Sep 1;43 Suppl 2:S62-9.

111. Owens RC, Donskey CJ, Gaynes RP, Loo VG, Muto CA. Antimicrobial-associated risk factors for Clostridium difficile infection. Clin Infect Dis 2008, Jan 15;46 Suppl 1:S19-31.

112. Spellberg B, Bartlett JG, Gilbert DN. The future of antibiotics and resistance. New England Journal of Medicine 2013;368(4):299-302.

113. Podschun R, Ullmann U. Klebsiella spp. As nosocomial pathogens: Epidemiology, taxonomy, typing methods, and pathogenicity factors. Clin Microbiol Rev 1998, Oct; 11(4):589-603.

114. Gaynes R, Edwards JR, National Nosocomial Infections Surveillance System. Overview of nosocomial infections caused by gram-negative bacilli. Clin Infect Dis 2005, Sep 15;41(6):848-54.

115. Ho J, Tambyah PA, Paterson DL. Multiresistant gram-negative infections: A global perspective. Curr Opin Infect Dis 2010, Dec;23(6):546-53.

116. Peleg AY, Hooper DC. Hospital-Acquired infections due to gram-negative bacteria. N Engl J Med 2010, May 12;362(19):1804-13.

117. CDC. Antibiotic resistance threats in the United States (2013): http://www.cdc.gov/drugresistance/threat-report-2013/

118. Stone PW, Braccia D, Larson E. Systematic review of economic analyses of health care-associated infections. Am J Infect Control 2005, Nov;33(9):501-9.

119. Kamada N, Seo SU, Chen GY, Núñez G. Role of the gut microbiota in immunity and inflammatory disease. Nat Rev Immunol 2013, May;13(5):321-35.

120. Xiong H, Carter RA, Leiner IM, Tang YW, Chen L, Kreiswirth BN, Pamer EG. Distinct contributions of neutrophils and CCR2+ monocytes to pulmonary clearance of different Klebsiella pneumoniae strains. Infect Immun 2015, Sep;83(9):3418-27.

121. Lewis BB, Buffie CG, Carter RA, Leiner I, Toussaint NC, Miller LC, et al. Loss of microbiota-mediated colonization resistance to Clostridium difficile infection with oral vancomycin compared with metronidazole. J Infect Dis 2015, Nov 15;212(10):1656-65.

122. Atarashi K, Tanoue T, Shima T, Imaoka A, Kuwahara T, Momose Y, et al. Induction of colonic regulatory T cells by indigenous clostridium species. Science 2011, Jan 21;331(6015):337-41.

123. Narushima S, Sugiura Y, Oshima K, Atarashi K, Hattori M, Suematsu M, Honda K. Characterization of the 17 strains of regulatory T cell-inducing human-derived Clostridia. Gut Microbes 2014;5(3):333-9.

124. Cummings JH, Pomare EW, Branch WJ, Naylor CP, Macfarlane GT. Short chain fatty acids in human large intestine, portal, hepatic and venous blood. Gut 1987, Oct; 28(10):1221-7.

125. den Besten G, van Eunen K, Groen AK, Venema K, Reijngoud DJ, Bakker BM. The role of short-chain fatty acids in the interplay between diet, gut microbiota, and host energy metabolism. J Lipid Res 2013, Sep;54(9):2325-40.

126. Stein RR, von Mering C, Bucci V, Toussaint NC, Buffie CG, Rätsch G, et al. Ecological modeling from time-series inference: Insight into dynamics and stability of intestinal microbiota. PLoS Comput Biol 2013, Dec 12;9(12):e1003388.

127. Khanna S, Pardi DS, Kelly CR, Kraft CS, Dhere T, Henn MR, et al. A novel microbiome therapeutic increases gut microbial diversity and prevents recurrent Clostridium difficile infection. J Infect Dis 2016, Jul 15;214(2):173-81.

128. Ratner M. Seres's pioneering microbiome drug fails mid-stage trial. Nat Biotechnol 2016, Oct 11;34(10):1004-5.

129. Pamer EG. Fecal microbiota transplantation: Effectiveness, complexities, and lingering concerns. Mucosal Immunol 2014, Mar;7(2):210-4.

130. Stiefel U, Nerandzic MM, Pultz MJ, Donskey CJ. Gastrointestinal colonization with a cephalosporinase-producing Bacteroides species preserves colonization resistance against vancomycin-resistant Enterococcus and Clostridium difficile in cephalosporin-treated mice. Antimicrob Agents Chemother 20x14, May 27.

131. Zeevi D, Korem T, Zmora N, Israeli D, Rothschild D, Weinberger A, et al. Personalized nutrition by prediction of glycemic responses. Cell 2015, Nov 19;163(5): 1079-94.

132. Arias CA, Panesso D, McGrath DM, Qin X, Mojica MF, Miller C, et al. Genetic basis for in vivo daptomycin resistance in enterococci. New England Journal of Medicine 2011;365(10):892-900.

133. Barrick JE, Yu DS, Yoon SH, Jeong H, Oh TK, Schneider D, et al. Genome evolution and adaptation in a long-term experiment with Escherichia coli. Nature 2009, Oct 29;461(7268):1243-7.

134. Raven KE, Gouliouris T, Brodrick H, Coll F, Brown NM, Reynolds R, et al. Complex routes of nosocomial vancomycin-resistant Enterococcus faecium transmission revealed by genome sequencing. Clin Infect Dis 2017, Apr 1;64(7):886-93.

135. van Schaik W, Willems RJ. Genome-based insights into the evolution of enterococci. Clin Microbiol Infect 2010, Jun;16(6):527-32.

136. Qin X, Galloway-Peña JR, Sillanpaa J, Roh JH, Nallapareddy SR, Chowdhury S, et al. Complete genome sequence of Enterococcus faecium strain TX16 and comparative genomic analysis of Enterococcus faecium genomes. BMC Microbiol 2012;12:135.

137 Palmer KL, Godfrey P, Griggs A, Kos VN, Zucker J, Desjardins C, et al. Comparative genomics of enterococci: Variation in Enterococcus faecalis, clade structure in E. faecium, and defining characteristics of E. gallinarum and E. casseliflavus. MBio 2012;3(1):e00318-1.

138. Paulsen IT, Banerjei L, Myers GSA, Nelson KE, Seshadri R, Read TD, et al. Role of mobile DNA in the evolution of vancomycin-resistant Enterococcus faecalis. Science 2003;299(5615):2071-4.

139. Leavis HL, Willems RJ, van Wamel WJ, Schuren FH, Caspers MP, Bonten MJ. Insertion sequence-driven diversification creates a globally dispersed emerging multiresistant subspecies of E. faecium. PLoS Pathog 2007, Jan;3(1):e7.

140. Willems RJ, van Schaik W. Transition of Enterococcus faecium from commensal organism to nosocomial pathogen . Future Microbiology 2009, Nov;4(9):1125-35.

141. Werner G, Fleige C, Geringer U, van Schaik W, Klare I, Witte W. IS element IS16 as a molecular screening tool to identify hospital-associated strains of Enterococcus faecium. BMC Infect Dis 2011;11:80.

142. Moradigaravand D, Gouliouris T, Blane B, Naydenova P, Ludden C, Crawley C, et al. Within-host evolution of Enterococcus faecium during longitudinal carriage and transition to bloodstream infection in immunocompromised patients. Genome Med 2017, Dec 27;9(1):119.

143. Fontana R, Grossato A, Rossi L, Cheng YR, Satta G. Transition from resistance to hypersusceptibility to beta-lactam antibiotics associated with loss of a low-affinity penicillin-binding protein in a Streptococcus faecium mutant highly resistant to penicillin. Antimicrob Agents Chemother 1985;28(5):678-83.

144. Williamson R, Le Bouguenec G, Gutmann L, Horaud T. One or two low affinity penicillin-binding proteins may be responsible for the range of susceptibility of Enterococcus faecium to benzylpenicillin. Microbiology 1985;131(8):1933-40.

145. Galloway-Peña JR, Nallapareddy SR, Arias CA, Eliopoulos GM, Murray BE. Analysis of clonality and antibiotic resistance among early clinical isolates of Enterococcus faecium in the united states. J Infect Dis 2009, Nov 15;200(10):1566-73.

146. Galloway-Peña JR, Rice LB, Murray BE. Analysis of PBP5 of early U.S. Isolates of Enterococcus faecium: Sequence variation alone does not explain increasing ampicillin resistance over time. Antimicrob Agents Chemother 2011, Jul;55(7):3272-7.

147. Grayson ML, Eliopoulos GM, Wennersten CB, Ruoff KL, De Girolami PC, Ferraro MJ, Moellering RC. Increasing resistance to beta-lactam antibiotics among clinical isolates of Enterococcus faecium: A 22-year review at one institution. Antimicrob Agents Chemother 1991, Nov;35(11):2180-4.

148. Fontana R, Cerini R, Longoni P, Grossato A, Canepari P. Identification of a streptococcal penicillin-binding protein that reacts very slowly with penicillin. J Bacteriol 1983, Sep;155(3):1343-50.

149. Rybkine T, Mainardi JL, Sougakoff W, Collatz E, Gutmann L. Penicillin-binding protein 5 sequence alterations in clinical isolates of Enterococcus faecium with different levels of beta-lactam resistance. J Infect Dis 1998, Jul;178(1):159-63.

150. Zorzi W, Zhou XY, Dardenne O, Lamotte J, Raze D, Pierre J, et al. Structure of the low-affinity penicillin-binding protein 5 pbp5fm in wild-type and highly penicillin-resistant strains of Enterococcus faecium. J Bacteriol 1996;178(16):4948-57.

151. Rice LB, Thomas RH, Lakticova V, Helfand MS, Donskey CJ. B-lactam antibiotics and gastrointestinal colonization with vancomycin-resistant Enterococci. Journal of Infectious Diseases 2004;189(6):1113-8.